

UNIVERSITY OF BELGRADE

FACULTY OF MEDICINE

Petar D. Milovanović

**NANOSTRUCTURAL AND  
MICROARCHITECTURAL BONE  
PROPERTIES OF HUMAN FEMORAL  
NECK: IMPLICATIONS FOR AGE-RELATED  
BONE FRAGILITY IN WOMEN**

Doctoral Dissertation

Belgrade, 2013

УНИВЕРЗИТЕТ У БЕОГРАДУ

МЕДИЦИНСКИ ФАКУЛТЕТ

Петар Д. Миловановић

**НАНОСТРУКТУРНЕ И  
МИКРОАРХИТЕКТОНСКЕ  
КАРАКТЕРИСТИКЕ ВРАТА БУТНЕ  
КОСТИ: УТИЦАЈ НА ПОВЕЋАНУ  
КОШТАНУ ФРАГИЛНОСТ СА  
СТАРЕЊЕМ КОД ЖЕНА**

докторска дисертација

Београд, 2013.

**PhD advisor:**

Professor Dr. Marija Đurić

University of Belgrade - Faculty of Medicine

**Members of the evaluation committee:**

1. Prof. Dr. Vladimir Bumbaširević, University of Belgrade - Faculty of Medicine
2. Assoc. Prof. Dr. Jelena Sopta, University of Belgrade - Faculty of Medicine
3. Prof. Dr. Nenad Filipović, University of Kragujevac - Faculty of Mechanical Engineering

**Date of public presentation:** \_\_\_\_\_

**Ментор:**

професор др Марија Ђурић,

Универзитет у Београду - Медицински факултет

**Чланови комисије за оцену и одбрану докторске дисертације:**

1. академик Владимир Бумбаширевић, Универзитет у Београду -  
Медицински факултет – председник комисије
2. доцент др Јелена Сопта, Универзитет у Београду - Медицински  
факултет
3. професор др Ненад Филиповић, Универзитет у Крагујевцу -  
Факултет инжењерских наука

**Датум јавне одбране дисертације:** \_\_\_\_\_

*I would like to thank all individuals who, each one in his/her own unique way, have helped me on the road to the end of my doctoral studies and inspired or encouraged me in my professional development.*

*First of all, I would like to express my greatest gratitude to Prof. Marija Đurić, the head of Laboratory for Anthropology and my PhD advisor for strong and enormous support during all these years. I am thankful for great and constructive guidance, wisdom, exceptional enthusiasm and impressive scientific vision, as well as continuous inspiration and numerous encouragements. Especially, I am grateful to her for creating Laboratory for Anthropology as an extraordinary and stimulating intellectual environment at our university, for accepting me as a member of her team, for believing in me more than I have believed in myself, and for teaching me (and all of us) the complexity and beauty of science in general and bones in particular.*

*I am very thankful to Assoc. Prof. Danijela Đonić and all my colleagues from Laboratory for Anthropology, especially Ksenija Đukić, for supporting me, tolerating me and trusting me for years. It would be hard to imagine any research without them.*

*I would like to thank the members of the PhD Advisory board for helpful comments regarding this thesis.*

*Apart from clear understanding of biological/medical context, the work on this thesis required learning many basic and advanced physical or chemical concepts and terminology pertinent to the materials science and engineering. In this context, the research has led me to many non-medical professionals and showed me new horizons and impressively different approach to medical problems. I am grateful to Dr. Zlatko Rakočević and his young team (Jelena Potočnik, Miloš Nenadović, Igor Peterka, Maja Popović and Mirjana Novaković) at Laboratory for Atomic Physics - Institute of Nuclear Sciences Vinča, as well as Dr. Olivera Nešković and Dr. Milovan Stoiljković from Department of Physical Chemistry - Institute of Nuclear Sciences Vinča, for fruitful collaboration during work on this PhD thesis. In particular, I have to thank Dr.*

*Zlatko Rakočević for his strong support in discovering and understanding the nano-world and for all the things I learned from him and his team during past three years – it was so constructive and interesting.*

*I express thanks to Prof. Slobodan Nikolić and Assoc. Prof. Vladimir Živković from Institute of Forensic Medicine, School of Medicine University of Belgrade for their significant support to our projects and excellent cooperation.*

*I would like to thank Dr. Michael Hahn, Dr. Bjoern Busse, Dr. Robert Percy Marshall, and Prof. Michael Amling from Institute of Osteology and Biomechanics, University Medical Center Hamburg-Eppendorf, for fruitful and exciting collaboration in the bone field, as well as Prof. H. J. Seitz from South-East-European Cooperation, University Medical Center Hamburg-Eppendorf for his support and trust.*

*Finally, I am grateful to my family and friends, who were important support during all my studies.*

**Title of the doctoral dissertation:**

NANOSTRUCTURAL AND MICROARCHITECTURAL BONE PROPERTIES OF HUMAN FEMORAL NECK: IMPLICATIONS FOR AGE-RELATED BONE FRAGILITY IN WOMEN

**Summary**

Background: Hip fractures are among the most important health problems in elderly population worldwide, particularly in elderly women. However, despite extensive research on age-related bone fragility, the factors leading to decreased bone strength in advanced age are not yet clear enough. Indeed, in clinical settings bone mineral density (BMD) assessed by dual energy X-ray absorptiometry has been used as an indicator of hip fracture risk. However, as it has been already pointed out that age-related decrease in BMD fails to fully explain the high increase in hip fracture risk with aging, other bone features also account for age-related deterioration in bone strength. Since bone is a hierarchically organized structure, it can be hypothesized that its strength depends on various features from nano-scale to macro-scale. Although numerous studies addressed macro- and microstructural basis of bone fragility, so far the direct data at microarchitectural level have been scarce. Moreover, nanostructure of the bone mineralized matrix has received insufficient attention with regard to effects of aging and its relation to bone fragility.

Hypotheses: Our hypotheses were that region-dependant worsening of bone microarchitecture in elderly women leads to increased femoral neck fragility, and that - besides the microarchitectural deterioration - the age-related nanostructural changes at the bone matrix level contribute to increased bone fragility in elderly women.

Material and methods: To test these hypotheses, we analyzed bone specimens from the femoral neck region obtained at autopsy in young and elderly women without hip fracture as well as in a group of postmenopausal women who sustained a hip fracture. Following sectioning process, micro-computed tomography was performed to assess bone microarchitectural properties. Bone nanostructure was analyzed via Topography and Phase modes of Atomic Force Microscopy (AFM), while chemical evaluation of

bone material composition encompassed energy dispersive X-ray spectroscopy, quantitative backscatter electron imaging, inductively coupled plasma optical emission spectroscopy and direct current argon arc plasma optical emission spectrometry. Nanoindentation and reference point indentation tests were used for assessment of mechanical characteristics at the bone material level.

Results and conclusions: Our results clearly demonstrated importance of microarchitectural and nanostructural bone features for bone mechanical integrity.

At the micro-level, our findings showed significant differences in trabecular microarchitectural properties between the postmenopausal women with hip fracture and age-matched controls. The fracture cases presented impaired parameters of trabecular bone microarchitectural organization, particularly in the superolateral neck region. Considering the fact that the femoral neck fracture typically starts in this subregion, the observed preferential impairment of the superolateral neck trabecular bone in women with hip fracture reveals the region-dependent microstructural basis of bone fragility in elderly women.

Using atomic force microscopy as a powerful tool for nano-level examination of the bone tissue revealed age-related effects on bone material, and provided new insights into greater bone fragility in elderly women by emphasizing distinct age-related deterioration at the bone matrix level.

Significant nanostructural differences between young and elderly women were found in the trabeculae of the superolateral femoral neck. In advanced age there was a bimodal distribution of the mineral crystal sizes, where - apart from small crystals similar in size to those in the young - the elderly individuals also expressed a group of larger crystals attributable to older tissue age of unremodeled bone areas. Given that chemical analyses showed unchanged calcium and phosphorus levels in the elderly trabeculae, the increase in mineral particle size could not be perceived as a consequence of an increased mineral content; rather, it suggests the reorganization of the existing bone mineral to larger grains in advanced age via coalescence of crystals.

Furthermore, we have introduced here the power spectral density (PSD) and fractal dimension analyses based on AFM topography images of the bone mineralized matrix, which have shown possible correlation with bone tissue age and proved useful



for explaining differential trabecular bone fragility across age. In particular, a decreased fractal dimension and less steep PSD trendline of the interfibrillar area of the femoral neck trabeculae in elderly individuals indicated age-related decrease in structural complexity and surface roughness, suggesting decreased energy dissipation during loading and consequent increases in brittleness and bone fragility in aged cohorts.

Assessment of nano-level mechanical behavior (combined with nanostructural evaluation) offered experimental evidence for particular mechanical consequences of bone matrix aging, separately from age-related effects at other hierarchical levels of bone structure. In this context, AFM nanoindentation tests showed that mechanical alteration already exists at the bone material level which showed less elastic behavior with greater propensity to fractures resulting from impact during a sideways fall in the elderly.

In contrast to trabecular bone, our AFM analysis of the external cortical surface of the femoral neck in young and aged women revealed small mineral grains and similar roughness (reflecting similar rate of mineral deposition) along with unchanged Ca/P ratios, thereby suggesting similar tissue age at the periosteal cortical surface in both age groups. Considering observed parallel age-related increase in the neck outer diameter, our data may confirm that the femoral neck undergoes periosteal expansion with aging due to continuous periosteal bone apposition.

The external cortical surface of the femoral neck in postmenopausal women with hip fracture displayed larger mineral crystals than in age-matched women without skeletal diseases. Based on observations that large-grained materials are accompanied by decreased mechanical properties in comparison with fine-grained fabrics, the findings of larger crystals in the fracture group offer additional explanation for reduced toughness and decreased strength of its cortical bone observed in this study. Moreover, along with increased crystal size, a shift to a higher mineralization profile and a tendency to increased cortical porosity and reduced osteocyte lacunar network delineate that cortical bone of the superolateral femoral neck in the fracture group bears distinct signs of fragility at various levels of its structural organization. These results contribute to the understanding of osseous alterations involving several hierarchical levels in age-related bone fragility. In particular, considering that we analyzed the very surface where

the fracture usually starts, these results contribute to the understanding of structural basis of age-related bone fragility.

**Keywords:** bone, nanostructure, microarchitecture, composition, femur, fragility, aging, women, hierarchical assessment, mechanical properties

**Scientific field:** Medicine

**Specific scientific field:** Skeletal biology

## **Наслов докторске дисертације:**

НАНОСТРУКТУРНЕ И МИКРОАРХИТЕКТОНСКЕ КАРАКТЕРИСТИКЕ  
ВРАТА БУТНЕ КОСТИ: УТИЦАЈ НА ПОВЕЋАНУ КОШТАНУ ФРАГИЛНОСТ  
СА СТАРЕЊЕМ КОД ЖЕНА

## **Резиме**

Увод: Преломи кука су један од најзначајнијих здравствених проблема код старих особа широм света, а посебно код старијих жена. Међутим, упркос многобројним истраживањима узрока фрагилности скелета код старијих особа, још увек се врло мало зна о чиниоцима који доводе до смањене чврстоће кости у старости. Минерална густина кости (bone mineral density, BMD) утврђена применом дензитометријске методе (dual energy X-ray absorptiometry, DXA) је дуго сматрана главним показатељем коштане чврстоће и до данас коришћена у клиничкој процени коштане фрагилности и ризика за прелом кука. Међутим, будући да је више аутора указало на податак да старосни пад BMD не може потпуно објаснити значајни пораст ризика од прелома кука код старијих особа, неопходно је испитати и допринос других коштаних карактеристика смањењу коштане чврстоће са старењем. Како је кост хијерархијски организована структура, може се претпоставити да њена чврстоћа зависи од различитих елемената коштане грађе од нанометарске до макро-скеале. Премда су се многобројне студије усредсредиле на испитивање макроструктурне и микроструктурне основе коштане фрагилности, још увек недостају директни подаци о микроархитектури костију код особа са преломом кука. Поред тога, старосним променама наноструктурних параметара самог материјала од кога је кост изграђена није посвећена одговарајућа пажња, као ни њиховом значају за коштану фрагилност.

Хипотеза: Наше хипотезе су биле да регион-зависно погоршање коштане микроархитектуре код старијих жена повећава њихов ризик за прелом кука, као и да се, осим микроструктурних промена, са старењем јављају и наноструктурне промене на нивоу коштаног матрикса које такође доприносе повећаној коштаног фрагилности код старијих жена.

Материјал и методе: Да бисмо испитали ове хипотезе, анализирали смо коштане узорке врата бутне кости добијене током обдукције код младих и старих жена без прелома кука, као и код постменопаузних жена које су доживеле фрактуру кука. Након припреме узорака, коштану микроархитектуру испитивали смо применом микрокомпјутеризоване томографије. Коштана наноструктура је утврђивана путем топографске и фазне анализе микроскопијом атомских сила (atomic force microscopy, AFM), док је хемијска евалуација коштаног материјала обухватала енергијски дисперзивну рентгенску спектроскопију (energy dispersive X-ray spectroscopy, EDX), квантитативни имиџинг повратним распршењем електрона (quantitative backscatter electron imaging, qBEI), као и оптичку емисиону спектроскопију са индуктивно куплованом плазмом (inductively coupled plasma optical emission spectroscopy, ICP-OES) и директно струјном плазмом (direct current argon arc plasma optical emission spectrometry, DCA ARC). Применом наноиндентације и микроиндентације одређене су механичке карактеристике на нивоу коштаног матрикса.

Резултати и закључци: Резултати ове студије су јасно показали значај микроархитектонских и наноструктурних карактеристика кости за њен механички интегритет.

На микро плану, пронађене су значајне разлике у трабекуларној микроархитектури између постменопаузних жена са преломом кука и контролне групе одговарајуће старости. Особе са фрактуром су имале погоршане показатеље трабекуларне микроархитектуре, посебно у пределу суперолатералног дела врата фемура. Имајући у виду чињеницу да преломи кука углавном почињу у овом пределу, нарочито пропадање трабекуларне кости у суперолатералном врату фемура открива регион-зависну микроструктурну основу коштане фрагилности код старих жена.

Применом микроскопије атомских сила као супериорног метода за испитивање наноструктуре коштаног ткива показани су ефекти старења на сам коштани матрикс, и пружени нови увиди у повећану крхкост костију код старијих жена.

Значајне разлике су пронађене у наноструктури трабекуларне кости између младих и старих жена у суперолатералном региону врата бутне кости. У позним годинама уочена је бимодална расподела величине минералних кристала: поред мањих кристала сличних по величини онима који су присутни код млађих особа, старије особе имају и групу већих кристала који се могу приписати неремоделираним зонама, тј. површинама са већом ткивном старости. С обзиром да су хемијске анализе показале непромењени ниво калцијума и фосфора код старијих трабекула, повећање величине минералних кристала се не може схватити као последица повећања количине минерала, већ је извесније да се постојећи кристали временом стапају градећи веће кристале код старијих особа.

Осим тога, применили смо анализу спектралне густине снаге (PSD) и фракталне димензије засноване на AFM топографским сликама минерализованог матрикса трабекуларне кости, показавши њихову могућу повезаност са старошћу коштаног ткива и степеном фрагилности трабекула током живота. Посебно, смањена фрактална димензија и мање стрм PSD линеарни тренд интерфибриларног простора трабекула врата бутне кости код старијих особа указује на смањење структурне сложености и површинске храпавости са старењем, сугеришући да је код старих особа смањена дисипација енергије током механичког оптерећења што корелира са повећаном кртошћу и, стога, повећаном подложношћу прелому.

Проценом механичког понашања кости на нанометарском нивоу упоредо са њеном наноструктурном евалуацијом, добијени су експериментални докази механичких последица старења коштаног матрикса, независно од ефеката на другим нивоима коштане хијерархијске организације. У том смислу, AFM наноиндентација је показала да, већ на нивоу самог материјала од кога је сачињена, кост старих особа показује измењене механичке карактеристике (смањену еластичност са већом склоношћу ка преломима приликом пада на кук).

За разлику од трабекуларне кости, наша AFM анализа спољашње кортикалне површине врата бутне кости код младих и старијих жена показала је постојање малих минералних кристала и сличну храпавост уз непромењен Ca/P однос указујући на међусобно сличну ткивну старост на периостеалној површини кортикалне кости у обе старосне групе. С обзиром на примећено повећање

спољашњег пречника врата фемура са старењем, ови резултати потврђују теорију да наведени регион подлеже расту у ширину путем сталне периостне апозиције нове кости током живота.

Спољашња кортикална површина врата бутне кости код постменопаузних жена са преломом кука показала је постојање већих минералних кристала него код здравих жена одговарајуће старости. На основу запажања да се крупнозрнасти материјали одликују смањеном механичком отпорношћу у поређењу са ситнозрнестим материјалима, налаз великих кристала у групи са фрактуром пружа додатно објашњење за смањење жилавости и пад чврстоће кортикалне кости. Поред тога, заједно са повећањем величине кристала, помак ка већем степену минерализације и тенденција ка повећаној порозности кортекса уз редуовану мрежу остеоцитних лакуна, показују да кортикална кост суперолатералног врата фемура код особа са фрактуром носи јасне знаке фрагилности на различитим нивоима коштане структурне организације. Ови резултати доприносе разумевању коштаних промена на више хијерархијских нивоа код повећане фрагилности кости са старењем. Нарочито, будући да смо испитивали саму површину на којој прелом обично почиње, наши резултати доприносе разумевању структурне основе коштане фрагилности код старих особа.

**Кључне речи:** кост, наноструктура, микроархитектура, састав, фемур, фрагилност, старење, жене, хијерархијски приступ, механичке особине

**Научна област:** медицина

**Ужа научна област:** биологија скелета (остеологија)



## CONTENTS

<b>1. INTRODUCTION</b>	1
1.1. Bone structure: hierarchical organization	2
1.2. Age-related changes in bone mineral density and geometry	5
1.3. Age-related changes in bone microarchitecture	6
1.4. Investigation of nanostructural bone properties	7
1.4.1. Morphological analysis using atomic force microscopy (AFM)	7
1.4.2. Mechanical characterization of bone mineralized matrix (determination of elasticity and hardness at the nano-level)	8
<b>2. RESEARCH HYPOTHESES AND GOALS</b>	10
<b>3. MATERIAL AND METHODS</b>	11
3.1. Study sample	11
3.2. Assessment of bone microarchitecture	11
3.2.1. Sample characteristics	11
3.2.2. Preparation of specimens	12
3.2.3. Micro-CT scanning procedure	12
3.2.3.1. Trabecular bone	12
3.2.3.2. Cortical bone	13
3.2.4. Micro-CT evaluation procedure	13
3.3. Assessment of bone nanostructure	14
3.3.1. Specimen selection and preparation	14
3.3.2. Atomic force microscopy	16
3.3.2.1. Basic characteristics of AFM	16
3.3.2.2. AFM imaging of bone specimens	18
3.3.2.3. AFM imaging. Determination of advanced nanostructural descriptors: Power spectral density (PSD) and fractal dimension (FD)	19
3.4. Quantitative chemical analyses	21



3.4.1. Evaluation of bone matrix composition via destructive analytical approach	21
3.4.1.1. Specimen preparation	21
3.4.1.2. Inductively coupled plasma optical emission spectroscopy (ICP-OES)	22
3.4.1.3. Direct current argon arc plasma optical emission spectrometry (DCA ARC)	22
3.4.2. Evaluation of bone matrix composition using non-destructive analytical approach	23
3.4.2.1. Energy dispersive X-ray spectroscopy (EDX)	23
3.4.2.2. Bone mineral density distribution analysis (BMDD) using quantitative backscatter electron imaging (qBEI)	23
3.5. Assessment of bone nanomechanical properties	25
3.5.1. Nanoindentation	25
3.5.1.1. Characteristics and preparation of the specimens	25
3.5.1.2. AFM imaging	26
3.5.1.3. AFM nanoindentation	26
3.5.1.3.1. Principle of nanoindentation	26
3.5.1.3.2. Nanoindentation test	27
3.5.2. Reference point indentation (RPI)	29
3.5.2.1. Characteristics and preparation of the specimens	29
3.5.2.2. Reference point indentation tests	29
3.6. Statistical analysis	31
3.6.1. Determination of sample size	31
3.6.2. Statistical analysis of data	31
<b>4. RESULTS</b>	<b>33</b>
4.1. Analysis of trabecular bone microarchitecture	33
4.2. Analysis of bone nanostructure and chemical composition	39
4.2.1. Age-related differences in nanostructure of trabecular bone	39
4.2.1.1. Advanced nanostructural analyses (PSD, FD) of trabecular interfibrillar surface in young vs. elderly women	44

4.2.2. Age-related differences in nanostructure of cortical bone	47
4.2.2.1. Advanced nanomorphological features: Power spectral density and fractal dimension in cortical bone of young vs. elderly women	53
4.2.2.2. Calcium/phosphorus ratio of the cortical bone in young vs. elderly women	54
4.3. Nanomechanical assessment of trabecular bone material in young vs. elderly women	54
4.4. Assessment of cortical bone in hip fracture cases vs. controls	59
4.4.1. Analysis of cortical bone nanostructure	59
4.4.2. Assessment of other levels of bone hierarchy	65
4.4.2.1. Analysis of cortical microarchitecture at the superolateral femoral neck	65
4.4.2.2. Assessment of osteocyte lacunar network	65
4.4.2.3. Evaluation of bone matrix composition	66
4.4.3. Reference point indentation assessment of the material properties of the cortical bone	68
4.4.4. Percentage of inter-group differences at various length scales	70
<b>5. DISCUSSION</b>	<b>71</b>
5.1. Microarchitectural basis of trabecular bone fragility	71
5.1.1. BV/TV and other microarchitectural parameters of the trabecular bone: Two sides of the same coin?	72
5.1.2. Aging process and age-related hip fractures: a microarchitectural perspective	73
5.2. Bone nanostructural changes during aging and bone compositional data show that the young and elderly women trabeculae differ even at the bone matrix level	75
5.2.1. Mechanical consequences of changed nanostructural pattern in aged trabecular bone	76
5.3. Power Spectral Density (PSD) and Fractal Dimension (FD): Advanced nano-roughness analyses in trabecular bone may reveal potential correlates of bone tissue age	78

5.3.1. Decreased fractal dimension in the elderly trabecular bone matrix suggests a decrease in bone toughness	79
5.4. Experimental evidence of deterioration in trabecular bone mechanical properties at the material level with aging	80
5.5. Young and aged individuals' bone nanostructural/compositional features at the external (periosteal) cortical bone surface suggest that this surface is not " <i>a Lazy Mary</i> "	84
5.5.1. Fresh bone at the external cortical bone surface: Periosteal bone apposition	86
5.5.2. Mechanical requirements may drive periosteal bone apposition during aging	87
5.6. Hierarchical assessment of cortical bone at the superolateral neck in the fracture and control groups reveals signs of bone fragility at various length scales	89
5.6.1. Microstructural basis of increased cortical bone fragility	89
5.6.2. Nanostructural signs of cortical bone fragility	90
5.6.3. Compositional imprints of increased cortical bone fragility: higher and more homogenous mineralization profile	91
5.6.4. Mechanical evaluation of the bone material provides experimental evidence of decreased bone toughness in cortical bone of the fracture group	92
5.7. Summary of structural and compositional determinants of age-related hip fracture	92
<b>6. CONCLUSIONS</b>	<b>94</b>
<b>7. REFERENCES</b>	<b>97</b>



## 1. INTRODUCTION

The fractures of the femoral neck (Figure 1A) represent one of the most important health problems in elderly population worldwide (Cooper et al., 1992). Most of these hip fractures in aged individuals develop after low-intensity trauma, usually after falling from the standing height (Cole et al., 2008). It is estimated that the number of hip fractures will even rise in future, from 1.66 million recorded in 1990 to 6.26 million in 2050 worldwide (Cooper et al., 1992). Hip fractures are particularly common in elderly women, and as shown in UK Million Women Study the incidence rate increases even 7-fold from the age 50-54 to 70-74 in females (Banks et al., 2009). Epidemiological studies in Serbian population for the period 1990-2000 revealed annual incidence rates of 185.9 per 100 000 women over 50 years of age (Lešić et al., 2007), while standardized incidence rates in the same period were 228 per 100 000 (Lešić et al., 2007) thus placing Serbia in the group of countries with a moderate fracture risk (Kanis et al., 2012). National projections pointed out that the number of hip fractures in women from Belgrade would probably increase up to 128.8% by the year 2020 (Lesić et al., 2005). However, the estimated number of hip fractures for the year 2010 (Lesić et al., 2005) was already exceeded by a third in 2009, and a continuous trend of increase in age-adjusted incidence rates has been shown in the Belgrade population for the period 2000-2009 (Senohradski et al., 2013).

Hip fractures are a significant burden for the society due to high mortality, high complication rates and high expenses (Tosteson et al., 2007; Cole et al., 2008). For instance, more than 30% of patients die within the first year after the fracture, and it is disappointing that mortality rates haven't declined since 1980s (Roberts and Goldacre, 2003), which urges for improving prevention. About 30% of hip fracture patients become permanently dependent on help of their families or specialized geriatric service (Melton, 1993). Moreover, the expenses of acute medical treatment are calculated to be more than 10 000 pounds per patient in the United Kingdom (Lawrence et al., 2005) or 8 000 Euros per patient in France (Maravic et al., 2005). Total annual costs due to hip fractures are estimated to 20 billion dollars in the United States (Braithwaite et al., 2003), 650 million dollars in Canada (Wiktorowicz et al., 2001) and nearly a billion pounds in the United Kingdom (Lawrence et al., 2005).

Considering aforementioned and given an estimated rise in the incidence of hip fractures in forthcoming years (Cooper et al., 1992; Senohradski et al., 2013), there is a strong need to improve the fracture prevention. It is apparent that the falls from the standing height are not a sufficient reason to break the femoral neck, since in those circumstances young persons would not sustain a fracture. Hence, the main cause of easy bone fracturing must originate from the characteristics of bone itself. However, despite the significance of this problem and extensive research on age-related bone fragility, current clinical understanding of age-related bone weakening is insufficient to allow appropriate detection of persons who are at a high fracture risk, and the factors leading to decreased bone strength in advanced age are not clear enough.

In order to unravel the basis of bone fragility, it is essential to further explore bone structure and identify the determinants of bone strength.

### **1.1. Bone structure: hierarchical organization**

Bone is a hierarchically organized structure (Currey, 2002), so it can be observed at different length scales: at the whole bone level, at micro-level, and at the level of bone material (nano-level) (Figure 1). As nicely noted by John Currey (Currey, 2002), bone is so complex that at no scale one can truly say that we are looking at “bone as such”. Therefore, one has to consider the bone features at various hierarchical levels to profoundly understand what bone really is, and to comprehend what determines bone strength.

Femoral neck, like other bones, consists of cortical and trabecular bone compartments (Figure 1B, D). Cortical bone is the outer bony layer with very low porosity (also called *compact bone*) (Bonucci, 2000) and finite element studies suggest that it bears 50% of the loading stress at the middle part of the femoral neck (Lotz et al., 1995). Trabecular (*cancellous* or *spongy*) bone is porous bone type consisting of a network of interconnected bony plates or rods (*trabeculae*) that fills the interior of the femoral neck (Jee, 2001; Currey, 2002) (Figure 1B, C). As trabeculae transfer the stresses imposed on the cortical shell, they can be regarded as structural support to the cortex during impact loads, thus contributing significantly to overall bone strength (Reich and Gefen, 2006). As a tissue, bone is composed of cells (bone-forming cells - osteoblasts, bone resorbing cells - osteoclasts, and the most numerous - osteocytes) (Jee,

2001) and extracellular matrix (Figure 1E, F). Since the exploration of bone mechanical behavior borrows the approach and terminology from the materials science and engineering, beyond strict histological definition of *extracellular matrix* it is quite common in literature to use the term “*bone material*” interchangeably with “*bone matrix*”, both denoting the very material which composes bony elements (Weiner and Wagner, 1998; Currey, 2002; Gupta et al., 2005; Roschger et al., 2008; Ritchie, 2011).

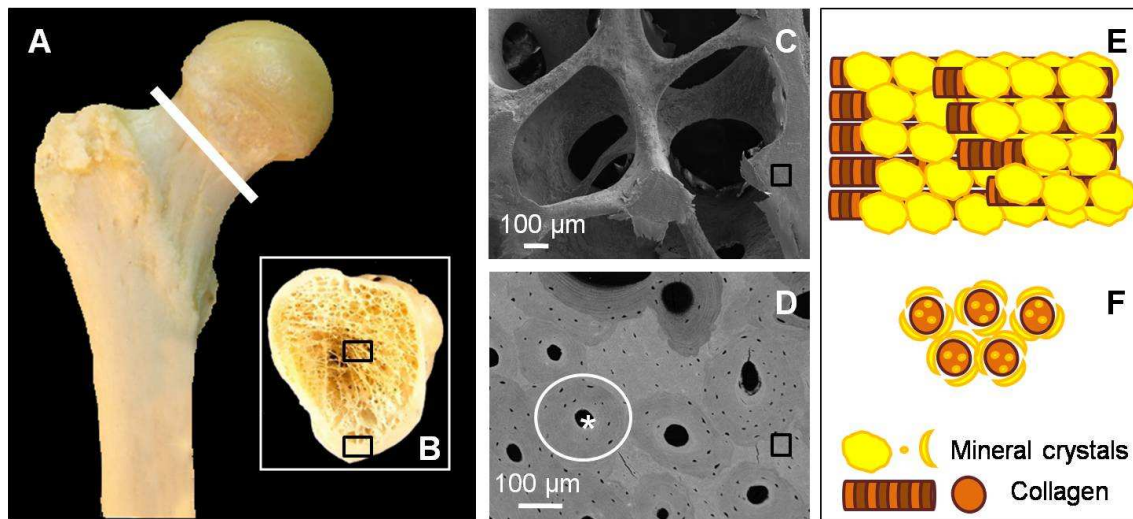


**Figure 1.** Levels of bone structural organization: Macroscopic (A, B), microscopic (C, D), nano-level (E, F). (A) A view on the proximal half of a human femur; (B) Section of the femoral neck showing that bone is organized in compact and trabecular bone compartments. Cortical bone is the outer layer while trabeculae fill the interior of the femoral neck. (C) Microscopic view (field emission scanning electron microscopy) of trabecular bone showing multiple interconnected trabeculae and large pores between them. (D) Microscopic view (backscatter electron microscopy) of cortical bone: Note that it is composed of numerous circular elements called osteons (white circle) containing Haversian canal (white asterisk) in the middle. At the level of material (matrix) bone is composed mainly of collagen fibrils and mineral crystals (schemes E, F). (E) Longitudinal view on collagen fibrils covered by mineral crystals. (F) Transversal section of collagen fibrils. Note that mineral crystals lie both between the collagen fibrils (interfibrillar mineral) and inside the collagen fibrils (intrafibrillar mineral). Non-collagenous proteins are not shown here for the sake of simplicity.

Observations at the lowest hierarchical level (*matrix level* or *material level*) revealed that bone is a nano-composite material composed of mineral part (65%), organic phase and water (Currey, 2002; An and Gruber, 2003; Thurner, 2009).

It is generally taken that bone mineral is represented by carbonated hydroxyapatite or dahllite. However, the exact chemical and physical characteristics of bone mineral are complex and still attract research attention (Paschalis et al., 1997b; Paschalis et al., 1997a; Boskey, 2001; Boskey, 2003; Rey et al., 2009; Xin et al., 2010). More precisely, bone mineral is poorly crystalline carbonated apatite with many cationic and anionic substitutions that are found within the lattice and on the surface of the apatite crystals (Boskey, 2001; Fratzl et al., 2004; Rey et al., 2009). It is believed that the mineral part mainly determines bone mechanical properties, especially hardness and strength of bone (Currey, 2003; Currey, 2012). Apart from chemical composition of mineral crystals and amount of mineralization, crystal perfection and size may be important contributors to mechanical properties (Boskey, 2001). Bone mineral is organized in particles of various sizes, and - although not yet decisive - they are mostly of plate-like rather than needle-like shape (Xin et al., 2010; McNally et al., 2012). Spatial organization of mineral crystals as well as their relation to other bone constituents is poorly understood. Moreover, exact contribution of various features of bone mineral to the bone material behavior remains unknown.

Collagen is the main constituent of the organic phase (90%), type I being the most abundant collagen form in the bone tissue (Bonucci, 2000; Currey, 2002). Collagen is organized in fibrils that are reinforced by mineral crystals (Figure 1E, F); however, the precise relationship between these bone nano-constituents is not yet clear (Bonucci, 2000; Currey, 2002). Majority of authors reported that about 70% of bone mineral is located around or between collagen fibrils (so called: *interfibrillar* or *extrafibrillar* mineral) (Pidaparti et al., 1996; Sasaki et al., 2002; Currey, 2012; McNally et al., 2012), in contrast to *intrafibrillar* mineral positioned mainly within the gap zones of collagen fibrils. The remaining 10% of organic phase are non-collagenous proteins, such as Phosphophoryn, Dentin matrix protein 2, Osteopontin, Bone sialoprotein etc. Although their function is not yet well understood, they probably provide attachment to collagen fibrils, mineral crystals and cells, have a key role in mineralization process and



participate in “sacrificial bonds” phenomenon which is important for bone toughness (Bonucci, 2000; Currey, 2002; Fantner et al., 2005; Turner, 2009).

## **1.2. Age-related changes in bone mineral density and geometry**

For a long time, bone mineral density (BMD) assessed by dual energy X-ray absorptiometry (DXA) has been considered as the main predictor of bone strength and used in clinical settings as indicator of bone fragility and subsequent hip fracture risk (Genant et al., 1999). According to World Health Organization criteria from 1999, more than 2.5 standard deviations decrease in BMD defines osteoporosis and suggests an increased fracture risk (Genant et al., 1999). It is well known that there is an age-related decrease in BMD which explains significant part of the fracture risk (Melton et al., 1993) and is statistically related to bone strength (Marshall et al., 1996; Veenland et al., 1997).

However, the age-related decrease in BMD fails to sufficiently explain such a high increase in hip fracture risk with aging (De Laet et al., 1997; Schuit et al., 2004). Namely, as demonstrated in the Rotterdam study, a 13-fold increase in hip fracture risk between 60 and 80 years was accompanied by less than 2-fold decrease in BMD (De Laet et al., 1997). Furthermore, the overall proportion of fractures attributable to a low BMD was modest in a large cohort of US elderly women (Stone et al., 2003). In particular, there is a significant overlap in BMD values between the hip fracture patients and controls (Cummings, 1985), and therefore, it becomes clear that other bone features also account for age-related deterioration in bone strength.

In order to provide more data about the fracture risk in addition to BMD, it was demonstrated that femoral neck length and width, as well as femoral neck angle contribute to the risk of structural failure in the femoral neck (Nakamura et al., 1994; Michelotti and Clark, 1999). Moreover, in the quest for improving prediction of hip fracture risk, it became apparent that mechanical characteristics should be estimated to extend the information that can be obtained by DXA. Therefore, Beck and colleagues developed a HSA software (HSA: *hip structure analysis* or *hip strength analysis*) to extract mechanical information from DXA images, based on geometric indices of bone cross-sections estimating bone resistance to bending, buckling and compression (Beck et al., 1990; Beck et al., 2000; Beck et al., 2006; Beck, 2007). Despite evident

simplifications and several approximations, this method has shown useful given that various studies reported age-related decreases in bone resistance to bending (decreased section modulus), buckling (increased buckling ratio) and compression (decrease in cross-sectional bone area) (Kaptoge et al., 2003; Uusi-Rasi et al., 2005; Beck et al., 2006; Yates et al., 2007; Djonic et al., 2011), allowing better distinguishing between different groups than possible with considering BMD alone (Djonic et al., 2011).

### **1.3. Age-related changes in bone microarchitecture**

Further analyses focused on the cortical and trabecular bone microarchitecture that soon became a gold standard in research of morphological basis of bone strength (Brandi, 2009; Rizzoli, 2010). Bone microarchitecture has been already assessed in the femoral neck of individuals of different ages showing a clear age-related deterioration in majority of cortical and trabecular parameters (Lundeen et al., 2000; Cui et al., 2008; Chen et al., 2010; Djuric et al., 2010). Those studies have further improved our understanding of age effects, suggesting a microarchitectural basis of age-related bone fragility.

However, relatively few studies compared the hip fracture and control groups in terms of trabecular bone microarchitecture (Faccini et al., 1976; Evans et al., 1981; Lips et al., 1982; Uitewaal et al., 1987; Hordon and Peacock, 1990; Ciarelli et al., 2000). Majority of those studies actually used iliac crest microarchitecture as a surrogate for that of the femur, and therefore, their results are of limited relevance since iliac bone's structural and biomechanical contexts differ from the femur's (Ciarelli et al., 2000). The exception is the study by Ciarelli et al. where trabeculae were directly assessed in the femur; however, while analyzing the femoral head which is not the site of frequent hip fractures in the elderly, the subregions of the femoral neck were not considered in that study (Ciarelli et al., 2000). In contrast to the cortical bone, no studies have directly compared the trabecular bone microarchitecture in the femoral neck of hip fracture patients *vs.* controls. Particularly, in view of recent data emphasizing regional differences in trabecular microstructure within the femoral neck due to differential stress and strain distribution in the subregions of the femoral neck during gait and falls (Verhulp et al., 2008), it is essential to determine separately the microarchitecture in two biomechanically and clinically relevant subregions of the femoral neck: the

superolateral neck – where the fracture usually starts (Bakker et al., 2009), and the inferomedial neck – which is more stable in aging (Djuric et al., 2010).

#### **1.4. Investigation of nanostructural bone properties**

Modern concept takes that bone fragility is dependent not only on bone macro- and microstructural features, but also on its nanostructure (Seeman, 2008). In recent years, there has been an increasing interest in exploring nanostructural characteristics of bone material. Some of age-induced changes in bone nanostructure and composition were revealed applying different methods for assessment of bone characteristics at nano-level, such as scanning electron microscopy (Green et al., 1985; Mackie et al., 1989a; Mackie et al., 1989b), backscattered electron microscopy (Roschger et al., 2008; Fratzl-Zelman et al., 2009; Fratzl-Zelman et al., 2011) and Raman spectroscopy (McCreadie et al., 2006; Yerramshetty et al., 2006; Yerramshetty and Akkus, 2008).

Since the bone at the matrix level may be viewed as a nano-composite material consisting of mineral grains and an organic phase, atomic force microscopy (AFM) which represents a powerful tool for characterization of nanomaterials has recently been applied to bones (Hassenkam et al., 2004; Thurner, 2009). AFM allows great spatial resolution without the need of excessive sample preparation. It uses an ultra sharp mechanical probe to “feel” the investigated surface, which allows three-dimensional surface imaging as well as distinguishing between different material properties of the surface (Jandt, 2001). One of the most important advantages of AFM is possibility to perform mechanical characterization of materials in addition to imaging (AFM nanoindentation method) (Thurner, 2009).

##### ***1.4.1. Morphological analysis using atomic force microscopy (AFM)***

Previous AFM studies were mainly qualitative, and tried to improve the knowledge on bone ultrastructure. Applying AFM on bovine trabecular bone from vertebrae, Kindt et al. showed that interfibrillar mineral crystals are not of uniform size and shape in the same bone (Kindt et al., 2005). Analysis of outer surface of human trabecular bone showed mainly bare collagen fibrils showing the characteristic 67 nm D-banding pattern (Fantner et al., 2006), while fracture surface of bovine trabecula showed mineralized collagen fibrils. The mineralized fibrils detected on fracture surfaces led to the

assumption that the mineral-mineral interface is the weakest link in bone and that fracture mainly develops in this zone (Fantner et al., 2006). AFM studies elegantly showed bovine collagen fibrils after removing the mineral particles using EDTA or NaF (Sasaki et al., 2002; Kindt et al., 2007; Thurner et al., 2007), similar like on elephant dentine after etching with  $H_3PO_4$  (Bozec et al., 2005). Conversely, collagenase treatment allowed better visualization of minerals in bovine cortical bone (Sasaki et al., 2002). Based on AFM analyses combined with alternative EDTA and collagenase chemical treatment, Sasaki et al. concluded that even 77% of bone mineral is extrafibrillar, while the rest is placed inside collagen fibrils (Sasaki et al., 2002). In addition to bone ultrastructure, AFM was applied to analyze the imprints of bone remodeling by visualizing resorptive lacunae in trabeculae in an excellent manner (Bozec et al., 2005; Hassenkam et al., 2006) or to explore structure of cortical bone lacuno-canalicular network (Reilly et al., 2001; Lin and Xu, 2011).

However, the previous AFM studies were only qualitative, and so far none of them has evaluated age-related differences at human bone matrix level. In particular, the effects of aging process on the femoral neck in terms of matrix nanostructure and mineral composition have been completely obscure, and it is unknown how nanostructural features of the mineralized matrix contribute to age-related bone fragility.

#### ***1.4.2. Mechanical characterization of bone mineralized matrix (determination of elasticity and hardness at the nano-level)***

Frequently researchers assessed bone mechanical properties, usually at the macro-level - representing mechanical behavior of the whole bone, or at micro-level - when trabecular bone cubes are analyzed (Njeh et al., 2004). Macro- and micro-mechanical properties depend not only on the bone material, but also on bone geometry, force directions, size, shape, micro-architecture (Njeh et al., 2004). It is, therefore, extremely difficult to link individual morphological or compositional features to particular mechanical properties. In contrast, nano-mechanical tests (*e.g.*, on a single trabecula) are capable of assessing mechanical behavior of the very bone material, quite independent on macro- and microstructural characteristics of bone (Rho and Pharr, 1999b). AFM provides opportunity to assess material's nanohardness (defined as resistance to penetration or

indentation by other solid) as well as its elastic modulus (Rho and Pharr, 1999b; Njeh et al., 2004). Bone nanohardness and elastic modulus obtained from AFM nanoindentation testing represent true material properties. Nanoindentation measures mechanical properties which depend on a combination of ultrastructural factors and not only on amount of mineral, and can be used to probe a surface and map its properties on a “spatially-resolved basis” (Rho and Pharr, 1999b; Njeh et al., 2004).

Previous nanoindentation studies focused mainly on comparing mechanical characteristics of various bone microstructural features within individual (Rho et al., 1997; Rho and Pharr, 1999a; Rho et al., 1999a; Rho et al., 1999b; Zysset et al., 1999; Hengsberger et al., 2001; Hengsberger et al., 2002; Hoffler et al., 2005). For instance, Hengsberger et al. showed differences in elastic characteristics of thick *vs.* thin osteonal lamellae of the human cortex in comparison with the trabeculae under dry and physiological conditions (Hengsberger et al., 2001; Hengsberger et al., 2002). Rho et al. reported variability of elastic properties when comparing interstitial and osteonal cortical bone from the tibia with trabecular bone from the vertebrae in an elderly person in two loading directions (Rho et al., 1999a), and compared osteonal lamellae from the center of the osteon and those on the periphery in middle-aged men (Rho et al., 1999b). Spatial heterogeneity of bone stiffness was assessed by Tai et al. (Tai et al., 2007) and Norman et al. (Norman et al., 2008a), while heterogeneity between different anatomical locations was studied by Hoffler et al. (Hoffler et al., 2000a). Several studies analyzed bone mechanical properties in individuals with a particular bone disease: in osteoporotic hip fracture (Fratzl-Zelman et al., 2009) and in osteogenesis imperfecta (Fan et al., 2006; Fan et al., 2007). Rho et al. noticed visual but not statistical differences in stiffness across age in human femoral cortex at the mid-diaphysis in men of various age (35-95 years) (Rho et al., 2002).

However, the studies dealing with humans of various ages are extremely scarce (Zysset et al., 1999; Hoffler et al., 2000b), and influence of aging on mechanical properties of the bone material remains obscure. Hence, further assessment of nano-level mechanical behavior (combined with nanostructural evaluation) of the bone matrix in individuals of different age may be essential to achieve a more profound understanding of particular mechanical consequences of bone matrix aging, separately from age-related effects at other hierarchical levels of bone structure.

## 2. RESEARCH HYPOTHESES AND GOALS

Our research hypothesis was that:

- a) region-dependant worsening of bone microarchitecture in elderly women leads to increased femoral neck fragility,
- b) besides the microarchitectural deterioration, age-related nanostructural changes at the bone matrix level contribute to increased bone fragility in elderly women.

In order to investigate the relationship between bone structural characteristics and mechanical resistance, the specific aims of our research were:

1. to assess the microstructural basis of the femoral neck fragility by analyzing trabecular bone microarchitecture in elderly women with hip fracture *vs.* women without hip fracture,
2. to assess how trabecular microarchitecture in elderly women with hip fracture *vs.* women without hip fracture varies between two biomechanically relevant subregions of the femoral neck (superolateral *vs.* inferomedial neck),
3. to analyze cortical microarchitecture in elderly women with hip fracture *vs.* women without hip fracture,
4. to analyze nanostructure of the mineralized bone matrix from the femoral neck cortex and trabeculae in young *vs.* elderly women using AFM,
5. to assess bone nanostructure by AFM in the femoral neck of elderly women without fracture *vs.* women who sustained hip fracture,
6. to analyze bone mineral composition of the trabecular and cortical bone of the femoral neck in young *vs.* elderly women via quantitative chemical methods,
7. to analyze bone mineral composition of the femoral neck in elderly women with hip fracture *vs.* age-matched controls by using quantitative chemical methods,
8. to perform nano-scale mechanical characterization of the bone matrix from the femoral neck of young *vs.* elderly women,
9. to perform nano/micro-scale mechanical characterization of the bone material from the femoral neck of elderly women without fracture *vs.* women who sustained hip fracture,
10. to address the relative contributions of particular morphological features at various hierarchical levels to overall bone fragility.

### **3. MATERIAL AND METHODS**

#### **3.1. Study sample**

The study sample comprised two groups of Caucasian female postmortem human subjects (n=35): women without hip fracture (young: aged 20-40 yrs., n=5; and elderly: aged 60-95 yrs., n=15), and postmenopausal women with a hip fracture (age: 60-95 yrs., n=15). The bone specimens originating from the femoral neck region were collected at autopsy at Institute of Forensic Medicine, School of Medicine, University of Belgrade, Belgrade. The inclusion criteria for this study were: female sex, defined age (young: 20-40 yrs., elderly: 60-95 yrs.), sudden or traumatic injuries as a cause of death. Exclusion criteria included: history of musculoskeletal diseases affecting the femur (except hip fractures in the fracture group), macroscopic and/or radiological signs of bone pathological changes, endocrine or metabolic diseases that affect the skeleton, and use of medications known to interfere significantly with bone metabolism (*e.g.*, anticonvulsants, corticosteroids, and hormonal therapy). Ethics approval was granted by the Ethics Committee of the School of Medicine, University of Belgrade, Belgrade.

#### **3.2. Assessment of bone microarchitecture**

##### ***3.2.1. Sample characteristics***

The sample set for microarchitectural analyses consisted of two groups of postmenopausal women: 15 individuals with hip fracture (fracture group: mean age 79.5 yrs., SD 8.5 yrs.), and 14 women without hip fractures (control, *i.e.*, non-fracture group: mean age 74.1 yrs., SD 9.3 yrs.). To avoid influence of confounding factors, the fracture group and the control group were not statistically different in age, body height and weight (t-test:  $p > 0.05$ ). All individuals included in the study were devoid of the signs of bone pathology, and had no history of skeletal pathology (apart from the fractures in the fracture group). In the donors who sustained hip fracture, the contralateral femur was taken in order to allow for scanning the femoral neck subregions in a consistent and precise manner. Contralateral femur has been considered appropriate for analysis given that the left and right sides do not differ significantly in densitometric parameters (Bonnick et al., 1996; Rao et al., 2000; Dane et al., 2001; Pierre et al., 2010) and no significant inter-side differences were found for any of the trabecular or cortical microarchitectural parameters in previous studies (Chappard et al., 2008).

### **3.2.2. Preparation of specimens**

After at least 2 weeks of storage in 70% ethyl alcohol, the proximal femora were cleaned of adherent soft tissue. The bone section in the middle of the femoral neck was excised using a water-cooled diamond saw (Exakt, Germany) (Figure 2).

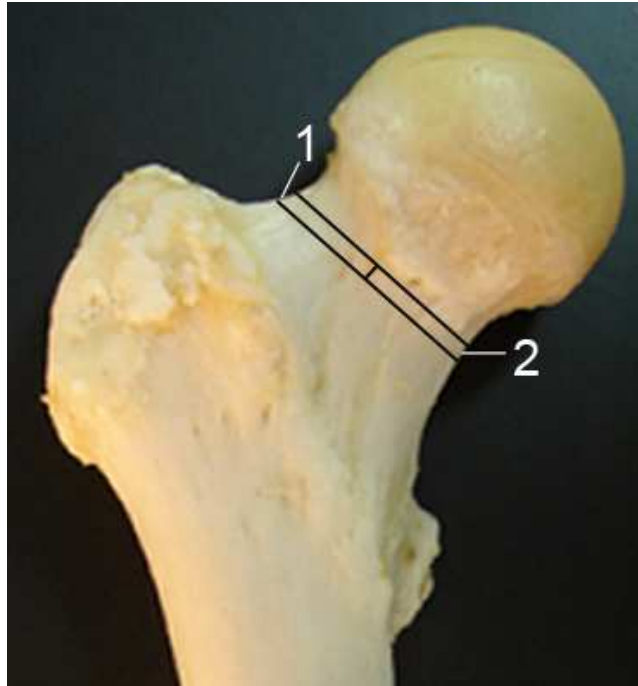


**Figure 2.** The regions of interest within the proximal femur. The femoral neck, a frequent fracture site in the elderly, is marked with a rectangle and its subregions with (1) the superolateral neck and (2) the inferomedial neck.

### **3.2.3. Micro-CT scanning procedure**

#### **3.2.3.1. Trabecular bone**

Each bone specimen was attached to a sample holder with a consistent proximal-distal orientation, and then the trabecular bone of the whole femoral neck section was scanned using micro-computed tomography (Scanco Medical  $\mu$ CT 40, Switzerland) in dry conditions. Micro-CT imaging was performed at Department of Osteology & Biomechanics, University Medical Center Hamburg-Eppendorf, Hamburg, Germany. The specimens were foam padded to avoid any movement artifacts during scanning. The scanning was operated at 55 kVp, 144  $\mu$ A, with nominal resolution of 36  $\mu$ m, isotropic, 1024 x 1024 pixels per slice. The integration time per projection was 300 ms.



### **3.2.3.2. Cortical bone**

Cortical bone specimens originating from the superolateral femoral neck region of five fracture cases and four age-matched controls were placed into a sample holder and foam padded to prevent any artifacts due to movements during the scanning procedure. For reliable evaluation of the cortical microarchitecture, the scanning was performed at a higher resolution (10  $\mu\text{m}$ , 2048 x 2048 pixels per slice) using Scanco Medical  $\mu\text{CT}$  40 (Switzerland) at 55 kVp, 144  $\mu\text{A}$  and integration time of 200 ms.

### **3.2.4. Micro-CT evaluation procedure**

Segmentation procedure comprised manual marking of the contours of the region of interest (ROI) on various slices, and using Morph function of the micro-CT program to interpolate contours to a stack of all slices – thus producing the volume of interest (VOI). Afterwards, the segmentation parameters were set (lower threshold 220, Gaus: sigma 0.8 and support 1.0) and bone microarchitecture was evaluated automatically using micro-CT evaluation program V6.5-1 with direct 3D bone morphometry.

The following trabecular microarchitectural parameters were determined: bone volume fraction (BV/TV, %), connectivity density (Conn.D,  $1/\text{mm}^3$ ), structure model index (SMI, dimensionless), trabecular number (Tb.N,  $1/\text{mm}$ ), trabecular thickness (Tb.Th, mm), trabecular separation (Tb.Sp, mm), and degree of anisotropy (DA, dimensionless). Bone volume fraction is the ratio between the mineralized bone tissue area and total area of the VOI, and most closely reflects the amount of bone, *i.e.*, “bone quantity” (Djuric et al., 2010). While trabecular number and thickness, as well as separation between trabeculae are also quite straightforward parameters related to “bone quantity”, other parameters that describe 3D arrangement of trabeculae need short explanation. Connectivity density is a nice quantitative measure of connectivity between trabeculae, and it is considered to be a sensitive feature of bone aging (Djuric et al., 2010). Structure model index is a dimensionless number used to describe overall shape of trabeculae; in trabecular bone it usually takes values between 0 (plate-like trabeculae) and 3 (rod-like trabeculae) (Hildebrand and Rüegsgiger, 1997). Degree of anisotropy depicts whether there is a preferred orientation of trabeculae in a particular direction (higher DA = higher anisotropy) or if their spatial organization is isotropic, *i.e.*, equally oriented in all directions (lower DA = lower anisotropy) (Ciarelli et al., 2000;

Homminga et al., 2002; Djuric et al., 2010). After analyzing the whole neck slice, we further evaluated its superolateral and inferomedial halves separately (Figure 2) in order to assess the region-specific pattern of trabecular microarchitecture.

For the cortical bone, the following microarchitectural parameters were determined: bone volume fraction (BV/TV, %), cortical porosity (Ct.Po, %) which is calculated as  $100\% - \text{BV/TV}$ , and cortical pore diameter (Po.Dm, mm), as well as apparent density of bone tissue (T.Dn, mg HA/cm<sup>3</sup>).

### **3.3. Assessment of bone nanostructure**

#### ***3.3.1. Specimen selection and preparation***

The bone samples from proximal femora of five younger women (age:  $31.6 \pm 5.5$  years) and five elderly women (age:  $82.2 \pm 8.5$  years) without diseases affecting the skeleton, as well as five aged women who sustained hip fracture (age:  $82 \pm 4.6$  years) were considered in the evaluation of bone nanostructure using AFM.

After storage in 70% ethanol for a minimum of 2 weeks, bones were cleaned of adherent soft tissue. After excising the femoral neck region (Figure 3A, B), a low-speed diamond wheel saw 650 (South Bay Technology Inc., USA) or SYJ-160 (MTI Corp., USA) with water soluble coolant and 0.3 mm thick diamond wheel was used to make bone sections in the lateral (*i.e.*, superolateral) region of the femoral neck, providing trabecular bone samples of approximately 5 mm x 5 mm x 1 mm each (Figure 3B, 3C), as well as corresponding cortical bone samples (Figure 3B, Figure 4). The specimens were afterwards ultrasonically cleaned in alcohol for 5 minutes to remove sectioning debris, and dried naturally at room temperature. All the specimens were prepared in the same manner in order to ensure validity of inter-specimen comparisons.

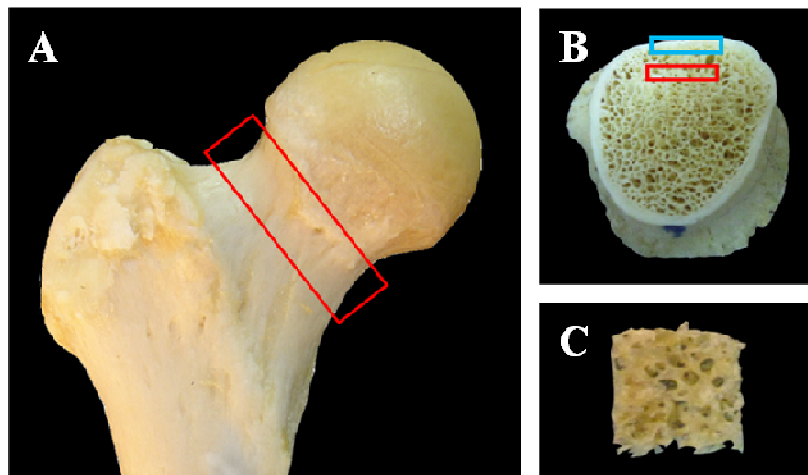


**Figure 3.** Bone specimens used for analysis of bone nanostructure: (A) Proximal femur (the red rectangle shows the neck region); (B) Excised femoral neck (the red and blue rectangle in the superolateral femoral neck depict the site from which the trabecular and cortical bone samples were taken, respectively); (C) A representative trabecular bone specimen used for AFM and chemical analyses (~5 mm x 5 mm x 1 mm).

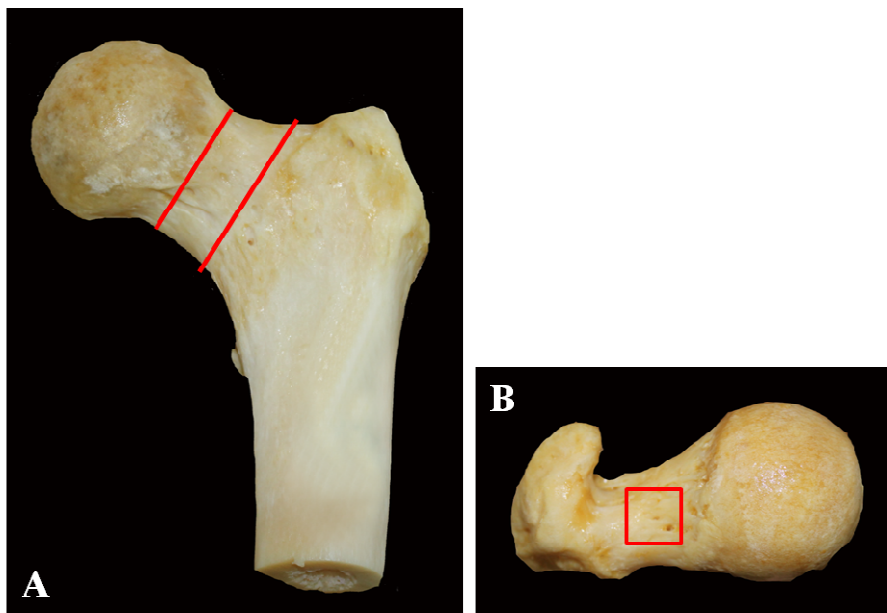


**Figure 4.** Cortical bone specimens used for analysis of bone nanostructure: (A) The proximal femur – anterior aspect (the red lines delineate the femoral neck); (B) The proximal femur – superior aspect. The red rectangle in the superolateral femoral neck depicts the site from which the cortical bone sample was taken and the surface (external cortical s. periosteal surface) that was subject to nanostructural analyses.

### 3.3.2. Atomic force microscopy

#### 3.3.2.1. Basic characteristics of AFM

Atomic force microscopy is a potent technique for nano-research, providing excellent imaging resolution without need of excessive sample preparation, dying and coating. It belongs to a family of scanning probe microscopies (SPM) developed by Binnig and co-workers (Binnig et al., 1986). In contrast to light microscopy and electron microscopes that use light or electron beams and system of lenses for obtaining the picture of the specimen, the AFM uses a sharp mechanical probe (Figure 5) which “feels” the investigated surface by coming in close “touch” with the surface and thus being able to provide an image of the 3D surface topography. AFM probe is basically a “nano-finger” which “touches” the investigated surface in a “gentle” and controlled way. It consists of a cantilever with a specific mechanical compliance (spring constant, *e.g.*: 40 N/m) which holds near its end an ultra-sharp tip with a radius of typically less than 10 nm (Figure 5). The tip is usually made of silicium nitride and represents the part of the probe that comes into a contact with the sample surface.

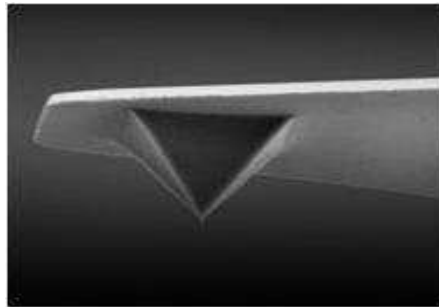


**Figure 5.** An AFM probe showing cantilever and a pyramidal ultra-sharp tip.

During scanning, the probe and the sample are moved relative to each other in a well defined and controlled manner (scan size, scan speed) line by line within *X-Y* plane (*raster scanning*) which is possible owing to microscope’s piezoceramic. Along each scanning line, the relative position of the probe is recorded, thus revealing *Z*-scale information that is directly dependant on the surface topography of the sample (Binnig et al., 1986; Jandt, 2001; Thurner, 2009).

The remaining parts of AFM actually measure and control the “tactile interaction” between the probe and the sample surface. Deflection of the cantilever is

detected using a laser beam that is focused onto the rear of the cantilever and reflects onto a special position-sensitive photodetector, and the signal is converted to the image and shown on the screen (Jandt, 2001).

While there are different operating regimes of AFM, it is mostly performed in “tapping mode” in which the tip oscillates over the sample surface near the resonant frequency, and contacts (lightly taps) the surface only intermittently. This mode allows good image resolution without damaging the surface (Jandt, 2001). The schematic explanation of AFM principle is shown in Figure 6. Briefly, as the AFM tip taps the scanned surface, it loses a part of the energy, which leads to a decrease in amplitude of its oscillation (Jandt, 2001). This amplitude is maintained constant via the system’s feedback loop by adjusting Z-position of the cantilever, while the photodetector records the position of the cantilever during its contact with the surface, thus visualizing three-dimensional surface topography of the analyzed specimen.

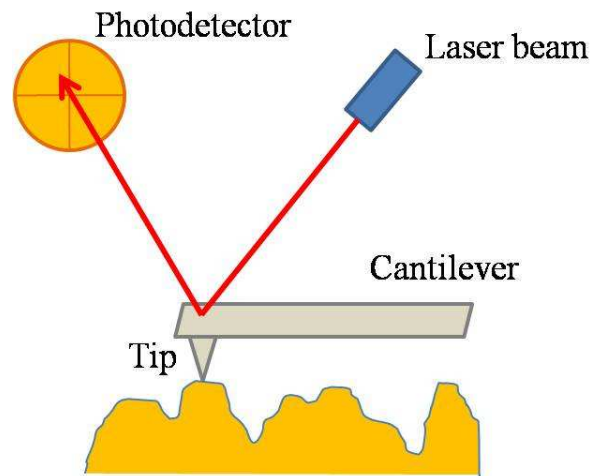


**Figure 6.** Basic operation principle of the tapping mode AFM (a simplified sketch). The cantilever with a pyramidal tip taps the surface of the specimen along X-axis (scan line). The vertical deflection of the cantilever (Z-axis) is related to the topography of the specimen. The position of the cantilever is detected by means of a laser beam that hits the rear of the cantilever and reflects onto the photodetector which records the vertical displacement (position) of the cantilever along a scan line. A series of parallel scan lines in X-Y plane (usually 256 lines per scan) gives information of the total scanned area. The position of the cantilever at each point is given a particular nuance of colour on the screen, reflecting Z-scale information, i.e., the topography of the specimen.

### ***3.3.2.2. AFM imaging of bone specimens***

Each bone sample was placed horizontally and glued on the sample disk, and imaged by Multimode quadrex SPM with Nanoscope IIIe controller (Veeco Instruments, Inc.) under ambient conditions. The topography and phase images were acquired simultaneously by standard AFM tapping mode using a commercial Solid Nitride Cone (SNC) AFM probe (NanoScience Instruments, Inc.) with cantilever length of 125  $\mu\text{m}$ , force constant 40 N/m, resonant frequency 275 kHz and the tip radius lower than 10 nm. Images were recorded with 256 lines per scan. While Height image displays topography of the sample, the Phase image reflects specific material properties of the sample (Bar et al., 1999; Jandt, 2001; García et al., 2007; Nenadović et al., 2012). Namely, the Phase mod is based on measuring the phase shift of the cantilever, which is directly related to local change in the energy dissipated in the sample during the tip-sample interaction (Anczykowski et al., 1999; García et al., 2007; Strbac et al., 2010). Simultaneous acquisition of Height and Phase images allows matching between the topographical elements and the material properties, distinguishing between materials of different mechanical properties, enhancing image contrast and improving detection of edges (Jandt, 2001).

In each sample, a minimum of 10 typical images were obtained from various locations, to assure representativeness of the observed features. The size of mineral crystals (grains) was recorded on AFM images by measuring maximum dimension of the grain, using Veeco Nanoscope III software version 5.31r1. Origin Lab (version 8) was applied for data analysis and curve fitting. The surface roughness was estimated from topography images using the subprogram packages of the Veeco NanoScope III. Surface roughness normally increases with increasing scan area but only up to a certain “saturation” value. This value (saturation roughness) was determined in trabecular bone specimens.

### **3.3.2.3. AFM imaging. Determination of advanced nanostructural descriptors: Power spectral density (PSD) and fractal dimension (FD)**

Power spectral density (PSD) analysis was performed on AFM topography images using the software WSxM (WSxM v5.0, developed by Horcas et al. (Horcas et al., 2007)). Power spectral density represents an advanced analysis of the surface roughness (Figure 7) based on Fourier decomposition of an image into the waves of particular wavelengths or frequencies (spatial frequencies) (Mitchell and Bonnell, 1990; Lita and Sanchez, 2000; Nenadović et al., 2012). Briefly, in the case of AFM topography data, PSD analysis deconvolutes the roughness as a function of unit length of the surface (Nenadović et al., 2012). Moreover, PSD analysis specifically correlates the vertical amplitude with the spatial frequency of surface features, revealing characteristics of the surface structure (Mitchell and Bonnell, 1990; Lita and Sanchez, 2000; Nenadović et al., 2012) and describing the contribution of various elements (features) to the surface roughness (Nenadović et al., 2012). Mathematical evaluation of the PSD function is complex and complete mathematical explanation can be found in other studies (Fang et al., 1997; Kitching et al., 1999). We used graphical presentation showing PSD [ $\text{nm}^4$ ] on the logarithmic scale on the *Y*-axis, while the *X*-axis is represented by the spatial frequency [ $1/\text{nm}$ ] and is also shown on a logarithmic scale.

In order to account for the contribution of features of various sizes to the bone surface, the power spectrum density data were extracted from the images of various sizes (from a minimum scan size of  $0.5 \times 0.5 \mu\text{m}^2$  to a maximum of  $5 \times 5 \mu\text{m}^2$ ). The data points collected from all images belonging to an individual were then plotted on a single graph showing *log* PSD vs. *log* spatial frequency of each individual. The data points were fitted linearly as previously suggested (Ulmeanu et al., 2000; Nenadović et al., 2012), and the slope of the obtained line was determined for each individual. The slope of PSD trendline was determined in this study since it has been used successfully for illustrating differences in spatial frequency distribution relatively independently on the area (Jiang et al., 2005).

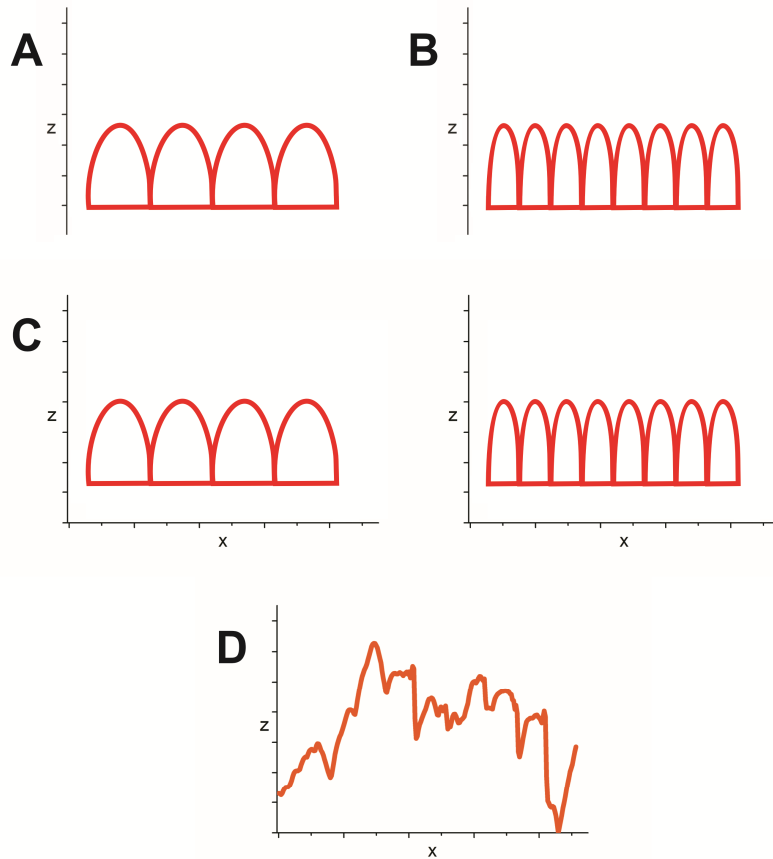


**Figure 7.** Roughness analysis. (A, B) Examples of ideally regular surface profiles showing “peaks and valleys” (2D profiles are shown for simplicity): Measures of roughness only consider the vertical (Z-axis) deviation from the mean surface, and therefore they cannot distinguish between A and B profiles which display the same roughness. However, the profiles A and B actually differ considerably, since B has more peaks and those peaks are narrower. (C) In contrast, PSD analysis considers not only vertical deviation, but also the width (X-axis values) of surface peaks (~wavelength), i.e., their number per unit length (spatial frequency = inverse wavelength). (D) A real example of a complex profile of bone surface. PSD is based on Fourier transformations which decompose the complicated wave to a number of ideal waves of particular wavelengths. For characterization of any surface, it is useful to know the vertical deviation of the peaks from the mean surface, but also the size (width) of those elements (peaks), as well as their relative contribution (power) to overall surface topography (see also the Results section).



Fractal dimension (FD) is a dimensionless number that describes the complexity of an object's structure (Dougherty and Henebry, 2001) and strongly corresponds to visual perception of roughness (Zawada and Brock, 2009). It depicts how an object occupies space (Ulmeanu et al., 2000), so that more plane surfaces have FD closer to 2, while FD of more complex or craggy surfaces approaches the value of 3 (Zawada and Brock, 2009). Moreover, fractal dimension measures the relative importance of high frequency fluctuations in surface patterns in comparison with low frequency fluctuations (Constantoudis and Gogolides, 2008). *Log* PSD vs. *log* spatial frequency graphs provide the ability to calculate the fractal dimension of each sample according to the following equation:

$$FD=0.5*(7-\beta),$$

where  $\beta$  represents the absolute value of the slope of PSD trendline (Pfeifer, 1984; Silk et al., 1998).

### **3.4. Quantitative chemical analyses**

#### ***3.4.1. Evaluation of bone matrix composition via destructive analytical approach***

##### ***3.4.1.1. Specimen preparation***

Trabecular and cortical bone specimens from individuals chosen for nanostructural analyses were powdered using electric grinder to micron sized particles (as proved using AFM). Subsequently, they were dried for 2 hours at 105° C. Then, 250 mg of powdered samples were weighted accurately into the teflon crucible. Hydrofluoric acid in combination with perchloric and nitric acid were used for sample dissolution. The solutions were evaporated to incipient dryness, preferably after warming the mixture at lower temperature for several hours, to remove the excess HF. When cool, a mixture of nitric and hydrochloric acid was added, and warmed to dissolve salts. Amonium acetate was added to dissolve lead chloride when it was formed. After cooling the solution was diluted to 100 ml with distilled water and stored in polythene bottles.

#### **3.4.1.2. Inductively coupled plasma optical emission spectroscopy (ICP-OES)**

An ICP-OES spectrometer (Spectroflame, Spectro Analytical Instrument, Germany), operating at 27.12 MHz and 2.5 kW was used to obtain the element content of the specimens, at Department of Physical Chemistry, Institute of Nuclear Sciences Vinca, Belgrade. This instrument is equipped with four polychromators for simultaneous determination of 30 elements and one monochromator for sequential analysis.

With the *SmartAnalyzer* software v. 2.20, it is possible to conduct and store scans of defined lines during quantitative measurements. The spectral lines for all elements were carefully selected to avoid possible interferences problems. After successfully completing reprofiling of the optics, at least 30 minutes after ignition of the plasma the measurements were performed. The user-friendly *Quick Quant procedure* has been used to compare the intensities for measured elements in a specimen with the intensities measured for standards with known concentrations. Calibration curves were calculated and the concentrations for the measured elements in the unknown sample were determined. The calibration standards were prepared in appropriate concentration range from elemental stock solutions. Matrix matched calibration standards were used. Peak identification, background subtraction and smoothing were performed prior to calculations of concentrations.

#### **3.4.1.3. Direct current argon arc plasma optical emission spectrometry (DCA ARC)**

The measurements were carried out on a U-shaped DC argon arc stabilized by combined gas and wall stabilization. Analyte solution containing different amounts of KCl (from 0 to 2%) were nebulized with a glass concentric nebulizer and introduced into the plasma tangentially to the arc axis. The horizontal part of the arc column with its axis parallel to the optical axis was focused on the entrance slit of a monochromator with photoelectric detection. Radial distribution measurements were performed by moving the arc device perpendicular to the optical axis of the monochromator. Square current modulation was realized using an electronic fast switch circuit. The current transition time (between 6 and 3 A) was a few microseconds, which was accomplished by careful optimization of the electric circuit, *i.e.*, by minimizing the reactive resistance of the circuit. The low current period lasted 5 ms with a repetition period of 25 ms. The

temporal responses were acquired using a digital storage oscilloscope controlled by a PC computer.

### ***3.4.2. Evaluation of bone matrix composition using non-destructive analytical approach***

#### ***3.4.2.1. Energy dispersive X-ray spectroscopy (EDX)***

Bone specimens were embedded in epoxy resins and, in order to provide a flat surface appropriate for EDX analysis, the specimens were finely polished using 4000 grit on Unipol 810 semiautomatic polishing machine (MTI Corporation, USA) under constant water irrigation. The specimens were then ultrasonicated for 5 minutes and left to dry naturally. The surface of specimens was coated with carbon and mounted in the scanning electron microscope (LEO 435 VP; LEO Electron Microscopy Ltd., Cambridge, England) operated at 20 kV and 1 nA at a constant working distance of 24 mm, in accordance with previous studies (Busse et al., 2010a). The spectra based on characteristic X-rays of different elements within the bone material were acquired using Energy Dispersive X-ray analysis (EDAX, DX-4, Mahwah, NJ) integrated with SEM. Elemental peaks reflecting the content of calcium (Ca) and phosphorus (P) in weight percent (Wt-%) were evaluated using EDX-ZAF software provided by the manufacturer (EDAX, DX-4, Mahwah, NJ), and calcium-to-phosphorus ratio - an estimate of the mineral composition of the bone material - was determined.

#### ***3.4.2.2. Bone mineral density distribution analysis (BMDD) using quantitative backscatter electron imaging (qBEI)***

The specimens were polished to achieve smooth coplanar surfaces using automatic precision grinding system under constant water irrigation (Exakt, Germany). Subsequently, they were carbon coated and mounted on the scanning electron microscope (LEO 435 VP, Cambridge, England) with a backscattered electron detector (Type 202, K.E. Developments Ltd., Cambridge, England) at Institute of Osteology and Biomechanics, University Medical Center Hamburg-Eppendorf, Hamburg, Germany. The imaging was operated in backscatter mode at 20 keV and 680 pA with a constant working distance of 20 mm. The beam current was controlled by use of a Faraday cup (MAC Consultants Ltd, England). Quantitative backscatter electron imaging (qBEI) was

performed to evaluate bone mineral density distribution (BMDD) in accordance with the application in previous studies (Roschger et al., 1998; Roschger et al., 2008; Busse et al., 2009; Regelsberger et al., 2012; Koehne et al., 2013). Briefly, to allow reliable inter-specimen comparisons all parameters were maintained stable during imaging and the gray levels were controlled using calibration standard with carbon (gray level:  $5 \pm 1$ ) and aluminum (gray level:  $222.4 \pm 1$ ). The relationship between gray levels and calcium concentration was evaluated based on the work of Roschger et al. (Roschger et al., 1998). Namely, a highly linear relationship ( $r = 0.98$ ) between the gray values of the backscattered signal intensities and the calcium content (Ca-Wt%) was reported previously by Roschger et al. (Roschger et al., 1998). The generated gray values represent the calcium content (Ca-Wt%) in each pixel. Evaluation of bone mineral density distribution based on gray level images of cortical specimens was performed using a custom routine in MatLab software (MathWorks, USA).

The following parameters were evaluated: mean calcium content (mean Ca, wt%), the most frequent calcium concentration within the scanned area (peak Ca, wt%), width of calcium content determined as FWHM (width at half-maximum of the curve) showing the homogeneity/heterogeneity of BMDD distribution (width Ca, wt%), percentage of low mineralized bone which denotes the bone area that is mineralized below the 5<sup>th</sup> percentile of the reference range of the control group (Ca low, % bone area) and percentage of high mineralized bone expressed as bone area containing Ca concentration above the 95<sup>th</sup> percentile of the reference range of the control group (Ca high, % bone area).

In addition, the osteocyte lacunar network was evaluated in recorded backscattered electron images. The number of osteocyte lacunae per bone area (N.Ot.Lc/B.Ar, #/mm<sup>2</sup>) was evaluated in accordance with previous studies (Busse et al., 2010a) and the current nomenclature guidelines of American Society for Bone and Mineral Research (ASBMR) (Dempster et al., 2013). All lacunae were counted manually while the reference bone area was determined using an image analysis software (ImageJ, 1.46q, National Institutes of Health, USA).

### 3.5. Assessment of bone nanomechanical properties

#### 3.5.1. Nanoindentation

##### 3.5.1.1. Characteristics and preparation of the specimens

The bone samples that were subject to testing nanomechanical properties derived from the femoral neck region of eight skeletal healthy women (five young:  $31.6 \pm 5.5$  years old, and three elderly:  $87.7 \pm 5.7$  years old).

The femoral samples were stored in ethanol, cleaned of adherent soft tissue and cut using a water-cooled diamond saw (Exakt, Germany) to detach the femoral neck region (Figure 8A, B). A low-speed diamond wheel saw 650 with water soluble coolant (South Bay Technology Inc., USA) was used to excise longitudinal trabecular bone specimens by cutting parallel to the femoral neck axis in the superolateral region of the femoral neck (Figure 8C-F).

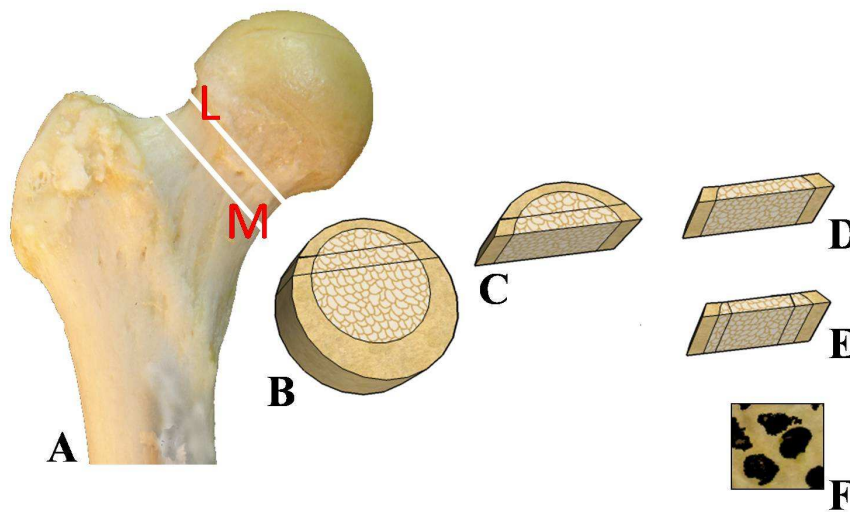


**Figure 8.** Schematic representation of the trabecular bone specimens' acquisition for nanoindentation measurements. (A) The proximal part of a human femur: the demarcated region shows the femoral neck region (L – superolateral neck, M – inferomedial neck); (B) Excised femoral neck: the cutting plane parallel to the femoral neck axis relieves the superolateral portion of the neck; (C-F) Excising the trabecular bone sample from the superolateral neck region.

The trabecular bone specimens were later embedded in epoxy resins under vacuum, and polished carefully using carbide papers of increasing smoothness (from 1200 up to 4000 grit) under constant water irrigation on Unipol 810 polishing machine (MTI Corporation, USA). Afterwards, the polished specimens were cleaned ultrasonically in alcohol for 5 minutes to remove any dirt, debris or particles resulting from the polishing procedure. The specimens were then allowed to dry naturally at room temperature at least 24 hours before nanoindentation tests. Every effort was made to prepare all the specimens in the same manner in order to secure the validity of inter-specimen comparisons.

### **3.5.1.2. AFM imaging**

Prior to embedding, each trabecular bone sample (after 5 minutes' washing in ultrasonic bath, and natural drying) was placed horizontally onto the sample disk, and imaged by Multimode quadrex SPM with Nanoscope IIIe controller (Veeco Instruments, Inc.) under ambient conditions in standard AFM tapping mode using a commercial Solid Nitride Cone (SNC) AFM probe (NanoScience Instruments, Inc.) (cantilever length 125  $\mu\text{m}$ , force constant 40 N/m, resonant frequency 275 kHz, the tip radius lower than 10 nm).

### **3.5.1.3. AFM nanoindentation**

#### **3.5.1.3.1. Principle of nanoindentation**

Nanoindentation method is based on penetration of a diamond tip (*i.e.*, *indenter*) of known proportion and geometry into the investigated surface at accurately defined loading force. In a typical indentation cycle, load is applied to the indenter that is in contact with the surface of the specimen. The load and depth of penetration (*i.e.*, load-displacement or force-penetration curve) are recorded as the load (force) is increased steadily up to a pre-defined maximum value while making an indentation on the surface (*loading phase*) and then decreased from maximum load back to zero while the tip is removed from the surface (*unloading phase*) (Figure 9). There are different variants of nanoindentation tests (quasi-static and dynamic), but Oliver-Pharr method is most commonly used in both material science and in the bone field (Oliver and Pharr, 1992). The detailed mathematical description of Oliver-Pharr's method is available in their

original publication (Oliver and Pharr, 1992) as well as in other studies (Rho and Pharr, 1999b; Rho and Pharr, 1999a; Rho et al., 1999a; Rho et al., 1999b; Thurner, 2009). Basically, this method allows calculating elastic modulus and nanohardness of the investigated material, based on indentation depth, load (force magnitude) and known geometry and properties of the indenter (Oliver and Pharr, 1992) (Figure 9).

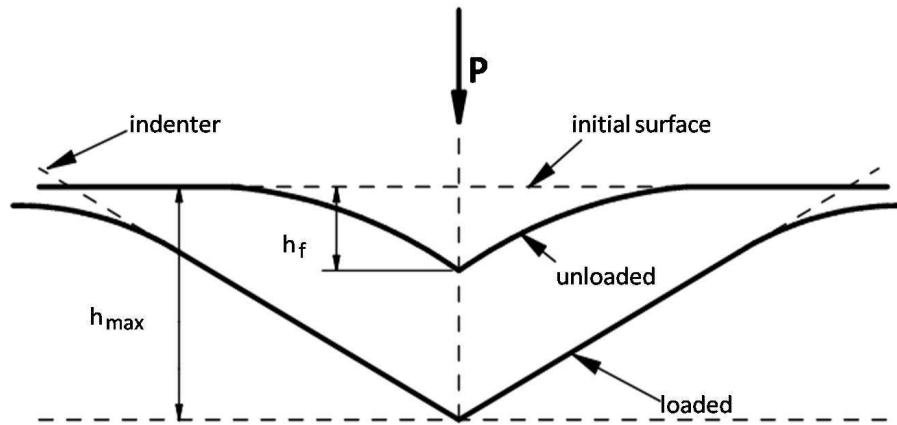


**Figure 9.** Scheme of the surface profile under maximum load based on Oliver and Pharr's method. It is noteworthy that the investigated surface partly recovers after the indentation due to elastic properties, while the remaining indent reflects persistent plastic deformation of the material. Oliver-Pharr's method calculates the nanohardness as the relation between maximum load and indentation area. ( $P$  – load,  $h_{max}$  – the maximum indentation depth, i.e., indenter's penetration depth at the maximum load at the end of loading phase,  $h_f$  – residual depth after removing the indenter).

### 3.5.1.3.2. Nanoindentation test

Nanoindentation was performed on Multimode quadrex SPM with Nanoscope IIIe controller (Veeco Instruments, Inc.) under ambient conditions in Force-indent mode using a commercial DNISP AFM probe (Veeco Instrument, Inc.) with a diamond tip suitable for nanoindentation applications (cantilever length of 350  $\mu\text{m}$ , resonant frequency 63 kHz, high spring constant of 243 N/m, tip radius 40 nm, Poisson's ratio of the tip 0.07 and elastic modulus of the diamond tip 1140 GPa). The force applied is

determined as the product of the spring constant of the cantilever and its deflection. Deflection sensitivity of the cantilever was calibrated by indenting a sapphire surface. The trabecular bone specimens were indented in the direction normal to the femoral neck axis, which resembles the direction of the fall impact in the elderly (Lotz et al., 1995).

We made series of indents using Auto Indent option which produces the indentation arrays automatically, after setting the number of columns and rows in the array and the spacing between them. A force-displacement curve was recorded for each indentation (Figure 10). A 10 x 5 array of indents, where the applied force increased along each row, were made on each specimen. The typical indentation forces ranged from 0.01 to 0.12 mN, and the tip was given an X-rotation of 25°.

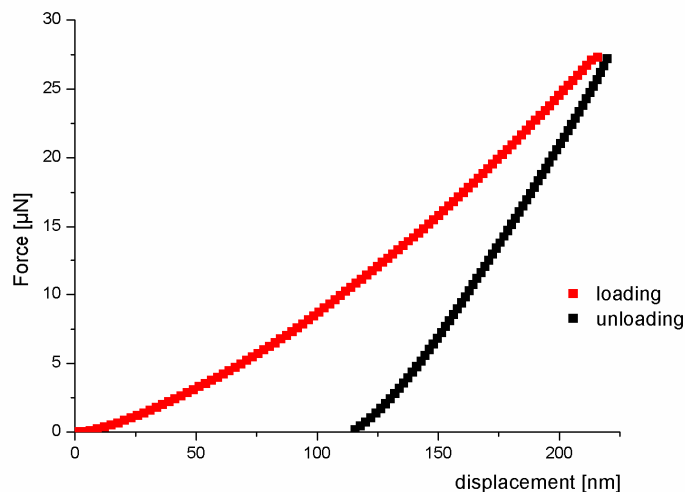


**Figure 10.** A typical force-displacement plot showing a single load-unload cycle. Maximum displacement corresponds to the depth of indentation at the end of the loading phase. During the unloading phase, the surface moves back towards the original position due to elastic properties. Note, however, that the surface never achieves the zero-position and even at the end of unloading phase it remains slightly indented indicating persistent (plastic) deformation. Elastic modulus information is extracted from the unloading part of the curve (elastic deformation region) using Oliver-Pharr method.



In each indentation cycle, the corresponding force-penetration depth plots were used to determine the elastic modulus and hardness value according to Oliver and Pharr method (Oliver and Pharr, 1992). In this method, the projected area of contact between the indenter and the sample at maximum load is calculated considering the geometry of the indenter and the depth of contact. Nanoindentation analysis software developed by Shuman and Costa (Shuman, 2006; Shuman et al., 2007) Dureza 1.1 was used to analyze the curve data, extracting the elastic modulus and nanohardness values of the specimens. Unload curve data were used for the non-linear numerical power-law fit, specifically the points from 20 to 100% were used for fitting following previous recommendations (Oliver and Pharr, 1992; Helvacı and Cho, 2005; Shuman et al., 2007). It should be noted that we performed nanoindentation tests on bone surfaces and also on the surrounding resin, in order to check for the effects of underlying acrylate on the measured bone values.

### ***3.5.2. Reference point indentation (RPI)***

#### ***3.5.2.1. Characteristics and preparation of the specimens***

The specimens that were subject to RPI testing comprised cortical specimens from elderly women who sustained hip fracture (n=5, age:  $82 \pm 4.6$  years) and age-matched control group of women (n=4, age:  $82 \pm 9.8$  years).

A low-speed diamond wheel saw SYJ-160 (MTI Corp., USA) with water soluble coolant was used to make bone sections in the superolateral region of the femoral neck, providing cortical bone samples each approximately 4 mm x 4 mm x 1 mm in size. The surface of cortical bone specimens was finely polished using 4000 grit on Unipol 810 semiautomatic polishing machine (MTI Corporation, USA) under constant water irrigation. The specimens were then ultrasonicated for 5 minutes and left to dry naturally before mechanical testing.

#### ***3.5.2.2. Reference point indentation tests***

Cortical bone specimens were mounted on a sample holder and placed on a BioDent Hfc instrument (Active Life Scientific Inc., Santa Barbara, CA, USA) in Institute of Osteology and Biomechanics, University Medical Center Hamburg-Eppendorf, Hamburg, Germany. Reference point indentation measurements were performed using a

commercial probe (type BP2, Active Life Scientific Inc., Santa Barbara, CA, USA) consisting of a *reference probe* which rests on the bone surface and a *test probe* which indents the bone during the testing (Hansma et al., 2008). Reference probe is a flat bevel with 5-mm-long cannula, whereas the test probe is 90° conospherical with less than 5 µm radius point.

The reference probe is driven to the bone surface. The principle of RPI involves 10 successive indentation cycles per measurement during which the test probe goes deeper into the bone with each cycle. Each cycle consists of three equally long phases: a *loading phase* with the applied force linearly increased to 2 N, a *hold phase* where the force is kept constant, and *unloading phase* in which the force linearly decreases to 0 and the probe is removed from the surface.

Based on the load-displacement curves that are recorded by the Biodent software, the following parameters were measured (Figure 11):

- first cycle indentation distance (ID 1, µm) which is a penetration depth achieved by the test probe during the first indentation cycle,
- total indentation distance (TID, µm) – distance from the initial touchdown distance to the maximum indentation distance in the last cycle,
- indentation distance increase (IDI, µm) – the increase in indentation distance from the first to the last cycle,
- average creep indentation distance (CID, µm) – additional distance traversed by the probe during the hold period, averaged over all indentation cycles, and
- the average energy dissipated (ED, µJ) which is a mean integrated area under the load-displacement curve (averaged during all cycles).

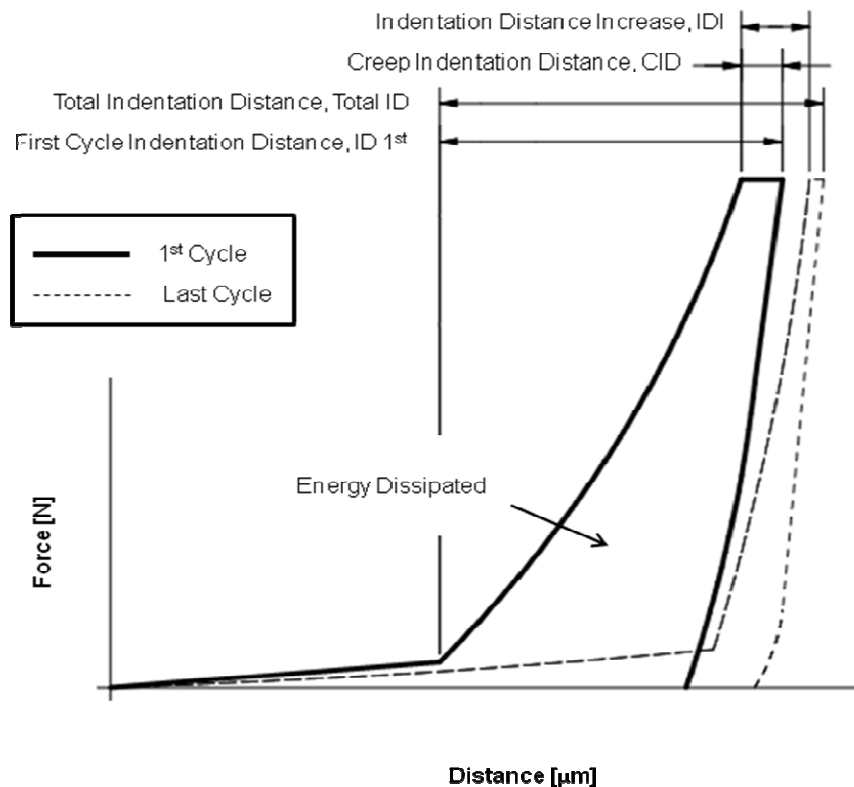


**Figure 11.** Schematic overview of material properties acquired using reference point indentation

### 3.6. Statistics

#### 3.6.1. Determination of sample size

Sample sizes needed for the analyses in this study were calculated in MedCALC statistical software (version 9.1.0.1) considering expected variability of the investigated parameters and biologically relevant level of differences intended to be detected, with type I error of 0.05 and type II error of 0.20.

#### 3.6.2. Statistical analysis of data

Kolmogorov-Smirnov test was applied to assess the normality of the data distribution of microarchitectural, nanostructural, compositional and mechanical parameters. Parametric tests (t-test, ANOVA, ANCOVA) in the case of normal distribution, or otherwise - appropriate non-parametric tests (Mann-Whitney test) - were used for assessing the differences in microarchitectural, nanostructural, compositional and mechanical parameters between the investigated groups. ANCOVA was used to check

for inter-group differences in various micro-CT parameters upon adjusting for BV/TV, and to check for inter-group differences in RPI parameters or cortical micro-CT parameters after age-adjustment. Linear regression analysis was used for determining the relationship of nanostructural parameters and mechanical properties of the bone matrix, as well as exploring the effects of age on nanostructural parameters of the bone matrix. Pearson's correlation analysis was used to assess the relationship between different parameters.

All statistical tests were performed in Statistical Package for the Social Sciences (SPSS) version 15, while curve analysis was performed in SPSS 15 and OriginLab 8. The p-values  $\leq 0.05$  were considered statistically significant.

## 4. RESULTS

### 4.1. Analysis of trabecular bone microarchitecture

We analyzed trabecular bone microstructural parameters of the femoral neck in 29 women belonging to two categories: non-fracture (control) group and fracture group. All microarchitectural parameters showed normal distribution (Kolmogorov-Smirnov test, Tables 1-4).

**Table 1.** Microarchitectural parameters in the superolateral neck of the control group: Kolmogorov Smirnov test for normality of data distribution.

	BV/TV	Conn.D	SMI	Tb.N	Tb.Th	Tb.Sp	DA
Mean	8.00	0.63	2.62	1.25	0.20	0.85	1.69
SD	4.00	0.55	0.47	0.06	0.05	0.05	0.29
Kolmogorov-Smirnov Z	0.45	0.88	0.39	0.88	0.54	0.85	0.77
<i>p</i> value	0.99	0.42	1.00	0.42	0.93	0.47	0.59

**Table 2.** Microarchitectural parameters in the inferomedial neck of the control group: Kolmogorov Smirnov test for normality of data distribution.

	BV/TV	Conn.D	SMI	Tb.N	Tb.Th	Tb.Sp	DA
Mean	14.00	0.84	2.26	1.27	0.27	0.82	2.30
SD	6.00	0.61	0.42	0.07	0.07	0.06	0.26
Kolmogorov-Smirnov Z	0.64	0.75	0.38	0.78	0.86	0.87	0.72
<i>p</i> value	0.80	0.62	1.00	0.57	0.45	0.44	0.68

**Table 3.** Microarchitectural parameters in the superolateral neck of the fracture group: Kolmogorov Smirnov test for normality of data distribution.

	BV/TV	Conn.D	SMI	Tb.N	Tb.Th	Tb.Sp	DA
Mean	3.6	0.21	2.94	1.22	0.17	0.89	1.67
SD	1.6	0.15	0.36	0.04	0.00	0.03	0.22
Kolmogorov-Smirnov Z	0.58	0.55	0.65	0.72	0.51	0.54	0.57
p value	0.89	0.92	0.80	0.68	0.95	0.93	0.91

**Table 4.** Microarchitectural parameters in the inferomedial neck of the fracture group: Kolmogorov Smirnov test for normality of data distribution.

	BV/TV	Conn.D	SMI	Tb.N	Tb.Th	Tb.Sp	DA
Mean	9	0.46	2.29	1.23	0.24	0.86	2.59
SD	4	0.43	0.44	0.06	0.04	0.07	0.33
Kolmogorov-Smirnov Z	0.42	0.97	0.40	0.97	0.49	1.20	0.46
p value	0.99	0.30	0.99	0.31	0.97	0.11	0.98

Comparison of the fracture and control groups showed that they differed most significantly in bone volume fraction (BV/TV: 6.3% in fracture cases vs. 11.2% in controls,  $p=0.002$ ), probably due to an overall trend to changes in both trabecular number and trabecular thickness. Moreover, the fracture cases had a lower connectivity density (Conn.D:  $0.33/\text{mm}^3$  vs.  $0.74/\text{mm}^3$ ,  $p=0.019$ ) and a higher trabecular separation (Tb.Sp: 0.87 mm vs. 0.83 mm,  $p=0.030$ ) (Table 5, Figure 12).

After division into the superolateral and inferomedial regions of interest, evident inter-site differences appeared: in particular, the superolateral neck displayed markedly unfavorable microarchitectural features (Table 6, Figures 12 and 13).

**Table 5.** Microarchitectural parameters in the fracture (FX) and control (CTL) groups in the femoral neck section.

	The femoral neck section			
	Control (n=14)	Fracture (n=15)	% of difference FX vs. CTL	<i>p</i>
Mean BV/TV (SE) [%]	11.2 (1.2)	6.3 (0.7)	-43.8	0.002
Mean Conn.D (SE) [1/mm <sup>3</sup> ]	0.74 (0.14)	0.33 (0.07)	-55.0	0.019
Mean SMI (SE)	2.44 (1.00)	2.61 (0.09)	7.1	0.207
Mean Tb.N (SE) [1/mm]	1.26 (0.02)	1.22 (0.01)	-2.8	0.081
Mean Tb.Th (SE) [mm]	0.23 (0.02)	0.21 (0.01)	-12.0	0.093
Mean Tb.Sp (SE) [mm]	0.83 (0.01)	0.87 (0.01)	4.8	0.030
Mean DA (SE)	2.00 (0.05)	2.13 (0.07)	6.6	0.124

The measured values are reported as mean with standard error of mean

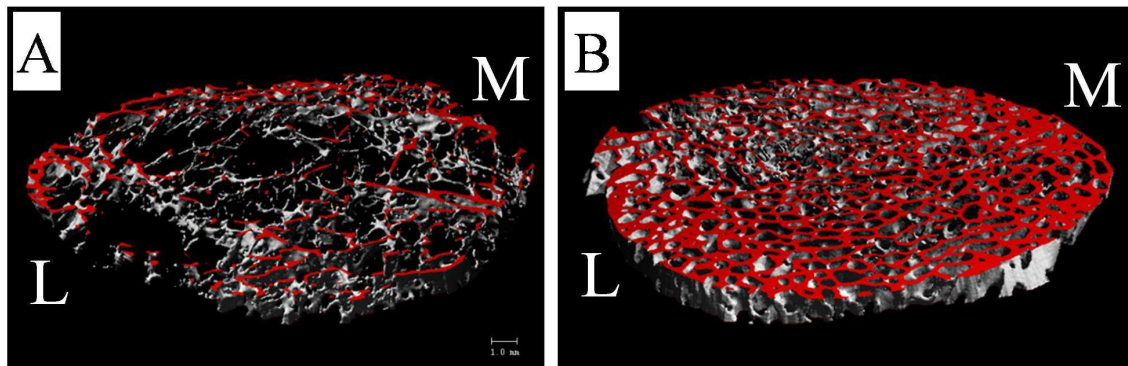


**Figure 12.** Representative 3D micro-CT reconstruction of the femoral neck trabecular bone in an elderly woman who sustained hip fracture (A) and in a woman without fracture (B). M – inferomedial neck region, L – superolateral neck region (The red layer represents exactly the osseous material of the top slice. The gray values represent all subsequent slices.)

In the superolateral neck the majority of parameters were impaired in the fracture group (Table 6, Figure 13). Especially, bone volume fraction and connectivity density demonstrated more than 50% lower values in the fracture group (BV/TV: 3.6 vs. 8.2%,  $p=0.001$ ; Conn.D: 0.21 vs. 0.63/mm<sup>3</sup>,  $p=0.008$ ). Other parameters showed smaller percentage of differences, but with attained statistical significance, except in the case of trabecular number and degree of anisotropy (Table 6). The superolateral neck of the fracture group displayed especially thinner trabeculae (0.17 vs. 0.20 mm,  $p=0.05$ ), higher separation between the trabeculae (0.89 vs. 0.85 mm,  $p=0.013$ ), and a higher SMI reflecting the predominance of rod-like trabecular elements (SMI: 2.94 vs. 2.62,  $p=0.049$ ) (Table 6).

**Table 6.** Microarchitectural parameters in the fracture and non-fracture (control) groups in the subregions of interest.

	Superolateral neck				Inferomedial neck			
	Control (n=14)	Fracture (n=15)	% *	<i>p</i>	Control (n=14)	Fracture (n=15)	% *	<i>p</i>
<b>Mean BV/TV</b>	8.2	3.6			14.3	9		
(SE) [%]	(1.1)	(0.4)	-56.1	0.001	(1.5)	(4)	-37.1	0.006
<b>Mean Conn.D</b>	0.63	0.21			0.84	0.46		
(SE) [1/mm <sup>3</sup> ]	(0.15)	(0.04)	-67.2	0.008	(0.16)	(0.11)	-45.8	0.059
<b>Mean SMI</b>	2.62	2.94			2.27	2.29		
(SE)	(0.13)	(0.09)	12.2	0.049	(0.11)	(0.44)	1.0	0.873
<b>Mean Tb.N</b>	1.25	1.22			1.27	1.23		
(SE) [1/mm]	(0.02)	(0.01)	-2.3	0.129	(0.20)	(0.02)	-3.2	0.113
<b>Mean Tb.Sp</b>	0.85	0.89			0.82	0.86		
(SE) [mm]	(0.01)	(0.01)	4.5	0.013	(0.17)	(0.02)	5.2	0.202
<b>Mean Tb.Th</b>	0.20	0.17			0.27	0.24		
(SE) [mm]	(0.01)	(0.01)	-14.8	0.05	(0.02)	(0.01)	-9.8	0.094
<b>Mean DA</b>	1.70	1.67			2.30	2.59		
(SE)	(0.08)	(0.06)	-1.3	0.821	(0.07)	(0.09)	12.4	0.016

\* - percentage of difference between the fracture group and the controls



In contrast, in the inferomedial neck only BV/TV and degree of anisotropy differed significantly between the fracture and non-fracture groups, where the fracture cases presented significantly lower values of BV/TV (9% vs. 14.3%,  $p=0.006$ ) and a higher anisotropy (2.59 vs. 2.30,  $p=0.016$ ) (Table 6, Figure 13).

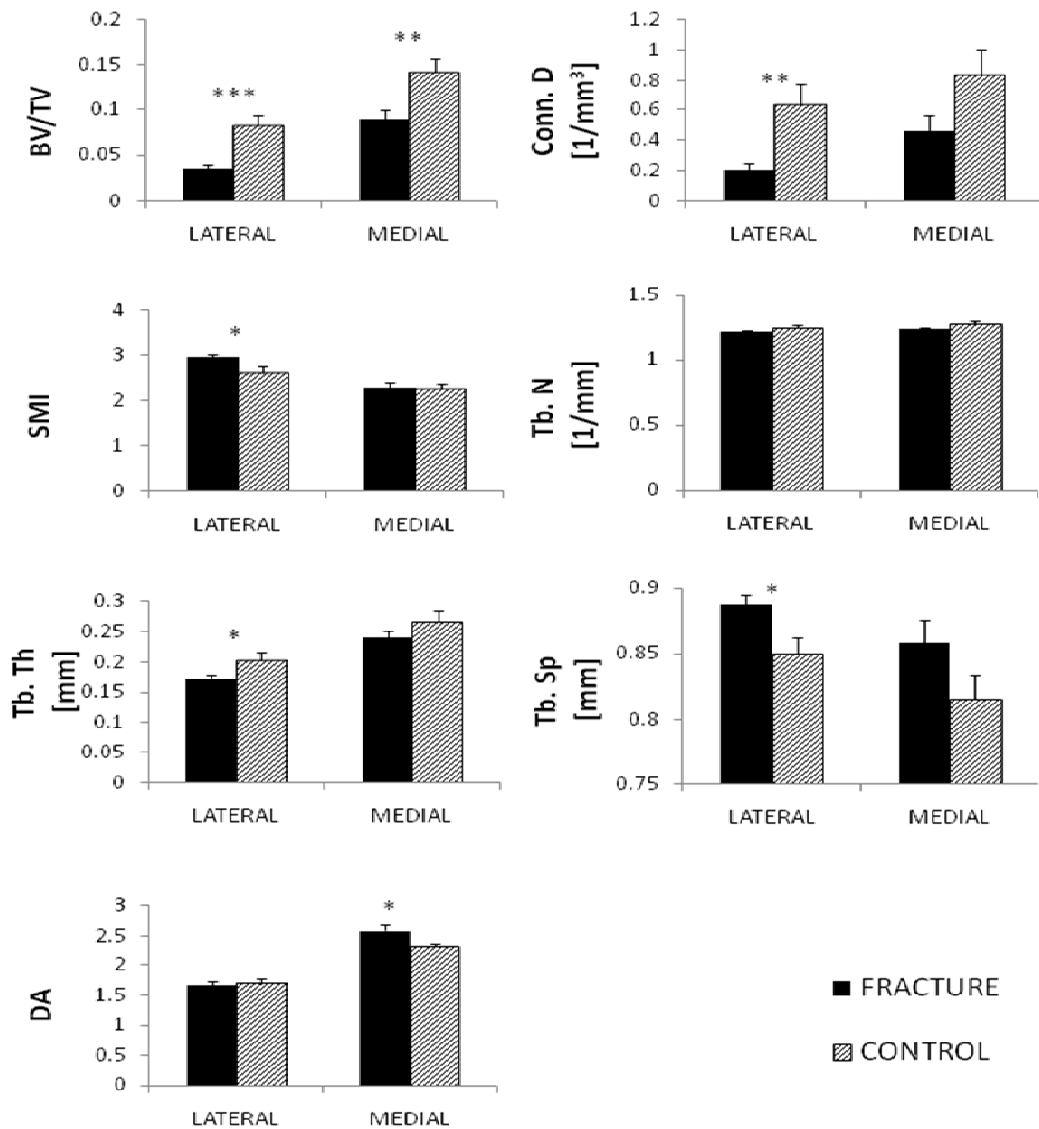


**Figure 13.** Comparison of the microarchitectural parameters between the fracture and non-fracture (control) group for the superolateral and inferomedial neck: BV/TV - bone volume fraction, Conn.D - connectivity density, SMI - structural model index, Tb.N - trabecular number, Tb.Th - trabecular thickness, Tb.Sp - trabecular separation, DA - degree of anisotropy. Bars indicate SE. (\*  $p \leq 0.05$ , \*\*  $p \leq 0.01$ , \*\*\*  $p \leq 0.001$ : Student's t-test)

In addition, bone volume fraction correlated significantly with all micro-CT parameters except with degree of anisotropy in both femoral neck subregions (Table 7). After adjusting for the effects of BV/TV, majority of inter-group differences disappeared (Table 8).

**Table 7.** Pearson's coefficient (*R*) for correlation between BV/TV and other micro-CT parameters.

Site		Conn.D	SMI	Tb.N	Tb.Th	Tb.Sp	DA
<b>Supero lateral neck</b>	<i>R</i>	0.885	-0.815	0.679	0.682	-0.802	0.317
	BV/TV <i>p</i> -value	<0.001	<0.001	<0.001	<0.001	<0.001	0.094
<b>Infero medial neck</b>	<i>R</i>	0.731	-0.680	0.676	0.682	-0.729	-0.151
	BV/TV <i>p</i> -value	<0.001	<0.001	<0.001	<0.001	<0.001	0.433

**Table 8.** Inter-group differences after adjusting for the effects of BV/TV (ANCOVA). Note that majority of inter-group differences disappeared.

	<b>Superolateral neck</b>	<b>Inferomedial neck</b>
	<i>p</i>	<i>p</i>
Conn.D	0.504	0.955
SMI	0.180	0.010
Tb.N	0.300	0.794
Tb.Th	0.712	0.459
Tb.Sp	0.788	0.715
DA	0.326	0.022

## 4.2. Analysis of bone nanostructure and chemical composition

We have performed an AFM characterization of nanostructure of trabecular and cortical bone specimens from the superolateral femoral neck region in young and elderly women to determine whether bone aging effects are visible at a nano-scale.

### 4.2.1. Age-related differences in nanostructure of trabecular bone

Analysis of AFM images revealed evident differences in nanostructure between the trabecular bone samples from the young and old females. Figure 14 shows AFM topography images of the bony trabeculae. The images shown here are representative of those acquired from various areas of the sample and depict features observed consistently.

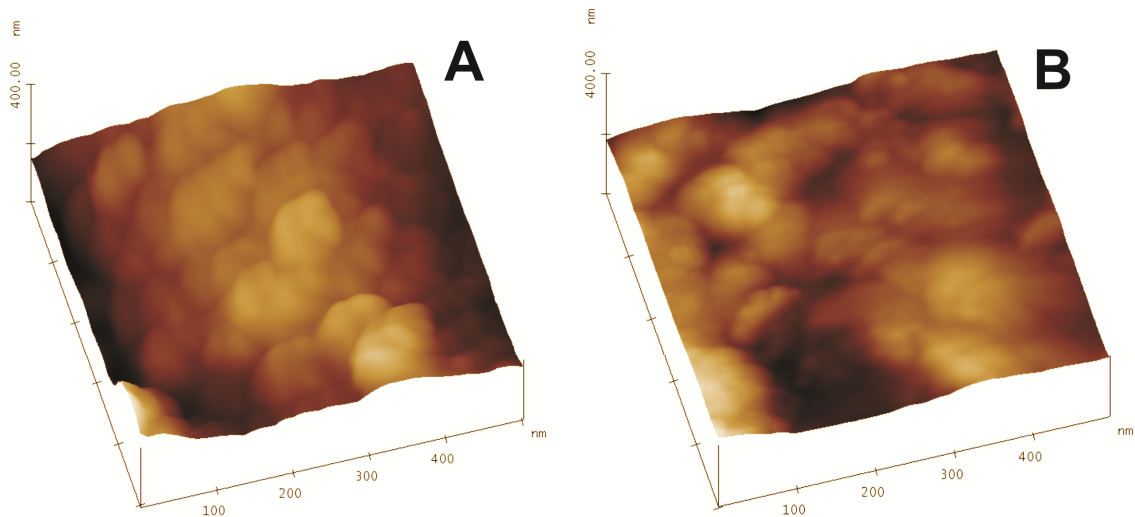


**Figure 14.** Trabecular bone from the superolateral region of the femoral neck in a young (A) and old woman (B): AFM 3D Topography image (500 nm x 500 nm). Note a lower surface roughness of the old woman trabecula.

In terms of materials, the observed bony surfaces represent a continuous phase, but with evident granular structure (AFM phase image, Figure 15).

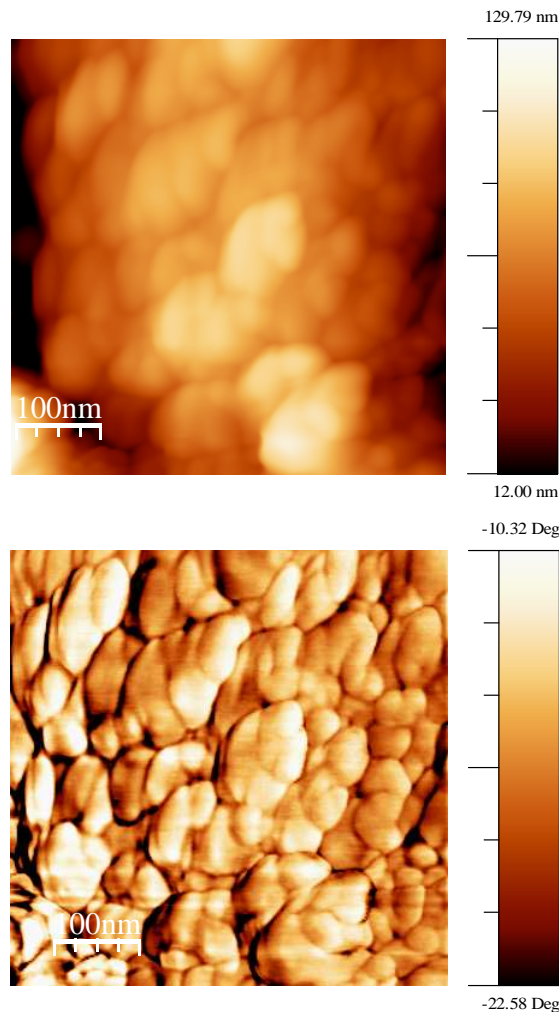


**Figure 15.** Representative AFM 2D Topography (up) and corresponding Phase image (down) of the trabecular bone from the superolateral region of the femoral neck in a young woman (500 nm x 500 nm). Note granular organization of the mineralized matrix. In 2D Topography image, the information on the third (Z) dimension is represented by different nuances of orange-brown colour: the highest parts (“the hills”) are lighter, whilst deeper parts of the surface topography (“the valleys”) are darker. The Phase image uses different colours to depict the areas of different material properties across the scanned area. In this case, the surface is composed of a single type of material in terms of physical and mechanical characteristics. It is evident that the surface is made of mineral grains of various sizes and shapes. Matching of Phase and Height images shows that the dark lines on the Phase image represent edges of the mineral grains, not different materials.

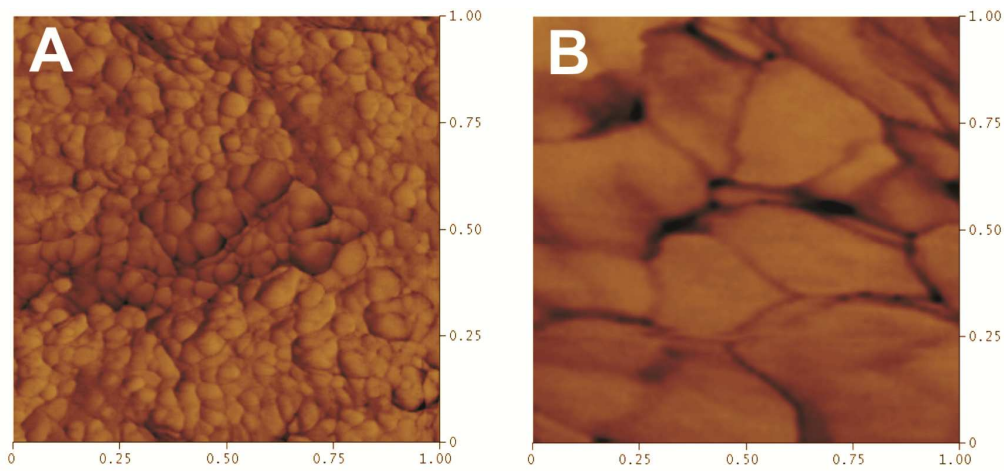


**Figure 16.** Representative AFM phase image of the trabecular bone from the superolateral region of the femoral neck in a young (A) and old woman (B) ( $1\ \mu\text{m} \times 1\ \mu\text{m}$ ). Domination of a single colour suggests that the observed surface is made of homogenous material in terms of material properties, although it is clear that the surface is granular (N.B. dark brown lines show the edges of individual mineral grains). Note larger mineral grains in an elderly woman's trabecula.

Size of the grains differed between the young and old individuals in a specific manner (Figures 16-18). In the elderly, the grains were larger on average (median: 95 nm vs. 59 nm; Mann-Whitney test,  $p < 0.001$ ), but also the variability was much greater (coefficient of variation: 60% vs. 38%; Figure 17). Old women displayed wide distribution of the grain sizes (26 nm - 445 nm), in contrast to young individuals where the grains were notably within a narrower range (21 nm - 129 nm, Figure 17).

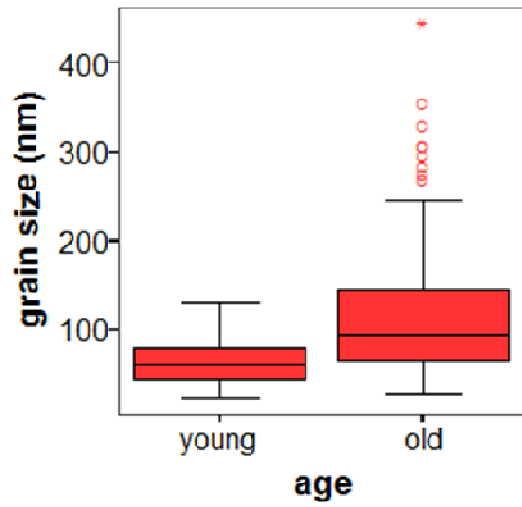


**Figure 17.** Boxplot diagram showing variability of the grain size distribution in the superolateral femoral neck trabecular bone in young and old women.

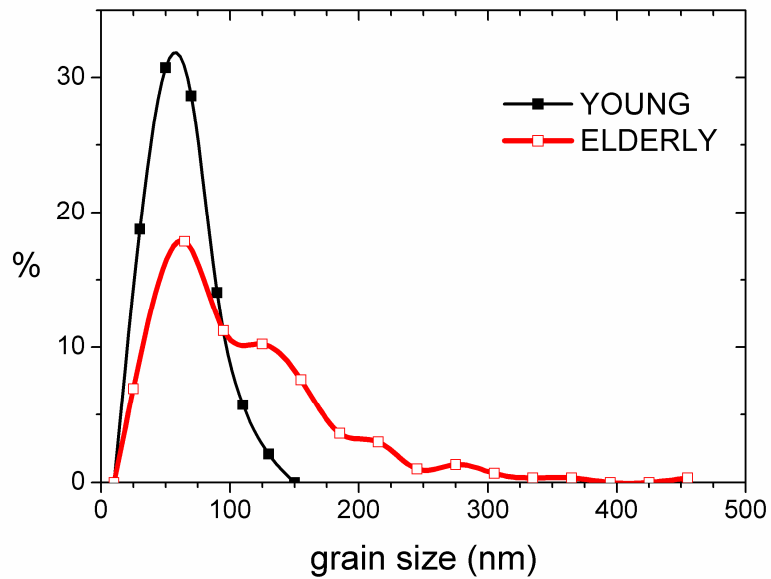


**Figure 18.** The superolateral femoral neck trabecular bone: The grain size distribution in the young and old women.

After deconvolution of the curve showing grain size distribution in old women, two peaks were identified (65 nm and 130 nm) using Origin Lab software (Figure 19). According to determination of the area under the curve, the smaller grains (which were of similar size to the grains of the young women) represented 44.8% of the grains in the elderly, while the remaining 55.2% were larger grains.

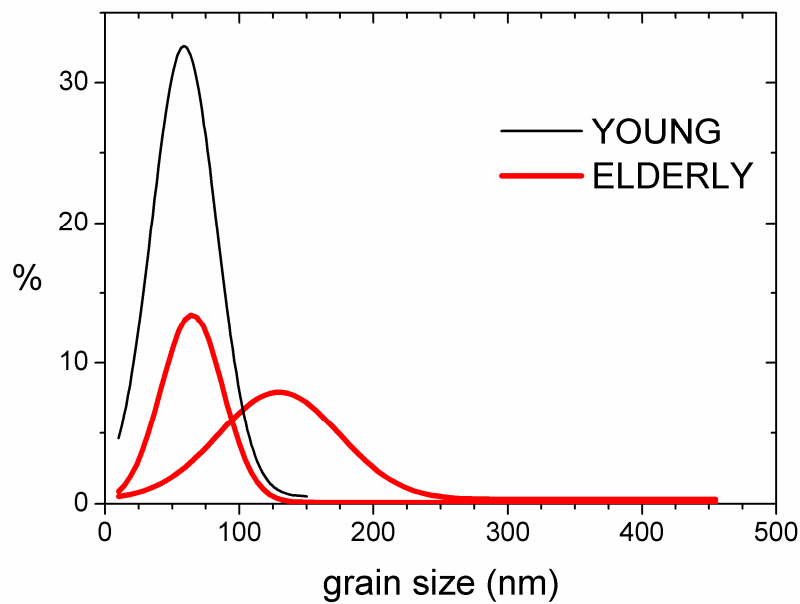


**Figure 19.** *The superolateral femoral neck trabecular bone: Fitted curves of the grain size distribution in the young and old women. Note that in old women there are two peaks indicating presence of small and large mineral grains, while the position of the peak in the young overlaps with the first peak of the elderly.*

In addition, we observed that old women showed unexpectedly a low mean saturation roughness of the trabecula (around 50 nm) (Figure 14) depicting that larger grains were flattened. In contrast, the mean saturation roughness in most of young cases was too high to be measured.

Chemical analyses showed unchanged levels of calcium and phosphorus in trabecular bone of elderly women (t-test:  $p=0.39$ ,  $p=0.84$ , respectively), without significant difference in Ca/P ratio (t-test:  $p=0.38$ ). Elemental composition of the bone matrix as revealed by spectroscopic analyses is shown in Table 9, revealing presence of

various trace elements in bone. Old bone contains more strontium and barium, and less iron (judging from mean values), however statistical significance was not achieved due to high variability in concentrations of these elements (*cf.* high SDs, Table 9).

**Table 9.** *Chemical composition of the human femoral trabecular bone (ICP-OES and DCA ARC quantitative analyses).*

	Young women		Elderly women	
	Mean	SD	Mean	SD
<b>Ca [wt %]</b>	22.55	3.01	24.38	2.55
<b>P [wt %]</b>	10.62	0.43	10.68	0.22
<b>Ca/P ratio</b>	2.12	0.26	2.28	0.23
<b>Mg [mg/g]</b>	3.25	0.26	3.08	0.64
<b>Sr [µg/g]</b>	54.25	2.22	89.25	76.75
<b>Fe [mg/g]</b>	2.40	3.90	0.21	0.21
<b>Ba [µg/g]</b>	<5.00	0.00	9.00	10.00
<b>K [mg/g]</b>	0.42	0.10	0.66	0.34
<b>Na [mg/g]</b>	25.28	5.28	27.90	4.96

#### **4.2.1.1. Advanced nanostructural analyses (PSD, FD) of trabecular interfibrillar surface in young vs. elderly women**

Illustrative AFM topography images of the trabeculae (Figure 20) revealed the nanostructural features of mineralized bone matrix, showing densely packed extrafibrillar bone minerals. The representative AFM images depict the features observed consistently at various locations within investigated human trabeculae. It was obvious from these images that the surface texture differed across age. To quantify differences in surface roughness and texture complexity, we extracted power spectral density curves and fractal dimensions data from the AFM topography images of the mineralized bone matrix of the femoral neck trabeculae in a group of young vs. elderly women.



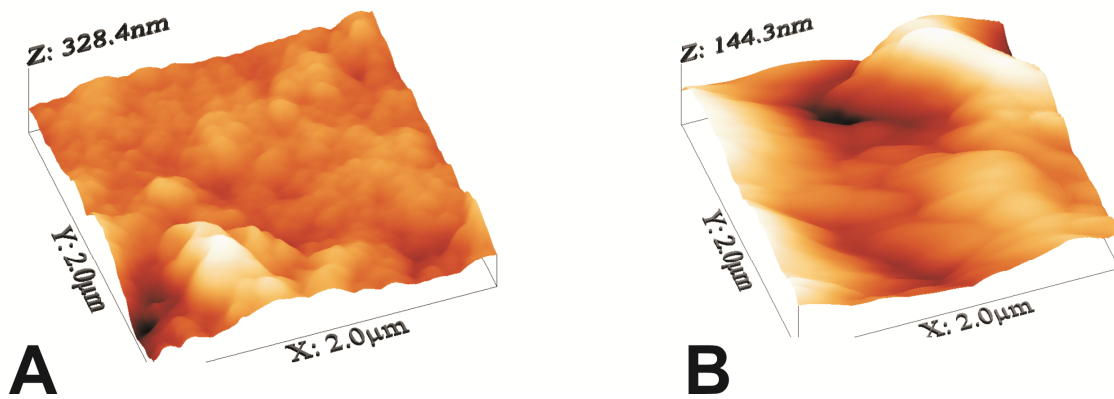


**Figure 20.** Representative AFM 3D surface plot (Topography images, scan dimensions:  $2\ \mu\text{m} \times 2\ \mu\text{m}$ ) of a young female (A) and an elderly female individual (B).

Power spectral density graphs showed the roughness density distribution in relation to spatial frequency. There was a decrease in magnitude of the power spectra with increasing spatial frequencies in all cases. In each individual, the PSD data originating from AFM images of different sizes were averaged. The observed relationship between the power spectra and spatial frequency could be approximated with a straight line in each individual ( $p < 0.05$ ). Figures 21A and 21B show linearly fitted PSD graphs of a young and an elderly individual, respectively.

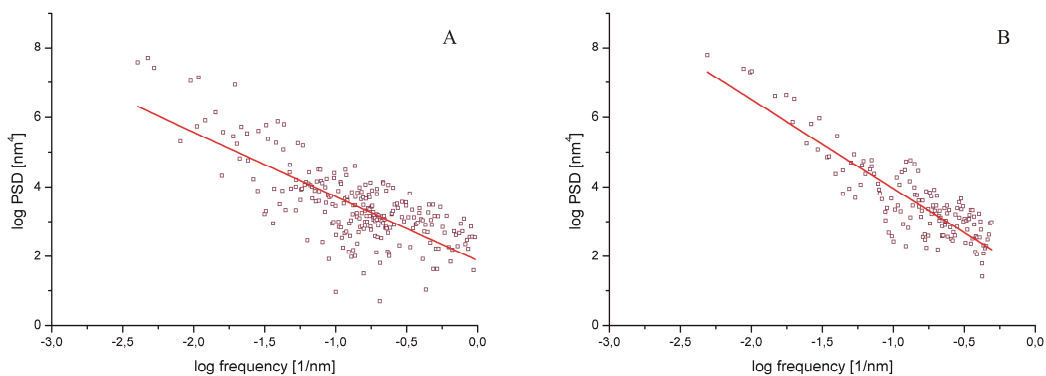


**Figure 21.** Power Spectral Density graph with linear fitting in a young female (A) and an elderly female individual (B). Note that both axes are with a logarithmic scale. Y-values (PSD=Power spectral density) correspond to the contribution of particular spatial frequency (X-value) to overall image roughness.

The slopes of the fitting lines were determined in both young and old individuals. The slopes showed negative values, illustrating decreased magnitudes with increasing spatial frequency. The absolute value of mean PSD slope in the elderly was higher than in the young specimens (2.374 compared with 2.066). Evaluation of the slopes of PSD trendlines in relation to age of individuals (Figure 22) suggests a tendency towards steeper lines in the elderly. There was statistically significant dependence of PSD slope on age according to the following law:

$$\text{PSD} = -0.007 * \text{age} - 1.828 \text{ (p<0.05)}.$$

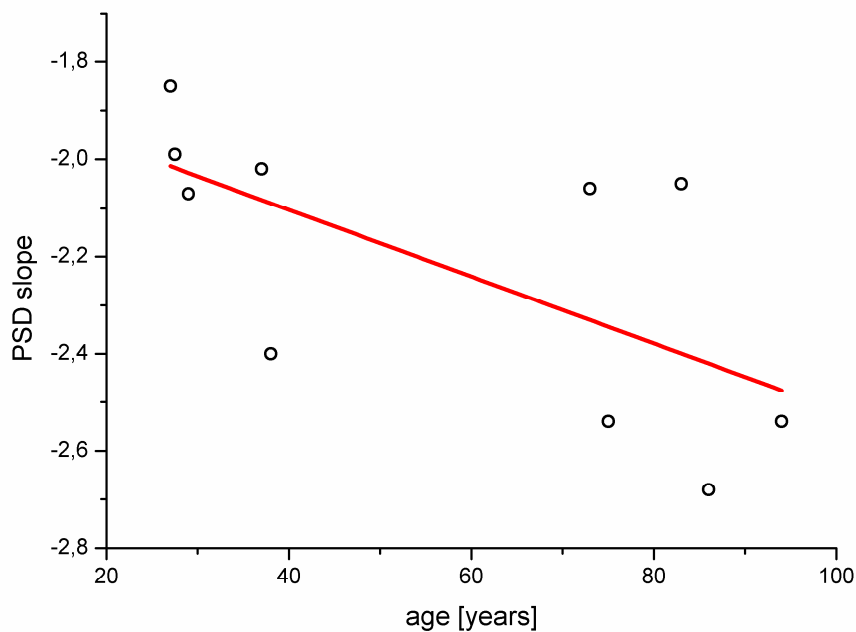


**Figure 22.** Age-dependence of PSD slopes.

PSD trendlines in each individual allowed subsequent calculation of the fractal dimension of their mineralized bone matrix. Younger specimens had higher average values of fractal dimensions (2.467) than the elderly (2.313). Individual fractal dimensions are shown in Figure 23. It was observed that the distribution of FD in young individuals was more homogenous, and only the FD in the oldest individual (38 years old) deviated towards the lower values. In contrast, elderly individuals presented with more disperse values of fractal dimension. In order to assess how the FD depends on the age of an individual, we have applied linear regression analysis. Evident negative

correlation was found in regression analysis between FD and age, which can be expressed with the following law:

$$FD = -0.003 * \text{age} + 2.586 \quad (r=0.65, p<0.05).$$

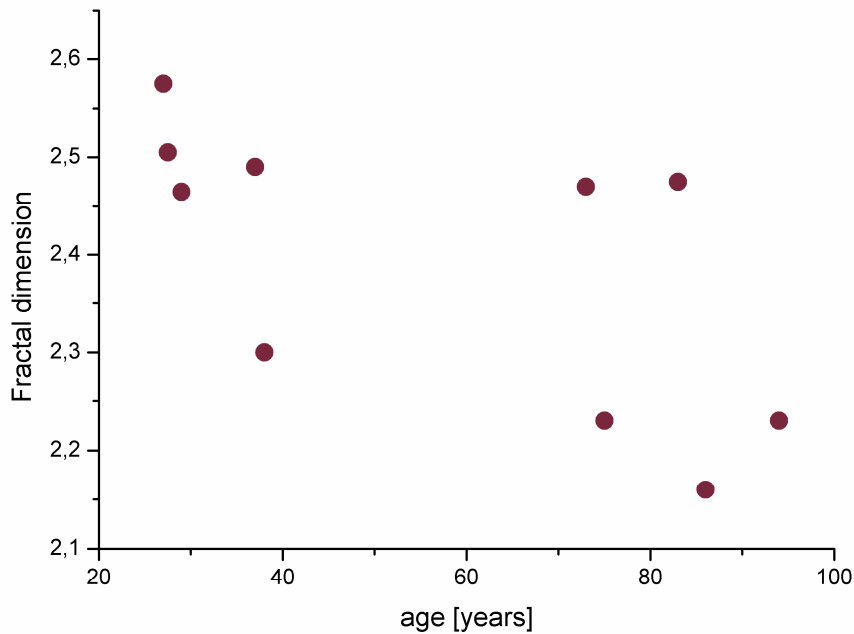


**Figure 23.** Age-distribution of fractal dimension of the bone mineralized matrix in the femoral neck trabeculae.

#### **4.2.2. Age-related differences in nanostructure of cortical bone**

Given that we observed a significant trend to increased femoral neck outer diameter in advanced age ( $R=0.844$ ,  $p=0.004$  – Figure 24), where the mean neck diameter was  $3.1 \text{ cm} \pm 0.2 \text{ cm}$  in the young vs.  $3.6 \text{ cm} \pm 0.2 \text{ cm}$  in elderly group ( $p=0.005$ ), we hypothesized that bone apposition happens at the periosteal cortical surface of the femoral neck. Therefore, we have performed qualitative and quantitative nano-scale characterization of the external cortical surface (periosteal surface) of the femoral neck in women of young and old age.

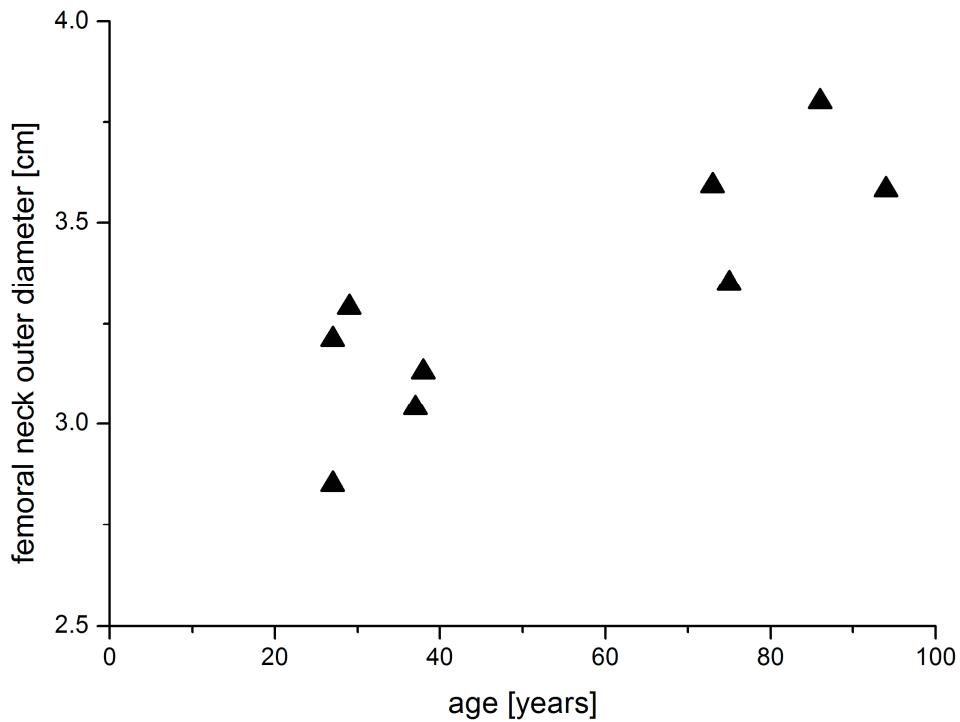


**Figure 24.** *The femoral neck outer diameter in relation to age of individuals.*

AFM Phase images that allow distinguishing between the materials of different properties have shown that the external cortical bone surface represents a continuous phase composed of mineral grains exclusively (Figure 25). The granular organization of the mineral phase was evident in Height and Phase images in both age groups of women (Figure 25 A, B, C, D). The minerals were densely packed, and they varied in shape. Usually they were plate-shaped rather than needle-shaped. The recorded features were consistently seen in AFM images in various locations within the cortical samples.

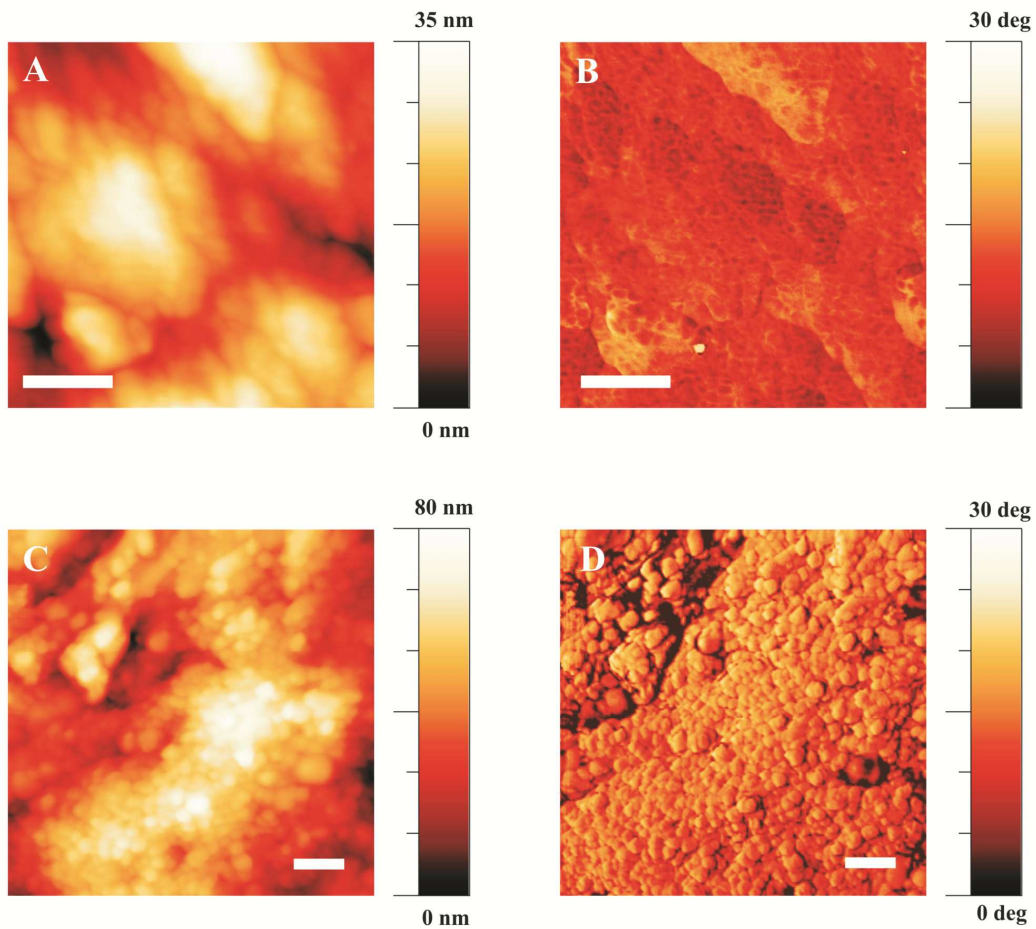


**Figure 25.** Representative AFM images of the external cortical bone surface of the femoral neck in a young (**A**, **B**) and elderly women (**C**, **D**). An AFM Height image (**A**), with corresponding AFM Phase image (**B**) of the external cortical surface in a young woman. (**C**) AFM Height image of the external cortical surface in an elderly woman, with corresponding AFM Phase image (**D**). Simultaneous acquisition of Height and Phase images allows matching nanostructural features with corresponding material properties. Note that in both individuals the observed surface represents a continuous phase composed of densely packed small mineral grains of various size and shape. Scale bar = 100 nm.

Matching of simultaneously acquired Height and Phase images allowed reliable identification of mineral grains and subsequent measurement of their size. The results revealed that small crystals dominated both in young and elderly external cortices (Table 10, Figures 25-27; Young vs. Old:  $p>0.05$ ). In young women, the size of mineral grains was in the range between 8 nm and 99 nm, with average diameter of 35 nm (Table 10). Likewise, the mean grain size in the elderly was 37 nm, with a range between 10 nm and 105 nm. Further analysis of the grain size distribution showed that minerals with diameter between 10 nm and 40 nm represented more than 60% of all mineral grains in both age groups (Figures 26 and 27).

**Table 10.** Grain size at the external cortical surface in young and old women femoral neck (CI – confidence interval).

Grain size						
age	Mean	SD	Lower	Upper	Min	Max
			95% CI of Mean	95% CI of Mean		
young	35 nm	18 nm	33 nm	36 nm	8 nm	99 nm
old	37 nm	18 nm	35 nm	38 nm	10 nm	105 nm

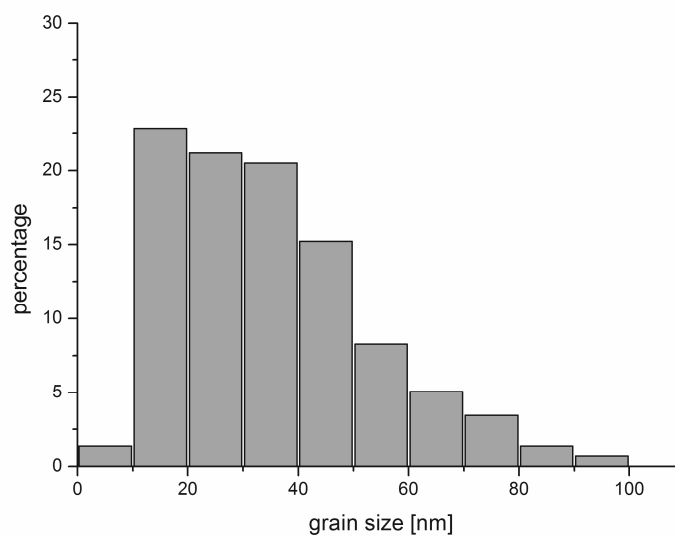


**Figure 26.** Histogram of grain size distribution in young women.

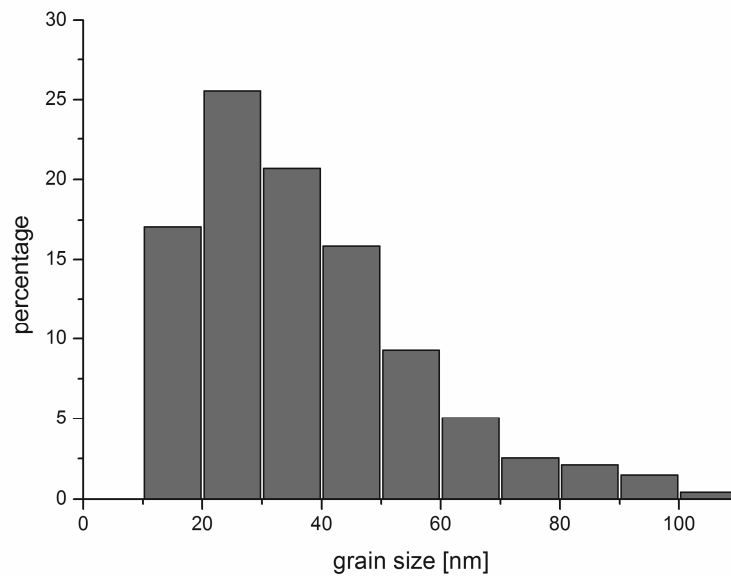


**Figure 27.** Histogram of grain size distribution in elderly women.

AFM topography images allowed 2-D and 3-D visualization of mineral crystals that cover the bone surface (Figure 25 A, C; Figure 28 A, B). Moreover, analyses of the spatial organization and packing of the grains revealed fiber-like structures densely covered by mineral grains (Figure 28). Those fibrils mostly had a fusiform shape, and appeared to be slightly interlaced with each other (Figure 28) or packed tight and parallel (Figure 29). They were obviously enveloped in aggregates of small crystals. The diameter of those fiber-like structures did not differ significantly between the age groups (Table 11;  $p > 0.05$ ).

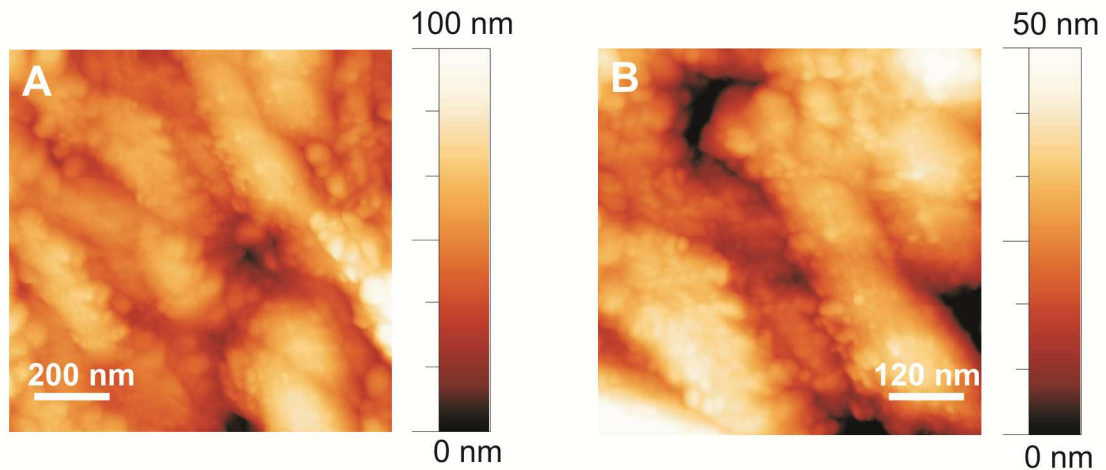


**Figure 28.** AFM Topography images showing mineralized collagen fibrils at the external cortical bone surface. (A) Note ~150nm-thick fibrils spreading mostly from the upper-left to lower-right angle of the image. (B) Higher magnification image showing two oblique fibrils. Note that the fibrils are coated with grains.

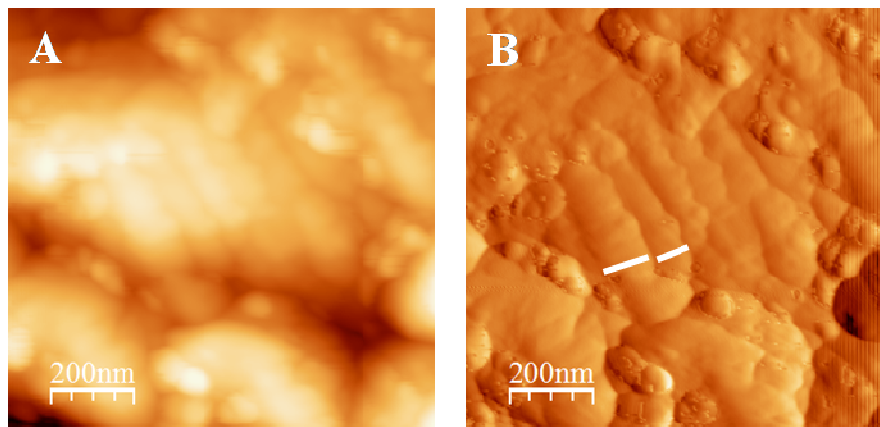


**Figure 29.** External cortical bone surface at the femoral neck region in a 38-year-old woman: AFM images ( $1\ \mu\text{m} \times 1\ \mu\text{m}$ ). (A) The Height image shows realistic topography of the external cortical bone surface (Z scale range 110 nm). (B) The corresponding Amplitude image. Amplitude image is a special type of AFM image which is edge-sensitive and usually shows the shapes (2D) of the surface elements more easily. Here it clearly shows several parallel fibril-like structures (two of them are marked by width using white lines) that might correspond to collagen fibrils coated with minerals (~100-150 nm in width). It is noteworthy that AFM Amplitude image does not contain height information, and therefore, its Z scale is meaningless in terms of surface structure.



**Table 11.** Diameter of mineralized fibrils at the external cortical surface in young and old women femoral neck.

<b>age</b>	<b>Mean</b>	<b>SD</b>	<b>Lower 95% CI of Mean</b>	<b>Upper 95% CI of Mean</b>	<b>Min</b>	<b>Max</b>
<b>young</b>	146 nm	40 nm	140 nm	152 nm	68 nm	235 nm
<b>old</b>	154 nm	33 nm	148 nm	160 nm	76 nm	233 nm

*CI – confidence interval*

**4.2.2.1. Advanced nanomorphological features: Power spectral density and fractal dimension in cortical bone of young vs. elderly women**

Power spectral density graphs from AFM topography images show contribution of surface morphological features of different sizes to overall surface roughness of the external cortex, where the slopes of PSD trendlines are taken as good descriptors of its surface roughness.

A representative graph of *log* PSD vs. *log* spatial frequency is shown in Figure 30, and denotes decreasing magnitudes with increasing spatial frequency in a linear manner ( $R > 0.95$ ,  $p < 0.001$ ). Based on the slope of PSD trendline, surface roughness did not differ between the age groups (-3.91 vs. -3.87;  $p > 0.05$ ).

Likewise, fractal dimension of the external cortical surface did not significantly change with age (1.54 vs. 1.56,  $p > 0.05$ ).

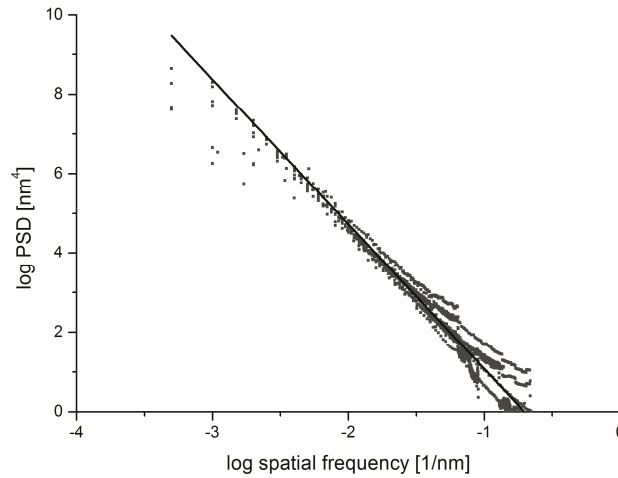


**Figure 30.** A representative AFM-derived PSD graph of the external cortical surface.

#### **4.2.2.2. Calcium/phosphorus ratio of the cortical bone in young vs. elderly women**

As determined using ICP-OES, calcium/phosphorus ratio (Ca-wt%/P-wt%) which may be taken as a measure of tissue age showed unchanged values between young and old specimens ( $1.92 \pm 0.19$  vs.  $1.82 \pm 0.25$ ;  $p > 0.05$ ).

### **4.3. Nanomechanical assessment of trabecular bone material in young vs. elderly women**

One of the principal advantages of AFM is its ability to extract information on mechanical properties of the specimens. Therefore, in addition to imaging, here we performed AFM mechanical characterization of young and elderly femoral neck trabeculae in order to assess age-related differences at the level of bone mineralized matrix using AFM nanoindentation method.

During loading phase of nanoindentation, the applied force was increased in each subsequent indent, and the maximum indentation depth at each indentation was recorded. In both age groups, increasing force led the tip deeper into the bone material resulting in higher indentation depths (Figure 31). Comparison of young and elderly trabeculae revealed that for the same applied load the indentation depth was shallower for elderly trabeculae than for the young, indicating that young bone is less stiff. After 300 nm - 400 nm of indentation depth there was a “kinking” phenomenon, where a

larger force increment was required for the same depth increment in both the young and elderly bone.

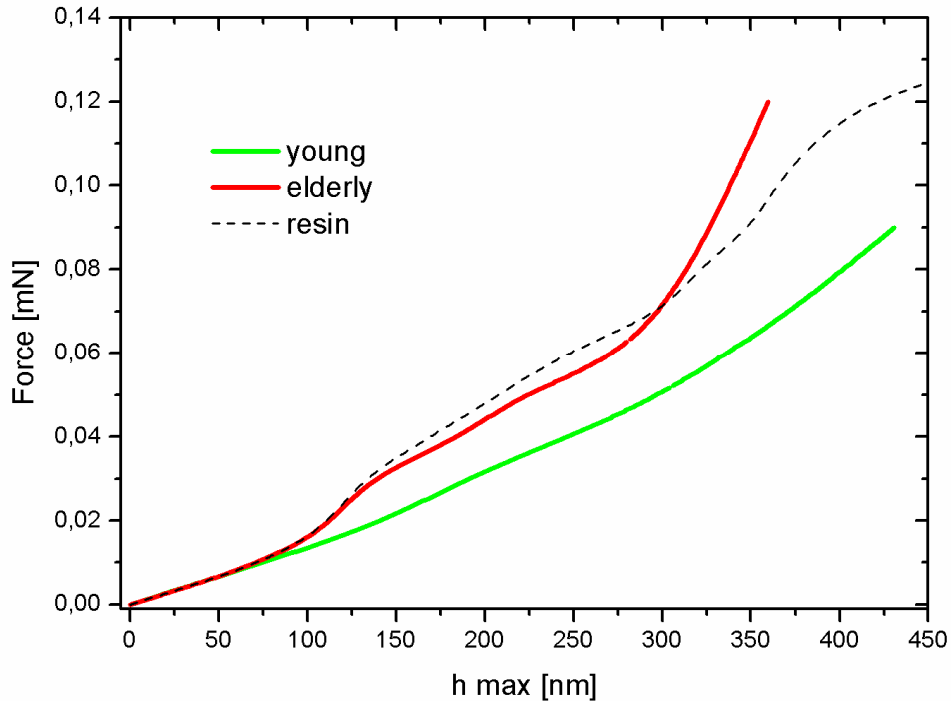


**Figure 31.** Force-indentation depth graph. Note that young bone is more deformable under the same load. Observe that after approximately 300 nm indentation depth there is a “kinking” possibly caused by delamination.

Analysis of the relation between elastic modulus and indentation depth has revealed that elastic modulus was generally higher for low indentation depths. However, with increasing penetration depth, the elastic modulus decreased towards the equilibrium value which determines the true tissue modulus. This was evident in each individual (an example shown in Figure 32 A) and each age group (summarized in Figure 33).

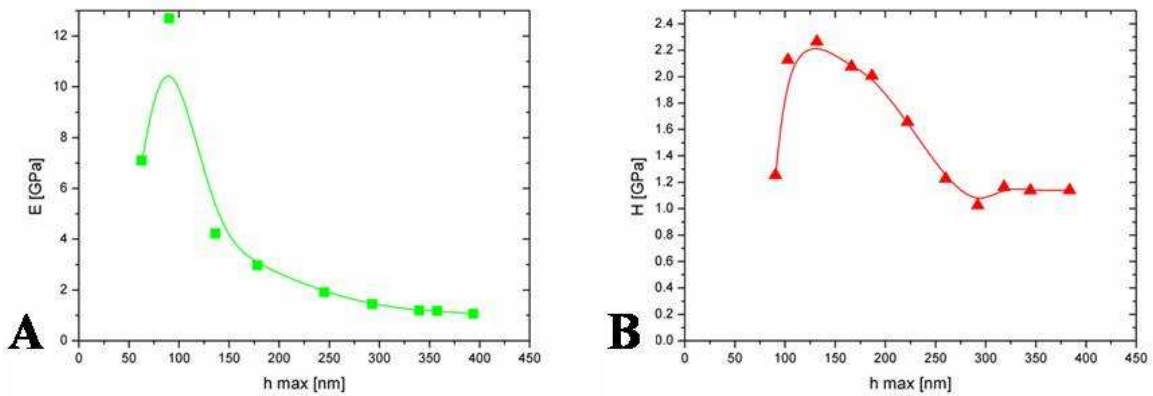


**Figure 32.** (A) Example of elastic modulus of the bone matrix as a function of indentation depth in an elderly individual. Note that with increasing indentation depth the calculated modulus decreases towards a steady value which represents the true tissue modulus. (B) Example of nanohardness in an individual, showing the same trend.

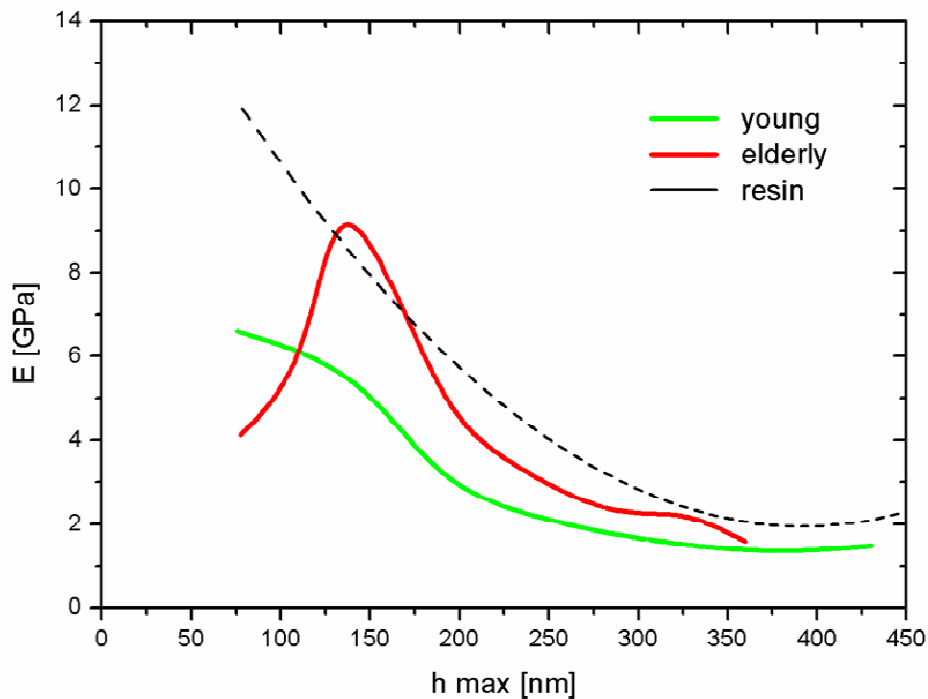


**Figure 33.** Elastic modulus as a function of indentation depth in young vs. elderly women. Note higher values of elastic modulus in the elderly. With increasing depth the modulus achieves a steady value in both age groups. The lines represent average values in given groups of specimens.

Comparison of elastic modulus - indentation depth curve between the age groups showed a clear trend of higher elastic modulus in the elderly for almost all indentation depths (Figure 33). In addition, mean true elastic modulus of elderly group was more than 50% higher than in the young (Table 12) and expressed greater variability (Figure 34). It might be noted that at the highest depths the values of modulus in both the young and old bone approached those of embedding resin (Figure 33).

**Table 12.** Nanostructural and nanomechanical properties of bony trabeculae in young vs. elderly women (\* - median).

		Mean	SE
Grain size [nm]	young	59*	3
	old	120*	18
Elastic modulus [GPa]	young	1.28	0.16
	old	1.97	0.52
Nanohardness [GPa]	young	0.59	0.15
	old	0.92	0.12

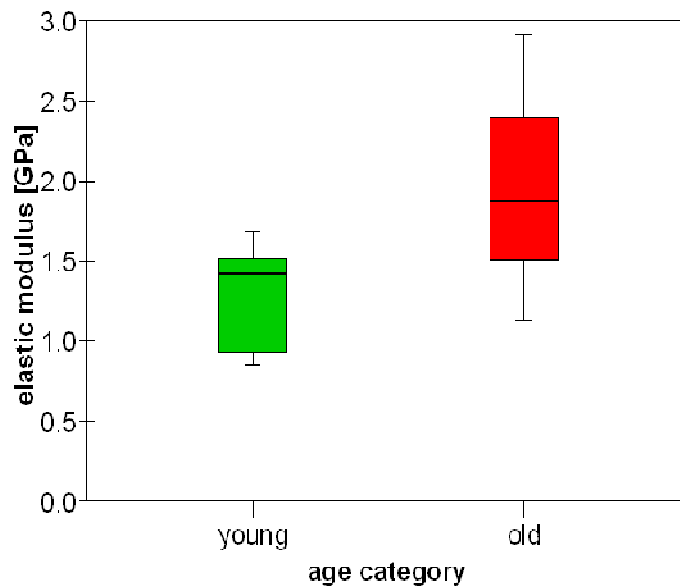


**Figure 34.** Box-plot diagram of elastic modulus of the bone matrix in young vs. elderly women.

Similar to elastic modulus, nanohardness was generally higher at low indentation depths, while increasing penetration depth led to a reduction in nanohardness down to a stable value (plateau) which corresponds to true tissue hardness. An example in an elderly individual is expressed at Figure 32B.

Analysis of relation between nanohardness and indentation depth showed higher nanohardness in the elderly for almost all indentation depths (Figure 35). Mean true nanohardness was more than 50% higher in the elderly (Table 12). It might be noted that at the highest depths the values of nanohardness in both the young and old bone had a tendency towards those of embedding resin (Figure 35).

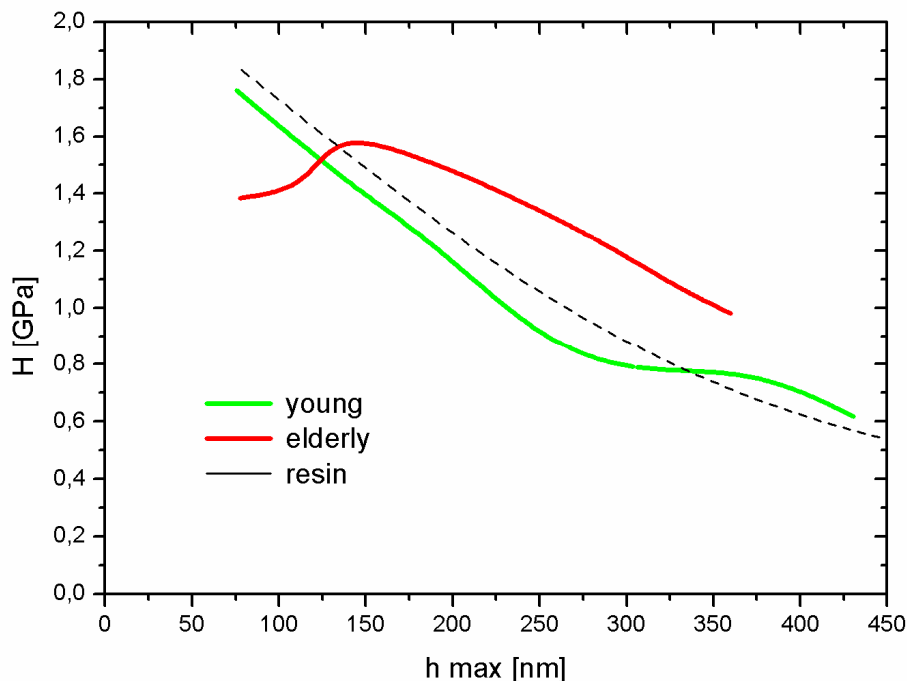


**Figure 35.** Nanohardness as a function of maximum penetration depth for young and elderly women. The lines represent averages in given groups of specimens.

Median size of bone mineral grains in the elderly (120 nm) was approximately two-fold larger than in the young (Table 12). Linear regression analysis between the median grain size and elastic modulus of bone showed their pretty high correlation ( $r=0.80$ ) and revealed that about 65% of variability in elastic modulus can be statistically explained by variability in median grain size (coefficient of determination

$r^2=0.64$ ,  $p=0.018$ ). The relationship between the mineral size and elasticity can be approximated by a linear statistical model, with the model equation as follows:

$$E = 0.19 + 0.018 * G,$$

where E is elastic modulus of the material, and G is median grain size (Figure 36).

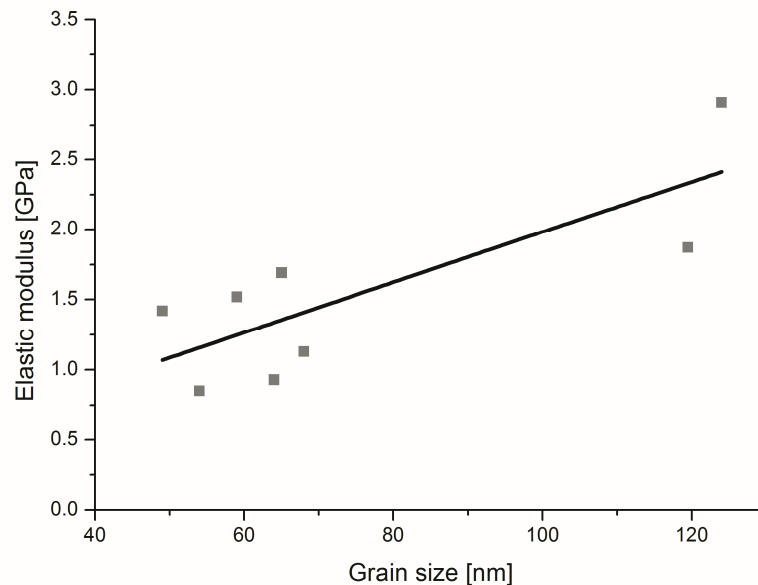


**Figure 36.** Relationship between the median size of mineral grains and elastic modulus of the bone matrix in the femoral neck trabeculae in women (Linear regression analysis,  $Elastic\ Modulus = 0.19 + 0.018 * Grain\ Size$ ).

#### 4.4. Assessment of cortical bone in hip fracture cases vs. controls

##### 4.4.1. Analysis of cortical bone nanostructure

To directly evaluate the significance of nanostructure on bone mechanical competence, another part of our study encompassed analysis of external cortical surface of the superolateral femoral neck of aged women who sustained hip fracture in comparison with age-matched healthy controls. Simultaneous acquisition of 3-D topography data and phase composition revealed granular organization of surface mineral phase in both groups (Figures 37-40).

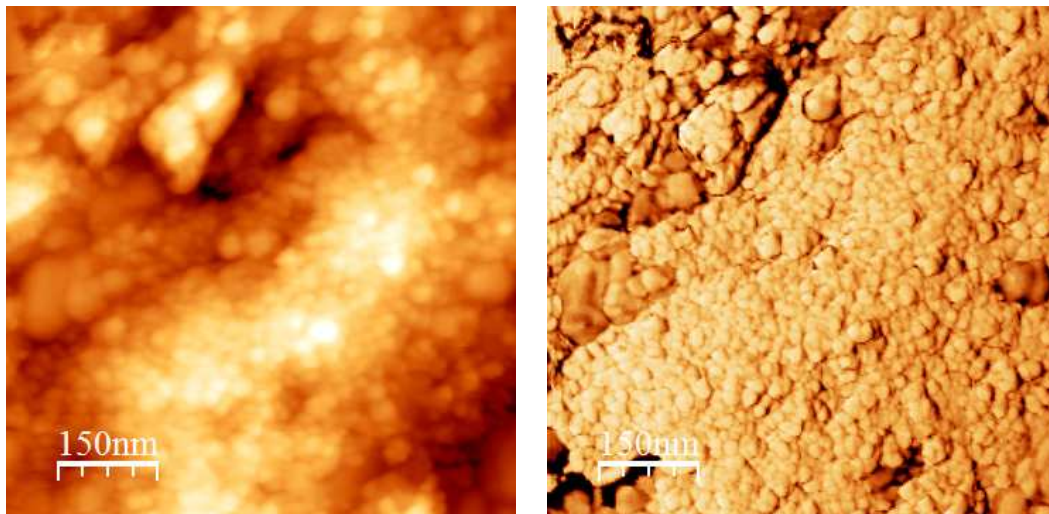


**Figure 37.** AFM Topography image (left) and Phase image (right) of the femoral neck cortical bone specimens in a 75-year-old female without bone diseases.

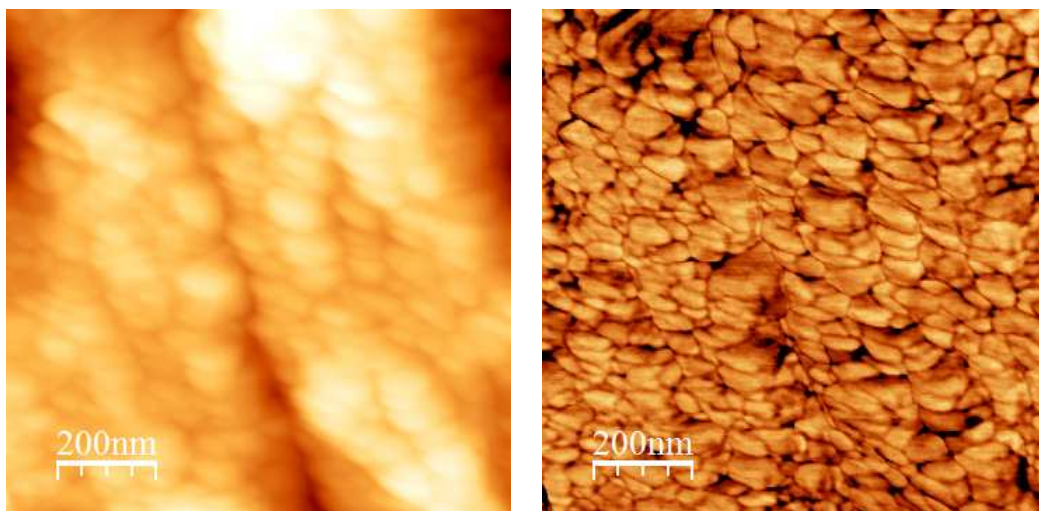


**Figure 38.** AFM Topography image (left) and Phase image (right) of the femoral neck cortical bone specimens in a 79-year-old female with hip fracture. Note larger mineral grains in comparison with the control group represented in Figure 37.



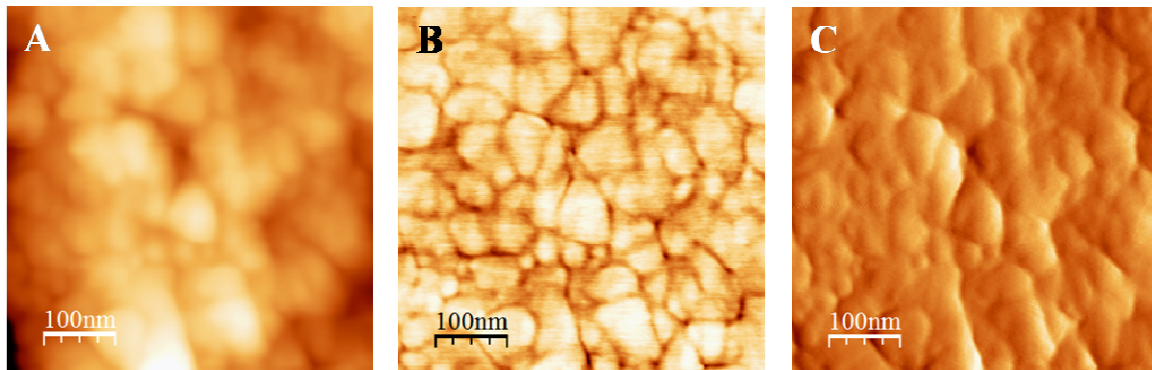


**Figure 39.** External cortical bone surface of the femoral neck region in an 87-year-old woman with sustained hip fracture: different image modalities of atomic force microscopy (500 nm x 500 nm images). (A) The Height image shows realistic topography of the external cortical bone surface. This is a two-dimensional image of the specimen's topography where the third (Z) dimension is represented by different nuances of orange colour: the hills, i.e., the highest parts are lighter, whereas the valleys, i.e., deeper parts are darker (Z scale range is 30 nm); (B) The corresponding Phase image shows that the surface is composed of a single type of material in terms of physical and mechanical characteristics (single colour depicts the same material properties across the scanned area) (Z scale range is 20° in this image). It is evident that the surface is made of mineral grains of various sizes and shapes, with domination of larger mineral plates (~100 nm). Matching of Phase and Height images shows that the dark lines on Phase image represent edges of the mineral grains. (C) The corresponding Amplitude image (Z scale range: 140 mV). The Amplitude image of the AFM is edge sensitive, so it nicely distinguishes between the individual elements of the surface pattern. However, we prefer the Phase image for measurements of grains' dimensions, since the Phase image also shows whether all elements belong to the same material. If the grains were measured only on Height or Amplitude images, it would not be possible to assure that all measured grains belong to the same material (e.g., mineral) which would lead to erroneous interpretations.

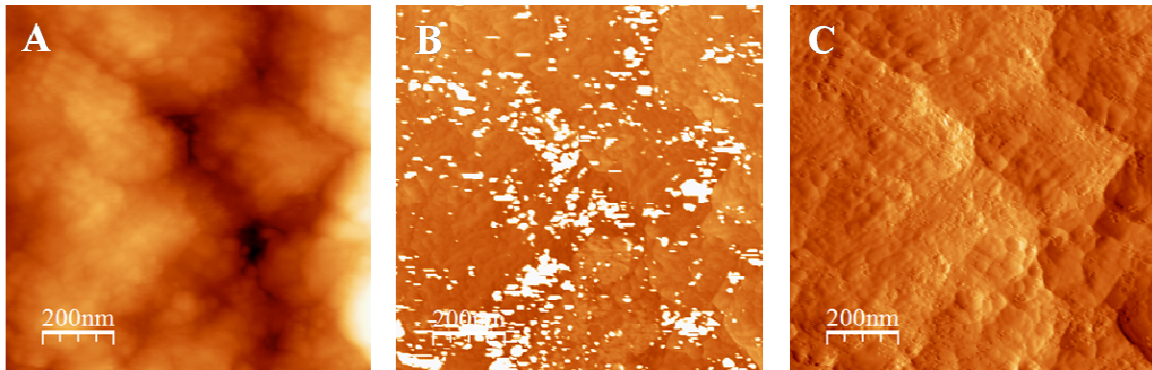


**Figure 40.** Atomic force microscopy images ( $1\ \mu\text{m} \times 1\ \mu\text{m}$ ) of the external cortical surface of an elderly woman with sustained hip fracture (age 78 years): (A) The Height image (Z scale range is 110 nm); (B) The corresponding Phase image (Z scale range  $60^\circ$ ). The Phase image uses different nuances of colour to depict the areas of different material properties across the scanned area. Here, note two different phases: the light brown-orange representing bone mineral and the white patches scattered throughout the surface indicative of surface dirt. (C) The corresponding Amplitude image (Z scale range: 600 mV). Without checking the Phase image, surface dirt can be mistaken for mineral grains and erroneously included in quantitative analysis.

Statistical analysis of mineral crystals showed a particular distribution of crystal sizes extending to higher values in hip fracture cases with a mean mineralite size of  $65.22\ \text{nm} \pm 41.21\ \text{nm}$ . In contrast, control cases displayed significantly smaller mineral crystals in outer cortical surface ( $36.75\ \text{nm} \pm 18.49\ \text{nm}$ ,  $p < 0.001$ , Figures 37 and 38).

The control group showed unimodal grain size distribution (peak position: 35 nm), while the data deconvolution revealed two distinct peaks in the fracture cases reflecting two groups of mineral crystals with respect to their maximum size. The peak positions in the fracture group were located at 36 nm and 84 nm (Figure 41) and the occupied areas under both curves were similar (Figure 41).

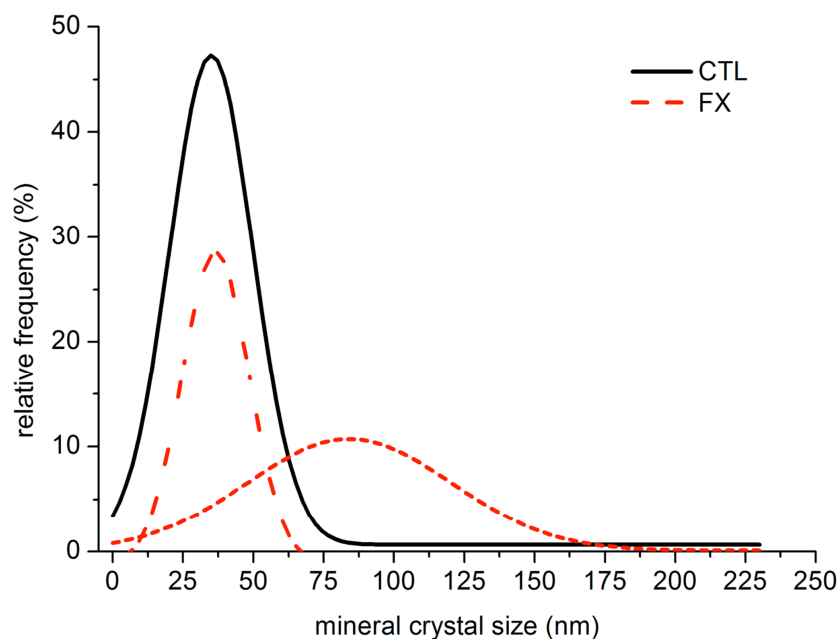


**Figure 41.** Deconvolution of mineral crystal sizes in the investigated subject groups. Note a bimodal distribution of the sizes in the fracture group (dashed lines, FX) with the peak positions at 36 nm and 84 nm, in contrast to unimodal distribution with peak position at 35 nm in the controls (full line, CTL).

Advanced nanomorphological analyses revealed certain differences in surface characteristics and morphological complexity of the cortical bone in investigated groups. Linear fitting of the PSD data allowed calculation of the PSD slope that is considered as a material/surface characteristic. It should be noted that PSD “curve” of the cortical bone in women with hip fracture showed steeper slope (Figure 42), which indicates that larger elements contribute more to the structure of the surface.

Roughness analysis in the cortical specimens in hip fracture group showed a trend towards a lower surface fractal dimension ( $1.40 \pm 0.13$  vs.  $1.56 \pm 0.14$ ) indicating lower and/or slower surface mineral deposition processes, which might suggest a decreased periosteal apposition in patients who would suffer from hip fracture.

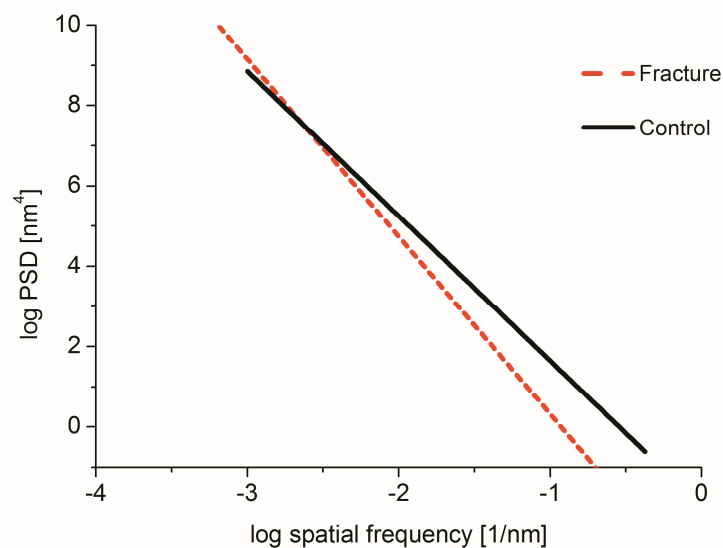


**Figure 42.** Fitted PSD curves of the fracture and control groups.

#### 4.4.2. Assessment of other levels of cortical bone hierarchy

##### 4.4.2.1. Analysis of cortical microarchitecture at the superolateral femoral neck

Micro-CT analysis of the cortical bone samples that stem from the superolateral femoral neck showed a tendency towards increased cortical porosity in the fracture group with larger pores and decreased apparent density of bone tissue ( $p>0.05$ ) (Table 13).

Pearson's correlation analysis showed that pore diameters significantly correlated with cortical porosity ( $R=0.766$ ,  $p=0.027$ ). Cortical porosity showed significant negative correlation with apparent density of the bone tissue ( $R=-0.783$ ,  $p=0.022$ ).

**Table 13.** Estimated marginal means for micro-CT parameters (age-adjusted).

Structural Indices	Groups	Mean	S.E.M.	95% CI	
				lower	upper
BV/TV [%]	control	92.1	2.1	86.7	97.4
	fracture	89.4	2.1	84.0	94.7
Ct.Po [%]	control	7.9	2.1	2.6	13.3
	fracture	10.6	2.1	5.3	16.0
Po.Dm [mm]	control	0.078	0.016	0.037	0.120
	fracture	0.107	0.016	0.066	0.149
T.Dn [mg HA/cm <sup>3</sup> ]	control	935	36.7	840	1029
	fracture	903	36.7	808	997

Abbreviations: S.E.M. – standard error of mean, CI – confidence interval, BV/TV – bone volume/tissue volume, Ct.Po – cortical porosity, Po.Dm – pore diameter, T.Dn – density of bone tissue

##### 4.4.2.2. Assessment of osteocyte lacunar network

The number of osteocyte lacunae, as a representative of osteocyte network, was evaluated per given bone area on recorded backscatter electron images of the cortical bone specimens. The fracture cases showed a less numerous osteocyte lacunar network, where mean osteocyte lacunar number per bone area was lower than in the controls ( $226 \pm 27 \text{ \#/mm}^2$  vs.  $247 \pm 32 \text{ \#/mm}^2$ ,  $p=0.05$ ).

#### 4.4.2.3. Evaluation of bone matrix composition

EDX analysis provided estimates of material composition and showed slightly higher amount of calcium in relation to phosphorus in the fracture group (Fracture group:  $2.38 \pm 0.01$  vs. control group:  $2.37 \pm 0.01$ ;  $p > 0.05$ ).

Analysis of bone mineral density distribution by qBEI in the superolateral femoral neck cortex showed significant differences between the fracture group and controls. Namely, the fracture group showed an overall shift to higher calcium content which is reflected in significantly increased mean Ca content, increased peak Ca content and significantly decreased percentage of bone area mineralized less than the 5<sup>th</sup> percentile of the reference range of the control group (Ca low) (Table 14, Figure 43). The FWHM of Ca distribution (Ca width) was lower in the superolateral neck cortex of the fracture cases demonstrating a more homogenous profile of tissue mineralization.

**Table 14.** Bone mineral density distribution in the cortical bone of the superolateral femoral neck in fracture group (FX) and control group (CTL) of elderly women.

Data are expressed as Mean  $\pm$  SE. (Wt% - weight percent,  $p$  -  $p$  value)

	<b>Ca mean</b> [Wt%]	<b>Ca peak</b> [Wt%]	<b>Ca width</b> [Wt%]	<b>Ca low</b> [% bone area]	<b>Ca high</b> [% bone area]
<b>CTL</b>	$25.162 \pm 0.142$	$25.824 \pm 0.121$	$4.894 \pm 0.175$	$5.15 \pm 0.60$	$5.16 \pm 0.66$
<b>FX</b>	$25.836 \pm 0.090$	$26.307 \pm 0.070$	$4.041 \pm 0.044$	$2.52 \pm 0.28$	$5.48 \pm 0.52$
<b><math>p</math></b>	$<0.001$	$0.001$	$<0.001$	$0.001$	$0.702$

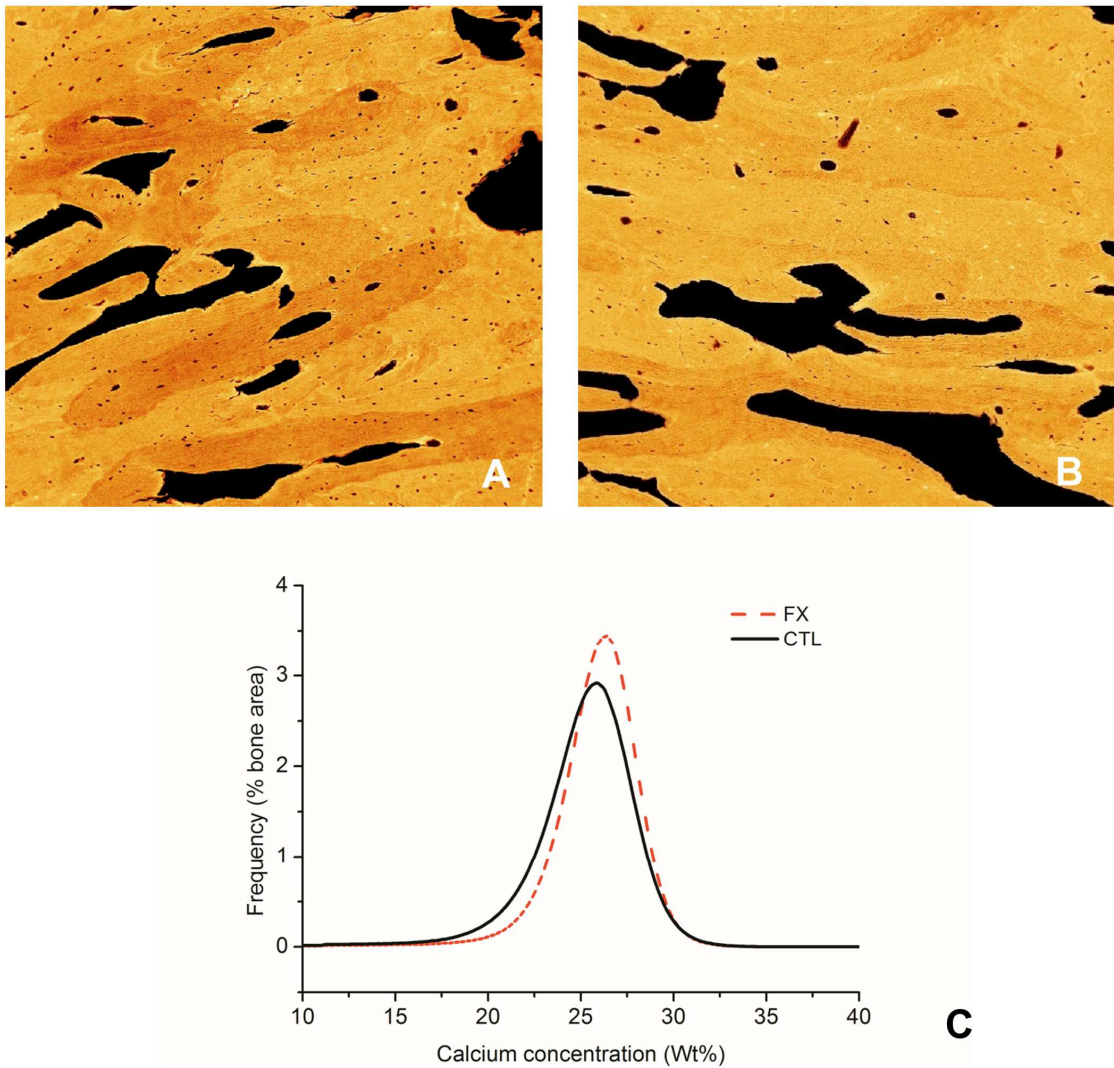


**Figure 43.** Differences between the fracture and control groups at the composition level. Backscattered electron micrograph of a representative cortical field in a control woman (A) and a woman with hip fracture (B) (calcium concentration is related to the nuance of colour, where lower calcium values in a particular spot are darker and higher calcium values lighter). (C) Bone mineral density distribution (distribution of calcium concentrations) in fracture (FX) vs. control group (CTL). Note that the fracture group shows a shift to a higher mineralization degree.

#### 4.4.3. Reference point indentation assessment of the material properties of the cortical bone

Reference point indentation was used to extract different mechanical properties of the cortical bone in both fracture and control cases. While the same force was applied on the test probe in both groups, the external cortex of the fracture group showed a tendency to achieve a higher 1<sup>st</sup> cycle indentation distance and a total indentation distance and a higher indentation distance increase (Table 15), however without achieving statistical significance.

In particular, indentation distance increase which refers to the difference between indentation distance of the first and last cycles showed approximately a 20% increase in the fracture group, revealing that successive indentations are more detrimental for them, compared to the control group.

**Table 15.** Age-adjusted estimated marginal means of the mechanical parameters obtained in RPI testing.

Reference Point Indentation Indices	Groups	Mean	S.E.	% of difference fracture vs. control
1st Cycle Indentation Distance (ID 1) [ $\mu\text{m}$ ]	control	12.63	1.180	10.55
	fracture	13.96	1.125	
Total Indentation Distance (TID) [ $\mu\text{m}$ ]	control	13.12	1.263	11.97
	fracture	14.70	1.204	
Indentation Distance Increase (IDI) [ $\mu\text{m}$ ]	control	1.290	0.215	20.54
	fracture	1.555	0.205	
Average Creep Indentation Distance (CID) [ $\mu\text{m}$ ]	control	0.658	0.038	2.58
	fracture	0.675	0.036	
Average Energy Dissipated (ED) [ $\mu\text{J}$ ]	control	2.705	0.155	-9.09
	fracture	2.459	0.148	



The average dissipated energy which corresponds to mean area under the load-displacement curve trended to lower values in women who sustained a fragility fracture, suggesting that these individuals require lower work to mechanical failure at micro-level (Table 15, Figure 44).

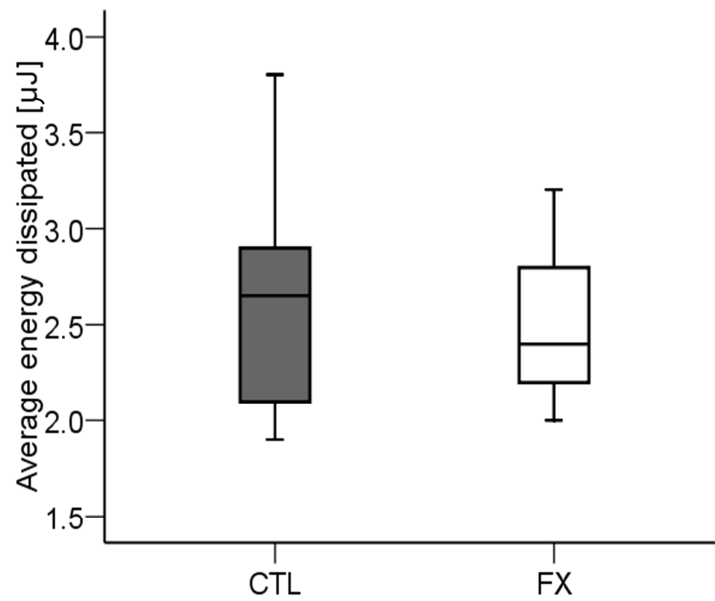


**Figure 44.** Box-plot diagram of average energy dissipated during indentations in control (CTL) and fracture (FX) groups.

#### 4.4.4. Percentage of inter-group differences at various length scales

Figure 45 shows percent of differences between the fracture and control groups at various hierarchical levels of the superolateral femoral neck cortex.

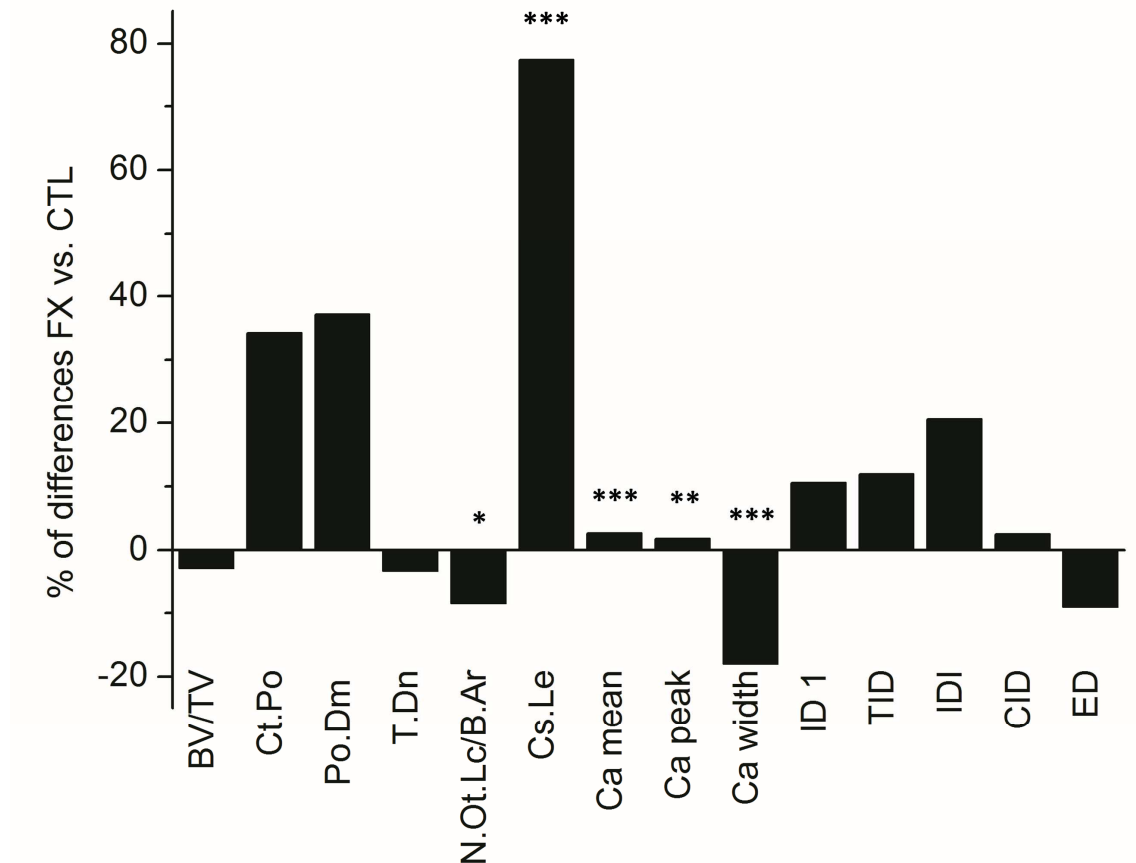


**Figure 45.** Multi-level differences between the fracture (FX) and control groups (CTL) in the cortical bone of the superolateral femoral neck (\*  $p < 0.05$ , \*\*  $p < 0.01$ , \*\*\*  $p < 0.001$ ). Abbreviations: BV/TV – bone volume fraction, Ct.Po – cortical porosity, Po.Dm – pore diameter, T.Dn – tissue density, N.Ot.Lc/B.Ar – number of osteocyte lacunae per bone area, Cs.Le – mineral crystal size (length), Ca – calcium, ID 1 – indentation distance in 1<sup>st</sup> cycle, TID – total indentation distance, IDI – indentation distance increase, CID – creep indentation distance, ED – average energy dissipated.

## **5. DISCUSSION**

In this study, we have undertaken a complex structural characterization of the femoral neck's trabecular and cortical bone compartments at various levels of bone hierarchical organization, in women of various ages and fracture statuses. Our approach comprised analyses of the trabecular bone microarchitecture, nanostructure and matrix composition, as well as assessment of bone mechanical behavior. Likewise, microarchitectural, nanostructural and compositional properties of the cortical bone were explored, along with consideration of bone mechanical competence. Taken together, this complex hierarchical evaluation revealed evidence of microarchitectural and nanostructural/compositional basis of increased bone fragility at the femoral neck in elderly women.

### **5.1. Microarchitectural basis of trabecular bone fragility**

It is generally held that bone microarchitecture is an important contributor to bone strength (Brandi, 2009; Rizzoli, 2010). However, although etiology of age-related hip fractures has been in focus for decades, there are still limited data on trabecular microarchitecture in the proximal femur of the hip fracture cases. Ciarelli et al. (2000) found a substantially lower bone volume fraction, trabecular number and connectivity in the individuals with fractures, thus documenting the importance of trabecular microarchitecture for sustaining hip fracture; however, it referred just to the femoral head region which is not the site directly involved in majority of hip fractures.

In this study we performed 3-D analysis of trabecular microarchitecture in the femoral neck of postmenopausal women with hip fracture and in a control group. Our findings revealed that the trabecular microarchitectural properties of the femoral neck differed significantly between the fracture and non-fracture groups in a *region-dependent manner*. Namely, particularly the superolateral region displayed outstanding trabecular microarchitectural weakness in elderly women who had sustained the femoral neck fracture. Human proximal femur is subject to a complex loading pattern during daily activities (Hert, 1994; Verhulp et al., 2008), where a larger proportion of the load on the femoral neck trabeculae is borne by the inferomedial group, while the

superolateral neck experiences only modest stresses and strains (Hert, 1994; Kalmey and Lovejoy, 2002; Rudman et al., 2006; Djuric et al., 2010). In contrast, the superolateral neck becomes severely loaded during a sideways fall and represents a fracture-initiating site (Verhulp et al., 2008; Bakker et al., 2009). The results of our study indicated that almost all microarchitectural parameters (trabecular bone volume fraction, connectivity density, SMI, trabecular separation and trabecular thickness) in the superolateral neck region were significantly worse in those women who had sustained hip fracture. These findings mirror diminished biomechanical competence of trabecular bone (Ciarelli et al., 2000; Legrand et al., 2000; Liu et al., 2006) and its failure to successfully disperse the forces exerted on the proximal femur during a fall. Therefore, it is likely that the interaction between severe impact load during a fall and weakened microarchitecture plays a crucial role in particular vulnerability of this femoral neck subregion. Moreover, some previous studies as well as the results from our study (*this thesis*) have reported deteriorated cortical microstructure in the superolateral neck of the hip fracture cases, which together with the observed trabecular deterioration may be a significant contributor to increased bone fragility (Bell et al., 1999b).

#### ***5.1.1. BV/TV and other microarchitectural parameters of the trabecular bone: Two sides of the same coin?***

Djuric et al. (Djuric et al., 2010) have recently reported that besides the bone volume fraction (a quantitative indicator of bone loss), other parameters more closely reflecting the bone internal organization and arrangement (*e.g.*: trabecular connectivity and separation) were significantly deteriorated in aged persons. The results of our present study show that apart from lower BV/TV and trabecular thickness, postmenopausal women with hip fracture displayed lower connectivity density, higher SMI and increased trabecular separation. After adjusting for the effects of BV/TV, the majority of inter-group differences disappeared, demonstrating that the microarchitectural changes are dependent on bone loss. Namely, bone loss manifests itself via the changes in trabecular microarchitectural parameters: trabecular thinning, rising the spacing between individual trabeculae, reducing trabecular connectivity and accentuating trabecular perforations leading to predominance of rod-like trabecular elements.

Only degree of anisotropy did not correlate with trabecular bone volume fraction; it expressed the independent role for hip fracture in the inferomedial neck irrespective of BV/TV. Increased trabecular anisotropy of the inferomedial neck in the fracture cases reflects preferential preservation of the trabeculae oriented in the direction of the dominant habitual stress. The phenomenon of increased anisotropy has been observed in aged femora (Djuric et al., 2010) and suggested as a mechanism to compensate for age-related net bone loss. However, although anisotropic trabeculae would be stronger and stiffer when loaded along the direction of dominant trabecular orientation (*i.e.*, during normal daily loading), such structure would be less resistant against collateral unusual (“*error*”) loads, such as falls (Ciarelli et al., 2000; Homminga et al., 2004; Djuric et al., 2010), like it was observed in our hip fracture cases.

### ***5.1.2. Aging process and age-related hip fractures: a microarchitectural perspective***

Majority of the previous studies regarding proximal femoral microstructure assessed microarchitectural changes during normal aging (Lundeen et al., 2000; Tsangari et al., 2007; Cui et al., 2008; Lochmuller et al., 2008; Chen et al., 2010; Djuric et al., 2010) and suggested (or indirectly concluded) the relevance of the changes in some of the micro-CT parameters for age-related bone fragility and hip fractures. However, since those studies are based on the data from normal subjects in normal aging, they cannot be fully extrapolated to the cases with fractures (Djuric et al., 2010). Aging process itself increases bone fragility via deterioration in bone microarchitecture (together with other mechanisms: (Beck et al., 2000; Busse et al., 2010a; Djonc et al., 2011)). It is corroborated by the details from the current study, given that the same micro-CT parameters that we found to be an important determinant of hip fracture had been previously demonstrated to change as a function of age (Djuric et al., 2010). However, our results further reveal that the women with hip fracture have more deteriorated trabecular microarchitecture than the controls, which raises the question of inter-individual variation in bone aging effects or additional factors leading to excessive damage in the microarchitecture in some persons. Given the cross-sectional nature of our study, it cannot be excluded that the persons who would eventually sustain a fracture have been already predisposed (in terms of unfavorable trabecular microarchitecture) even before reaching the observed age, which might be related to

genetic determinants of bone microstructural design. Beyond the causes of insufficient trabecular microarchitecture in hip fracture cases, our study points out that it is a significant determinant of bone fracture susceptibility.

Our microarchitectural analysis is limited by inherent restraints of cross-sectional studies, as it does not track an individual's aging process and sustaining fracture, but compares two different groups (fracture cases and the controls). A relatively small sample is due to analyzing cadaveric material; however, the sample size is quite consistent with other micro-CT studies. This study assessed only region-dependence of trabecular microarchitecture, without analyzing cortical compartment which is also important for overall bone strength, since certain data on regional variability in cortical bone were already available from other studies (Bell et al., 1999b). In the fracture group, contralateral (unfractured) hip bone was analyzed, in order to allow for scanning the femoral neck subregions of interest in a consistent manner. The contralateral hip was considered appropriate for analysis given that left and right sides reportedly did not differ significantly in densitometric and microarchitectural parameters (Bonnick et al., 1996; Rao et al., 2000; Dane et al., 2001; Chappard et al., 2008; Pierre et al., 2010). Since our intention was to scan complete femoral neck, such sample size had to be scanned in 36  $\mu\text{m}$  nominal resolution. Like in all imaging techniques the resolution limits the lowest detectable values (Djuric et al., 2013); therefore the findings of the present study are limited by the micro-CT scanning resolution of 36  $\mu\text{m}$  which could have affected the lower boundary of values of detected trabecular elements. However it is similar to many other human bone studies, allowing inter-study comparisons. In addition, although very thin trabeculae may be present, it is not much likely that such thin trabeculae would be a prevalent issue both in normal and fracture cases based on the range of trabecular dimensions in human bone reported in various classical histomorphometric studies (Ciarelli et al., 2000; Hordon et al., 2000; Ostertag et al., 2009). Therefore, although absolute values may be affected indeed, it is unlikely that such statistically significant differences would be neutralized.

## **5.2. Bone nanostructural changes during aging and bone compositional data show that the young and elderly women trabeculae differ even at the bone matrix level**

Atomic force microscopy was shown as a useful technique for bone nanostructural characterization, which was capable to discriminate between the young and aged bone materials.

AFM phase images have shown that the observed trabecular surface in terms of materials represents a continuous phase, which is consistent with the SEM findings on bovine femur trabeculae (Chen et al., 2011); nevertheless, granular organization of the phase was evident in our sample. Based on appearance and size of the grains, the material corresponds to extrafibrillar bone mineral, located on the surface of collagen fibrils (Landis et al., 1996; Sasaki et al., 2002; Hassenkam et al., 2004), forming a continuous scaffold (Hassenkam et al., 2004; Chen et al., 2011). However, we demonstrated that in contrast to the grains of young women, the mineral grains<sup>1</sup> in the elderly were larger on average, with bimodal size distribution. Diverse techniques applied in several species and various bones (mostly on isolated bone minerals) (*e.g.*: TEM, XRD, FTIR, SAXS) showed that bone mineral particles usually increased in size and crystallinity with age (Handschin and Stern, 1995; Paschalis et al., 1997b; Kuhn et al., 2008). However, some of the XRD studies on human material suggested that there was practically no change after the age of 30 (Handschin and Stern, 1995). Previous AFM studies which focused on mineral size only analyzed the dimensions of isolated crystals from immature (Tong et al., 2003) and mature bovine bones (Eppell et al., 2001), and suggested that crystals grow during maturation. However, the reported age-related crystal growth is not enough to explain such a large mineral grain size in elderly individuals observed by AFM in our study. Apart from crystal growth, there are two additional processes by which minerals can become bigger: crystal secondary nucleation leading to crystal proliferation, and aggregation (coalescence) of preformed crystals (Zinke-Allmang et al., 1992; Boskey, 2001). Given that our quantitative chemical analyses revealed unchanged calcium and phosphorus levels (as well as Ca/P ratio) in the elderly, increased mineral grain size in old women cannot be explained by raised

---

<sup>1</sup> In this study the term “mineral grain” or “mineral particle” has often been used instead of the term “mineral crystal” as it is beyond atomic force microscopy to determine the level of crystal perfection; however, whereas in materials science “grains” are a common term, it is usual in bone literature to refer to mineral constituents of bone matrix as “mineral crystals” regardless of their crystal perfection.

amount of mineral. Rather, our findings indicate that in aging the existing mineral is reorganized by coalescence to form larger grains, similar like it was suggested for turkey leg tendon maturation (Landis et al., 1993; Landis et al., 1996). As a rule of thumb, the surfaces with larger grains are expected to express a higher roughness; however, our observation of lower roughness in spite of larger grains in the elderly also gives support to the reorganization hypothesis, where fused grains form a larger flattened structure. However, for direct assessment of the mechanisms of grain enlargement experimental studies are warranted.

Despite the process of crystal enlargement, nearly 45% of mineral grains in elderly individuals are small grains which are similar in size to those observed in the younger women. Given that small mineral size has been attributed to more freshly remodeled bone - younger bone (Su et al., 2003), the small grains found in our elderly cases could correspond to new (remodeled) bone. In contrast, large grains might denote the areas which were devoid of remodeling process for a considerable amount of time. The question remains whether the large mineral grains could be a consequence of reported low rate remodeling process in the elderly (Noble, 2003; Busse et al., 2010a), or those crystals have just been too large or too mature to be remodeled (Boskey, 2001). The latter option is supported by the observation that degradation of calcium phosphate ceramics depends inversely on grain size (Grynopas et al., 2002), and the fact that the surfaces with larger grains weaken the cell-material interactions (Bose et al., 2010), which could also account for insufficient osteoclastic removal of such grains.

### ***5.2.1. Mechanical consequences of changed nanostructural pattern in aged trabecular bone***

In spite of general notion that bone mineral properties (amount of mineral; crystal size, shape and perfection) are significant determinants of bone mechanical status (Boskey, 2002), the precise effect of changes in the mineral phase on bone mechanical properties is not yet fully understood (Burr, 2002a). It was suggested that cracks could appear easier in more mineralized bone due to decreased amount of plastic deformation before ultimate failure (Burr, 2002a). However, the chemical analyses in our sample showed similar calcium content in the trabecular bone of young and elderly women. Apart from mineral content, changes in the morphology of mineral crystals were assumed to be



relevant for altering tissue local stress distribution (Mongiorgi et al., 1983) and increasing bone brittleness (Burr, 2002a). Generally, in various materials (including pure hydroxyapatite) the smaller grain size is associated with increased stiffness, higher compressive and tensile strengths and high fracture toughness of the material (Rezwan et al., 2006; Wang and Shaw, 2009; Bose et al., 2010). Given that strength of ceramics is inversely proportional to the square root of the grain size (Carter and Norton, 2007; Wagoner Johnson and Herschler, 2011), the structure with larger grains is mechanically disadvantageous in comparison to that with smaller grains. As a result, when during a fall the previously underloaded superolateral femoral neck is suddenly subject to high compressive stresses (Lotz et al., 1995; Beck et al., 2006), the stress is less well tolerated which can lead to fracture. Therefore, an age-related increase in mineral crystals' size as observed in our study suggests that altered nanostructure of the superolateral part of the femoral neck can be considered as one of the determinants of its particular fragility in advanced age.

Our nanostructural observations of the trabecular bone are limited by inherent limitation of cross-sectional observational studies, as we analyzed the individuals of various ages without possibility to follow the same persons during aging process. There are some restrictions of AFM technique as well, as the AFM probe tip radius (less than 10 nm) and scan size limit the minimum size of observable elements. In addition, AFM assesses the surfaces, without supporting bulk morphological evidence. Given that the thickness of the diamond wheel used for specimen sectioning was 3 orders of magnitude higher than the average grain size, the observed grain sizes could not be an artifact of the preparation procedure. On the other hand, the roughness might have been influenced by the sectioning; however, inter-specimen comparisons were possible since all the samples were prepared in the same way. In order to clarify the exact mechanisms of crystal growth, combining AFM with diffraction techniques would be particularly beneficial in further experimental studies.

### **5.3. Power Spectral Density (PSD) and Fractal Dimension (FD): Advanced nano-roughness analyses in trabecular bone may reveal potential correlates of bone tissue age**

The shape of PSD curves in materials science has been considered to reflect particular physical and chemical processes that participated in building the material surface (Lita and Sanchez, 1999; Lita and Sanchez, 2000; Jiang et al., 2005; Castro et al., 2007). Such connection has not yet been evaluated in a biological context, so it remains unknown whether the surface patterns of the mineralized bone matrix may reflect the process of bone remodeling. In that context, given that the remodeling process affects bone structure by substituting old bone tissue with fresh bone tissue, AFM analyses might elucidate differential nanostructural features that are potentially attributable to different tissue age. Based on characteristics of fractal dimension reported for other systems (Dimri, 2005), our findings of higher fractal dimension of the interfibrillar surfaces in the trabecular bone of young women suggest a greater degree of roughness and more structural complexity. Moreover, it was reported that a large fractal dimension indicates the significant contribution of high-frequency (*i.e.*, small-wavelength) fluctuations in the surface patterns (Constantoudis and Gogolides, 2008). Such frequent spatial fluctuations may correspond to our finding of smaller mineral grains dominating trabecular bone structure in younger individuals. Since smaller mineral crystals indicate the presence of younger bone (Su et al., 2003), higher fractal dimension of the bone matrix may correlate with a more recently remodeled structure.

Steeper PSD slope with a decreased fractal dimension in the trabeculae of elderly women denotes the dominance of large-dimension (low spatial frequency) surface patterns. These large morphological features of the mineralized bone matrix surface may reflect larger dimensions of the interfibrillar mineral grains that we observed by AFM. In contrast to small mineral grains, the larger crystals denote older unremodeled areas of bone. Bone remodeling is a key process in bone tissue, consisting of coupled and balanced bone resorption and bone formation phases (Parfitt, 1987; Martin, 2000; Burr, 2002b; Parfitt, 2004; Busse et al., 2010a). Several studies pointed out that the bone remodeling process might be hampered in aged human bone, causing accumulation of microcracks and hypermineralized lacunae, as well an increase in tissue age (Schaffler et al., 1995; Noble, 2003; Norman et al., 2008b; Busse et al., 2010a).

Without remodeling, senescing bone mineral would remain “*in place*” long enough to undergo energy-driven physicochemical processes leading to increased size and perfection of the mineral crystals, which was observed in the trabeculae of the elderly (Paschalis et al., 1997b). As these crystals grow, they reprecipitate in a dynamic equilibrium during which the mineral structure becomes more ordered and the interfibrillar surface less complex, decreasing the fractal dimension in the elderly as we observed in this study.

### ***5.3.1. Decreased fractal dimension in the elderly trabecular bone matrix suggests a decrease in bone toughness***

The present findings from advanced structural analyses have particular mechanical implications. Detection of only mineralized fibrils on the fracture surfaces led to the assumption that the mineral-mineral interface is the weakest link in bone (Fantner et al., 2006) and that bone usually cracks within interfibrillar space (Fantner et al., 2005; Fantner et al., 2006; Ebacher et al., 2012). Many failure modes and energy dissipation mechanisms are based on the separation of mineralized fibrils (Fantner et al., 2005; Gupta et al., 2005). Increased roughness and greater topographical complexity of interfibrillar matrix that we observed in young trabeculae would increase the interface available for cracking between the mineralized fibrils. In that way, increasing amounts of energy can be dissipated at the nano-level during the loading. Moreover, the presence of many grain boundaries in such a material might interact with crack propagation, interrupting it and/or increasing the tortuosity of the crack path. Overall, both mechanisms lead to increased bone toughness, where local nano-level failures can be regarded as a means of energy dissipation with the ultimate goal being to prevent a macroscopic bone failure (Ritchie, 2011). In addition, since it has been suggested that nanogranular friction between mineral particles increases yield resistance (Tai et al., 2006), higher surface roughness of the mineralized fibrils would have further positive effects on bone strength. In sharp contrast to the young individuals, lower surface roughness and reduced topographical complexity (decreased FD) in the elderly signify a decline in bone toughness, which renders their bone brittle and more susceptible to fracture. Reduced toughness is also the result of changes in collagen cross-linking in aged cohorts (Viguet-Carrin et al., 2006; Barth et al., 2010). Given that bone resistance

to fracture originates from various features at all levels of bone hierarchical organization (Busse et al., 2010a; Launey et al., 2010; Ritchie, 2011), it is important to try and extract the individual contributions of each feature to overall bone strength. In that context, our AFM study showed the particular contributions of the mineralized bone matrix from the morphological point of view. However, further experimental studies are necessary to provide direct demonstration of mechanical behavior at the interfibrillar level.

Additional studies are warranted to determine how the age-related changes in PSD and FD shown in the present study might interact with larger scale characteristics of tissue organization. For example, it would be important to determine how these nano-scale parameters might correlate with trabecular bone packets (Parfitt, 1979), which are an important toughening mechanism in trabecular bone because they create interfaces and potentially increase mineral heterogeneity as a consequence of differences in their mean tissue age (Roschger et al., 2008; Busse et al., 2009; Ciarelli et al., 2009; Smith et al., 2010).

In addition, the PSD curve presented as a straight line with a constant slope in both age groups of individuals indeed resembles the shape of PSD curve of a randomly rough surface with self-affine characteristics, which implies that vertical and lateral surface elements vary in a constant manner (Buchko, 1997; Cui et al., 2001). The constant slope appearance is a property of fractal objects (Cui et al., 2001; Dobrescu et al., 2004). Therefore, our data suggest fractality of mineralized bone matrix, albeit limited only to the investigated range of spatial frequencies at nano-scale due to the complex hierarchical organization of bone (Currey, 2012).

#### **5.4. Experimental evidence of deterioration in trabecular bone mechanical properties at the material level with aging**

By using AFM nanoindentation method, we have analyzed age-distinct nanoscale mechanical characteristics of bony trabeculae in the region where age-related hip fractures usually start (the superolateral region of the femoral neck). This study reveals experimental data that the bone trabeculae of elderly women express less elastic behavior at the material level, which (along with other features) makes them more vulnerable to unusual impact loads such as those originating from a fall.

In the literature the values for elastic moduli of bone material extend over two orders of magnitude depending on the study, reflecting both biological and methodological variability (Turner, 2009). Therefore, quantitative comparisons between the studies are problematic. However, inter-specimen comparisons within the study are relevant (Turner, 2009), as we made efforts to prepare and test all the specimens in a consistent manner. Our study showed a clear trend of lower elastic moduli of the bone matrix in the femoral neck trabecular bone in young women in comparison with the elderly. According to Currey's extensive tests on inter-relation of various bone mechanical properties (Currey, 2004), the higher modulus that we found in the elderly suggests decreased bone toughness reflecting less ability to absorb energy in the post-yield region of the stress-strain curve. Moreover, higher modulus of bone would be associated with decreased impact energy absorption and higher notch sensitivity (Currey, 2004). Notch sensitivity shows the propensity of material to fracture when a notch or a crack is present. The superolateral region of the femoral neck (which we analyzed in this study) does not experience significant stress during normal locomotion; however, it becomes subject to a high impact load during a fall on the trochanter in the elderly (Verhulp et al., 2008). Considering low elasticity of the bone found in elderly women, the impact would be less well tolerated, which can lead to a fracture in that femoral subregion. Moreover, in the case of already existing microcracks, increased notch sensitivity in the elderly would also contribute to weakened resistance to impact of a fall.

Bone is a nano-composite material consisting of mineral and organic phases (Fantner et al., 2006). Therefore, the changes in bone material properties may be regarded as a consequence of the changes in each of the phases and/or their interaction. In this study, we found larger mineral crystals in the trabecular bone of elderly women (enlarged due to crystal growth and/or coalescence processes), which might contribute to its decreased mechanical competence during an impact of a fall. The results from the current nanoindentation tests add experimental evidence to this assumption, based on strong correlation between the grain size and measured elastic modulus. In addition, the remaining part of variability in matrix elastic modulus which cannot be explained by increased mineral size could originate from age effects on other features, such as chemical composition of bone mineral and/or alterations in organic phase. We believe

that organic phase (mainly collagen, but perhaps non-collagenous proteins as well) contributes to age-dependent differences in elasticity; namely, based on collagen's low turnover rate the age vestiges reflected in morphological and chemical alterations in collagen were recorded in aged individuals (Nalla et al., 2006; Saito and Marumo, 2010). However, more detailed description of age-collagen interaction requires further studies.

It is evident that there is a higher elastic modulus at small indentation depths in both age categories; however, with increasing penetration depth, the elastic modulus decreases towards the stable value which can be considered as the true tissue modulus. The same behavior was evident for nanohardness. This observation resembles the phenomenon known in materials science as the *indentation size effect* (Mishra and Ghose, 2006) and is considered as a consequence of the strain gradient plasticity (Nix and Gao, 1998). In addition, our study suggests a technical matter in nanoindentation studies dealing with trabecular bone embedded in epoxy resins. Namely, in previous studies the effects of underlying acrylate on nanoindentation properties of bone were neglected (Rho et al., 1997; Fan et al., 2006; Gan et al., 2010). In contrast, the influence of an underlying material on the nanomechanical properties of thin films and coatings is a known issue in materials science, called *substrate effect* (Helvacı and Cho, 2005; Mishra and Ghose, 2006). In our study, it seems that at the highest indentation depths in both the young and old bone trabeculae, the values of elastic modulus and nanohardness converge towards the values of resin (see Figures 33 and 35). Indeed, the core idea in embedding is to support the bone tissue with the resin which resembles the bone hardness as much as possible (An and Gruber, 2003); however, since the resin fills the space all around trabeculae it is also possible that in the case of high indentation depths there is already an influence of the underlying resin on the measured values of the bone layer. Therefore, our findings might suggest that with indentation depths exceeding 400 nm the effects of embedding resin should be considered when interpreting the results.

Macro- and/or micromechanical tests on bone specimens were applied previously by various authors (*e.g.*, Martens et al., 1983; Ciarelli et al., 2000; Fantner et al., 2004; Passi and Gefen, 2005; Reich and Gefen, 2006). However, since bone is an extremely complex hierarchical structure, those tests bear combined information from the material and structural properties, and it is impossible to extract the relative effects

of particular micro- or nanostructural features. The value of our study is that it succeeded in isolatedly assessing the age-related changes of the bone mineralized matrix and its mechanical significance, without interference from other hierarchical levels of bone structure. Therefore, the data from this study show that even if the macro- and microstructural parameters were the same between the young and elderly, elderly bone would still be more fragile due to lower quality and subsequent particular vulnerability of the material which it is composed of.

Apart from numerous advantages of nanoindentation method which are related to extracting material properties (Rho and Pharr, 1999b), this type of study has its restraints. Namely, this study is liable to inherent limitations of observational cross-sectional study design; *i.e.*, it does not follow the same person during aging process. The purpose of this study did not include analysis of femora with fractures, but focused just on skeletal healthy individuals (young *vs.* old). The size of the sample is limited, but still it is quite comparable (Bar et al., 1999; Fan et al., 2006; Fan et al., 2007; Fratzl-Zelman et al., 2009), or sometimes even superior to other nanoindentation studies (Rho et al., 1997; Rho and Pharr, 1999a; Rho et al., 1999a; Rho et al., 1999b; Hengsberger et al., 2001). In addition, Oliver-Pharr method has certain limitations: it considers the material as elastic with time-independent plasticity, it fixes Poisson's ratio of the bone to 0.3, and assumes isotropic nature of bone (Oliver and Pharr, 1992; Thurner, 2009). However, it is the method most commonly used in material science and there is a lot of experience with its application to the bone (Rho and Pharr, 1999b; Thurner, 2009). Although nanoindentation of bone under dry conditions does not give absolutely correct values, it is very common and reliable method (Rho et al., 1997; Rho and Pharr, 1999b; Rho et al., 1999a; Rho et al., 1999b; Gan et al., 2010). In order to minimize the drying artifacts, the samples were kept dry for more than 24 hours before the analysis, since it was previously shown that the modulus value stabilizes after 24 hours of drying (Hengsberger et al., 2002). Nevertheless, the concerns with Oliver-Pharr method are not deleterious for the results of this study, since we were less interested in absolute values, but rather focused on the young *vs.* elderly inter-specimen comparisons which were appropriate since all the specimens were treated and analyzed in the same way.

### **5.5. Young and aged individuals' bone nanostructural/compositional features at the external (periosteal) cortical bone surface suggest that this surface is not “a *Lazy Mary*”**

Several AFM studies have recently assessed the cortical compartment of animal or human bone (for a review see: Sasaki et al., 2002; Bozec et al., 2005; Thurner, 2009; Wallace, 2012). However, quantitative analyses of human cortical bone nanostructural features have been insufficient. Given that our quantitative analysis of bone nanostructure revealed that bony trabeculae bear *tissue age information*, we were interested to determine whether age effects in nanostructure are also visible at the external cortical (periosteal) surface of the femoral neck which is a frequent fracture site in elderly persons.

The periosteal surface of the cortical bone in the human femoral neck still represents an unsolved riddle since its nanostructure has not been explored and there is considerable controversy about the existence of bone apposition process at this surface (Cullinane and Einhorn, 2002; Orwoll, 2003; Seeman, 2003; Blizotes et al., 2006; Seeman, 2007). Based on the hypothesis that the analysis of nanostructure may provide evidence of bone surface dynamics and tissue age, in this study we performed AFM nano-scale characterization of the external cortical surface from the femoral neck in young *vs.* elderly women. Our aim was to address age-related differences in bone nanostructure and explore the presence or absence of nanostructural signs of periosteal bone activity in young *vs.* elderly women in the femoral neck region.

While other studies focused on different areas of cortical bone in various species (Hengsberger et al., 2001; Reilly et al., 2001; Wallace et al., 2010; Lin and Xu, 2011), our AFM study on the human femoral neck in young *vs.* elderly females represents the first qualitative and quantitative AFM characterization of the periosteal (external) cortical bone surface. Namely, in contrast to other bone surfaces, the external or periosteal cortical bone surface has been widely neglected in previous research, which resulted in many still unresolved issues about its structure and dynamics (Seeman, 2007). Whereas the role of periosteum is more straightforward in growing bones (Rauch, 2007), there is a dilemma regarding the periosteal surface in adults, particularly in the femoral neck region. Namely, while the clinical literature mainly indicates that it is a quiescent and inactive surface (Cullinane and Einhorn, 2002) with less cellular



periosteum when compared to other bone sites (Allen and Burr, 2005), other studies speak for existence of active re/modeling events: adding new bone to the surface without prior osteoclastic resorption (periosteal apposition) (Parfitt, 2002; Power et al., 2003), or bone formation following bone resorption processes (bone remodeling) (Orwoll, 2003).

Assuming quiescent periosteal surface (Cullinane and Einhorn, 2002) and given that outer cortical lamellae are unreachable by intracortical remodeling (Akkus et al., 2003), the periosteal bone surface would possibly store *time information*, bearing clear signs of increased tissue age with person's aging. Namely, when the mineral crystals stay "in place" undisturbed long enough, the processes of crystal growth and/or aggregation can take place leading to an increased crystal size (Boskey, 2001). However, our AFM findings showed consistent bone nanostructural patterns at the external cortical surface in both age groups. Specifically, both in young and elderly women the investigated bone surface was composed of small densely packed mineral crystals that were similar to small mineral grains that we observed using the same in situ AFM technique in trabecular bone specimens of young women. Furthermore, several spectroscopic and microscopic bone studies, as well as our AFM data in trabecular bone, demonstrated that smaller mineral crystals were a sign of newly deposited or more freshly remodeled bone (Eppell et al., 2001; Akkus et al., 2003; Su et al., 2003), while dominance of larger minerals was suggestive of older tissue age (Paschalis et al., 1997b; Eppell et al., 2001).

Our advanced nanostructural analyses (power spectral density and fractal dimension) showed similar surface texture and unchanged morphological complexity of the external cortical surfaces between young and elderly women, suggesting that both express similar tissue age (based also on our analyses in trabecular bone) and similar rate of mineral deposition at the surface (Sahoo et al., 2006). Namely, as portrayed in experimental studies in materials science that the power spectral density (PSD) slopes depended on the rate of particle deposition on the surface, slow surface deposition rate of the material would result in smooth and less complex surface morphology (lower roughness, lower fractal dimension) (Sahoo et al., 2006).

Apart from the size of mineral crystals which was linked to bone tissue age in several studies of cortical and trabecular bone (Su et al., 2003; Kuhn et al., 2008),

composition of matrix minerals which can be expressed in the form of Ca/P ratio has been also regarded as an indicator of bone age (Legros et al., 1987; Grynepas, 1993; Skedros et al., 1993; Huja et al., 2006; Kuhn et al., 2008; Roschger et al., 2008; Busse et al., 2009; Busse et al., 2010a; Busse et al., 2010b). Our spectroscopic analysis showed consistent Ca/P ratio between the groups. Therefore, two independent measures of bone tissue age in our study (crystal size and relation of calcium to phosphorus) showed the same range of values between the groups, suggesting similar surface tissue age at the external cortex between young and elderly women. Moreover, domination of small crystals at the cortical surface in both age groups and low fractal dimensions may support the theory of slow but continuous new bone deposition at the periosteal surface, especially considering the parallel increase in neck outer diameter. These results are in line with several studies showing that periosteal apposition continues during adulthood (Beck et al., 2000; Szulc et al., 2006; Seeman, 2008; Djonic et al., 2011), which is considered as a compensatory mechanism for offsetting age-related net bone loss (Beck et al., 2000; Seeman, 2008; Djonic et al., 2011).

In addition, our observation of AFM topography images frequently revealed fibril-like packing of mineral crystals that might correspond to mineralized collagen fibrils, *i.e.*, basic building blocks of the bone matrix as shown in previous studies (Hassenkam et al., 2004; Hassenkam et al., 2005; Kindt et al., 2005). However, since the main focus of our study was on organization and appearance of mineral plates, our experimental protocol did not encompass demineralization that would allow direct visualization of collagen fibrils (Kindt et al., 2007; Thurner et al., 2007; Wallace et al., 2010). Nevertheless, the diameters of the mineralized fibrils are compatible with the range of diameters of the collagen fibrils reported in the literature (Thurner, 2009), and we found no significant age-related differences in morphology or size of those fibrils at the external cortical surface.

#### ***5.5.1. Fresh bone at the external cortical bone surface: Periosteal bone apposition***

Although signs of periosteal remodeling were found in nonhuman primates (Bliziotis et al., 2006), it is still unknown whether remodeling indeed takes place at the periosteal surface in the human femoral neck. Our findings of new (young) bone at the human external cortical surface may actually be indicative of bone modeling, *i.e.*, periosteal

apposition. The latter is further supported by a clear tendency to increase femoral neck outer diameter in analyzed subjects with advanced age (Figure 24). In that context, the presence of “young” bone at the external cortical surface even in a 94-year-old woman suggests that the process of periosteal apposition in women might be continuous throughout life. Our results are in line with several studies which suggested that periosteal apposition continued during adulthood (Beck et al., 2000; Szulc et al., 2006; Seeman, 2008; Djonic et al., 2011), trying to preserve the deleterious effects of age-related net bone loss (Beck et al., 2000; Seeman, 2008; Djonic et al., 2011). Namely, periosteal apposition increases bone outer diameter, where distributing bone tissue just a little bit further from the neutral axis leads to a significantly increased cross-sectional moment of inertia and consequently improves bone resistance to bending (Beck et al., 2000; Beck, 2007; Seeman, 2008; Djonic et al., 2011).

Indeed, our data suggest that outer cortical surface is renewed throughout life, and the characteristics of its surface dynamics might be important element of bone quality. In this regard, mechanical properties of outer cortical surface received attention in nice recent work by Diez-Perez et al. (Diez-Perez et al., 2010; Güerri-Fernández et al., 2013). Namely, these authors introduced a novel method - “reference point indentation” - which represents a microindentation technique for in vivo measurement of tissue material properties at the external cortex in humans (Diez-Perez et al., 2010). It was reported that mechanical probing of the external cortical surface better discriminated between the patients with fragility fracture and healthy controls than did the standard densitometry (Diez-Perez et al., 2010). Another study additionally showed usefulness of such methodological approach since it revealed that among long-term bisphosphonate(BP)-treated osteoporotic patients those that experienced BP-related atypical fractures showed inferior material properties of the external cortical surface (Güerri-Fernández et al., 2013). Therefore, periosteal cortical surface may indeed represent a valuable tissue for assessment of bone health.

### ***5.5.2. Mechanical requirements may drive periosteal bone apposition during aging***

The exact “driving force” for periosteal bone apposition is still unknown. The hormonal theory suggesting that postmenopausal estrogen deficiency removes a constraint on periosteal apposition (Seeman, 2003) is not fully supported by our study, since there

were no nanostructural differences in periosteal cortical surfaces between premenopausal and postmenopausal women. Moreover, experimental studies in materials science portrayed that the power spectral density (PSD) slopes depended on the rate of particle deposition on the surface (Sahoo et al., 2006). In that context, our findings of unchanged power spectral density graphs and fractal dimension in elderly women suggest that their rate of periosteal bone apposition is not altered significantly. Therefore, instead of hormonal theory, the “mechanostat” theory assuming that periosteal apposition is regulated by mechanical requirements (van der Meulen et al., 1996) seems much more likely in this context. More specifically, widening of the femoral neck via periosteal apposition was suggested to occur in response to weakening of the cortex due to its “trabecularization” by negative bone turnover in aged persons (Power et al., 2005). However, our AFM data indicated traces of periosteal dynamics irrespective of age, *i.e.*, there were nanostructural signs of bone formation activity not only in elderly but also in young adult women. Therefore, our findings reinforce the observation that, in the case of bending loads, there is a strain gradient through the cortex where the maximum strains are reached at the periosteal surface (Beck et al., 2000; Tanck et al., 2006; LaMothe and Zernicke, 2008; Busse et al., 2010a) throughout life. In that context, since bone structurally adapts to predominant mechanical stimuli (LaMothe and Zernicke, 2008; Djuric et al., 2010; Skedros et al., 2012), these high strains are most likely responsible for the observed periosteal bone formation across life.

The cross-sectional design of the study imposes certain limitations since the processes can be only inferred, which cannot replace direct dynamic observations. The AFM analyses are performed on relatively small sample size, due to analyzing human cadaveric material; however, the sample is larger than in majority of other AFM studies, even those analyzing animal bones (Hengsberger et al., 2001; Tong et al., 2003; Hassenkam et al., 2004; Hassenkam et al., 2005; Kindt et al., 2005; Thurner et al., 2005; Hassenkam et al., 2006; Kindt et al., 2007; Lin and Xu, 2011). Since our previous AFM analysis of the nanostructural signs of young *vs.* old tissue showed that they are notably different (*this thesis*), and given that in this study confidence intervals for nanostructural and chemical properties in both age groups were almost completely overlapped, it is unlikely that increasing sample size would bring up significant differences. Although

absolute values of the parameters analyzed in this study (mineral grain size, Ca/P ratio) might be dependent on the applied techniques, uniform processing of all specimens allowed reliable inter-specimen comparisons.

## **5.6. Hierarchical assessment of cortical bone at the superolateral neck in the fracture and control groups reveals signs of bone fragility at various length scales**

Using a combined analysis that focuses on size-scales ranging from the nano-to-micro levels in cortical bone from the superolateral femoral neck, we showed a wide range of differences between the fracture group and control cases. In particular, our study suggests that a number of detrimental changes at various hierarchical levels of cortical bone may render bone fragile and thus help to explain a higher susceptibility to macroscopic failure with advanced age.

### ***5.6.1. Microstructural basis of increased cortical bone fragility***

Already at the level of the cortical microarchitecture, the fracture group showed higher porosity with larger pores, however, without reaching statistical significance. In the previous studies, Bell and co-workers also reported high porosity values in the cortical femoral neck in the fracture cases (Bell et al., 1999a; Bell et al., 1999b; Bell et al., 1999c; Bell et al., 2000; Bell et al., 2001). It was suggested that merging adjacent clustered osteons during the bone resorption phase leads to increasing porosity in fracture cases (Jordan et al., 2000). However, even in the non-fracture cases, the superolateral femoral neck shows higher porosity than the inferior neck or the femoral diaphysis due to significant enlargement of pores (Chappard et al., 2013). Increasing porosity in the fracture group would favor local stress concentrations and flaws, thus promoting deleterious effects on bone integrity.

In contrast to large-sized cortical pores (~ 100  $\mu\text{m}$ ), osteocyte lacunae were less frequent in the fracture group. This denotes a hampered network for detecting microcracks and launching bone repair processes (Qiu et al., 2005; Busse et al., 2010a; Bernhard et al., 2013; Milovanovic et al., 2013) which is particularly harmful considering a higher degree of mineralization in the fracture group.

### 5.6.2. Nanostructural signs of cortical bone fragility

Different bone mineral characteristics, such as mineral content and composition, crystal shape and size, have been recognized to be potentially important for bones' mechanical integrity (Paschalis et al., 1997a; Boskey, 2002; Boskey, 2003; Boskey, 2007; Donnelly et al., 2010). While the composition and size of mineral crystals have repeatedly been assessed in bone via different spectroscopic methods (Thompson et al., 1983; Fratzl et al., 1991; Simmons et al., 1991; Handschin and Stern, 1995; McCreadie et al., 2006; Kuhn et al., 2008; Yerramshetty and Akkus, 2008; Gourion-Arsiquaud et al., 2009), their morphological evaluation due to direct visualization in bone remains of particular importance (Hassenkam et al., 2004; Hassenkam et al., 2005; Chen et al., 2011). In this context, our AFM data showed that the external cortex of the superolateral subregion in the femoral neck demonstrated distinct nanostructural patterns between the fracture and control group in elderly women, where an increased proportion of larger mineral particles was observed in the fracture group. In human trabecular bone, it has been shown that bone nanomechanical properties significantly depend on mineral crystal size, where larger crystals correlated with decreased mechanical competence (*this thesis*). Additionally, studies dealing with synthetic hydroxyapatite particles showed that lower material strength occurred with larger grain size (Wagoner Johnson and Herschler, 2011). In nanocrystalline synthetic hydroxyapatites increased grain sizes of up to 140 nm without any phase changes were shown to substantially decrease the indentation toughness (Wang and Shaw, 2009). While smaller grains are able to deflect the crack path, intergranular fractures lead to higher dissipated energy and improved toughness. In contrast, larger grains are associated with transgranular cracking with inhibited crack deflection, thereby reducing the energy dissipation (Wang and Shaw, 2009) and increasing bone fragility.

There is a strain gradient through the cortex where the maximum strains are reached at the external cortical surface (Beck et al., 2000; Tanck et al., 2006; LaMothe and Zernicke, 2008; Busse et al., 2010a) throughout life. Because previous studies showed that the superolateral femoral neck undergoes significant impact stress during a sideways fall (Lotz et al., 1995) and hip fracture normally starts in the cortex of the superolateral femoral neck (Bakker et al., 2009), the changes in its osseous nanostructure may represent a crucial factor in fracture risk.

### ***5.6.3. Compositional imprints of increased cortical bone fragility: higher and more homogenous mineralization profile***

Distribution of the cortical bone mineralization at the femoral neck was analyzed in recent quantitative backscatter electron imaging or microradiography studies. In this context, conflicting results were reported in regard to the mineralization level in the fracture group (Loveridge et al., 2004; Fratzl-Zelman et al., 2009; Wu et al., 2009; Bousson et al., 2011). While some authors found a decreased degree of mineralization in the femoral neck in hip fracture patients (Loveridge et al., 2004; Fratzl-Zelman et al., 2009), others showed significantly increased mineral content in the inferomedial femoral neck (Wu et al., 2009). In our fracture group, we found a shift towards higher mineralization levels and a more homogenous mineralization profile. In general, during maturation the bone material accumulates more mineral which is essential for achieving bone mechanical strength (Currey, 2002). However, it has to be borne in mind that various bone mechanical properties do mutually compete, so that any structural and compositional alteration may result in mechanical imbalances as some mechanical properties would be improved while others are hampered (Currey, 2003; Currey, 2004; Ritchie, 2011). Therefore, increasing mineral content is beneficial for mechanical strength primarily in the elastic region of the stress-strain curve (*pre-yield zone*), whereas - in contrast - excessive calcium content has been shown to result in deleterious *post-yield* mechanical behavior of bone (Currey, 2004). In other words, increasing mineral content leads to increased stiffness, whereas the absorbed impact energy and bone toughness decline simultaneously (Currey, 2003; Currey, 2004; Currey, 2012). In this context, altered mineralization pattern that we found in the cortex of the superolateral femoral neck of the fracture cases may jeopardize bone toughness and impact energy absorption (Busse et al., 2009) which are both crucial properties relevant for avoiding bone failure under impact load during a sideways fall. Moreover, higher mineralization heterogeneity in control group may be beneficial as it creates interfaces and increases the path of the microcracks, thus increasing energy dissipation and preventing a macroscopic bone failure.

#### ***5.6.4. Mechanical evaluation of the bone material provides experimental evidence of decreased bone toughness in cortical bone of the fracture group***

Reference point indentation has the potential to reflect osseous changes at the nano/micro-level (Diez-Perez et al., 2010; Güerri-Fernández et al., 2013). Our findings from reference point indentation testing of the femoral neck cortical bone showed a tendency towards increased indentation distances (first cycle indentation distance, total indentation distance and indentation distance increase). This confirms data from an *in vivo* study using RPI on the external cortex of the human tibia that showed increased IDI, TID and CID in hip fracture patients (Diez-Perez et al., 2010). It has to be noted that RPI does not solely indent the surface, but rather indentation also produces micro-cracks similar like in bone fractures (Diez-Perez et al., 2010). We found a 20% increase in the indentation distance increase (IDI) which is a measure of damage resulting from repeated loading (Hansma et al., 2008). This suggests a decline in crack growth toughness in the fracture cases in comparison to the control cases (Diez-Perez et al., 2010; Gallant et al., 2013). Average energy dissipation signifies the amount of work until failure. In our fracture group, a tendency towards lower energy dissipation indeed reflects a higher fracture risk.

These analyses have a few limitations, first a cross-sectional study design implies that we cannot follow the same individuals and track whether they would sustain a fracture. Another limitation is a relatively small sample size, however it is comparable or superior to other studies with AFM and mechanical tests (Hassenkam et al., 2004; Hassenkam et al., 2005; Hassenkam et al., 2006; Lin and Xu, 2011).

#### **5.7. Summary of structural and compositional determinants of age-related hip fracture**

Our hierarchical characterization of the femoral neck's trabecular and cortical bone compartments revealed that deterioration in bone microarchitecture (decrease in trabecular bone volume fraction, trabecular thinning, trabecular perforations and loss of connectivity, as well as increased cortical porosity and cortical pore diameters) and reduction in osteocyte lacunar network (decreased osteocyte lacunar number per cortical bone area), as well as alteration in bone nanostructural (increased mineral crystal size, decreased surface roughness) and compositional features (increased mineral content



with more homogenous calcium distribution) were associated with age-related hip fragility (Figure 46). Each of these age-related deteriorations at various levels of bone organization contribute to increased bone fragility, by altering stress distribution in the bone and/or facilitating microcrack growth, hampering bone repair mechanisms and reducing bone toughness (Figure 46).

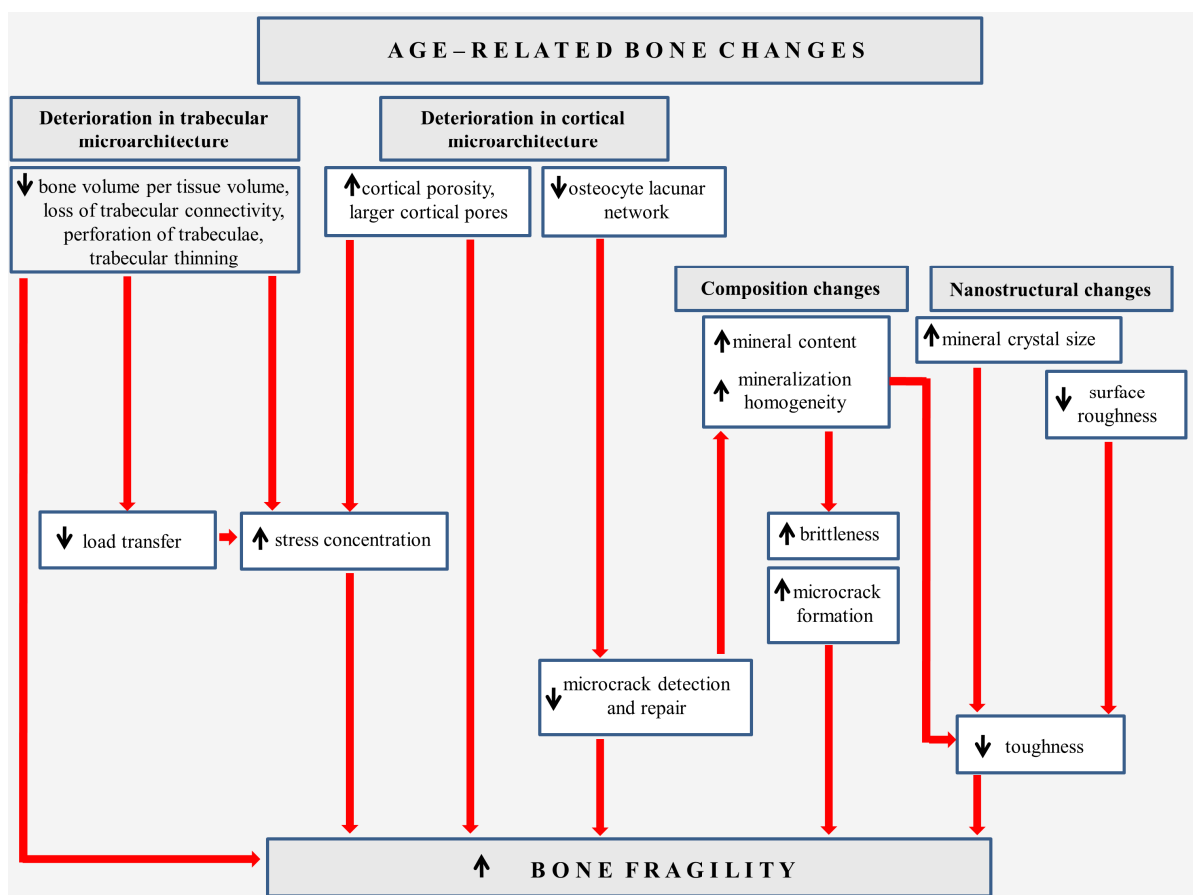


**Figure 46.** The determinants of age-related bone fragility at the femoral neck region in women

## 6. CONCLUSIONS

The results of this study yielded evidence for importance of microarchitectural and nanostructural bone features in age-related decline of bone mechanical properties.

Not only does the aging lead to deterioration in trabecular bone microarchitecture of the femoral neck region, but also, as our results revealed, there are significant differences in trabecular microarchitectural properties between the postmenopausal women with hip fracture and age-matched controls. The fracture cases presented impaired parameters of trabecular bone microarchitectural organization, particularly in the superolateral neck region. Considering the fact that the femoral neck fracture starts in that region, the observed preferential impairment of the superolateral neck trabecular bone in women with hip fracture reveals the region-dependent microstructural basis of bone fragility in elderly women.

Using atomic force microscopy as a powerful tool for nano-level examination of bone tissue provided new insights into the age-related effects on bone material and increased bone fragility in elderly women. Assessment of nano-level mechanical behavior (combined with nanostructural evaluation) of the bone matrix in individuals of different ages proved essential to achieve a more profound understanding of particular mechanical consequences of bone matrix aging, separately from age-related effects at other hierarchical levels of bone structure.

Namely, our in situ AFM study revealed differences in the trabecular bone nanostructure of the superolateral femoral neck between young and elderly women. In particular, we observed a bimodal distribution of the mineral crystal sizes in advanced age, showing that - apart from small crystals similar in size to those in the young - the elderly individuals also expressed a group of large crystals that could correspond to areas that were devoid of remodeling for considerable time. Given that chemical analyses showed unchanged calcium and phosphorus levels in the elderly bone, the increase in mineral particle size could not be a consequence of an increase in the mineralization degree; rather, it suggests the reorganization of the existing bone mineral to form larger grains in advanced age possibly by means of grain aggregation and fusion (coalescence). Based on the mechanical disadvantage of large-grained structures (decreased material strength), these nanostructural differences contribute to our

understanding of the increased fragility of the superolateral part of the femoral neck in aged females.

Analyses of AFM-derived power spectral density and fractal dimension at the nanometer scale have shown themselves useful for explaining differential trabecular bone fragility across age, and how their specific patterns may potentially correlate with bone tissue age. Namely, our findings showed decreased fractal dimension and less steep PSD trendline of the interfibrillar area of the femoral neck trabeculae in elderly individuals, adding new evidence for age-related differences at the level of mineralized bone matrix. Lower structural complexity and surface roughness of the interfibrillar area in elderly individuals, which was reflected in a decreased fractal dimension, may suggest a decreased energy dissipation during loading (decline in the bone toughening mechanism), which may in turn lead to increased brittleness and bone fragility in aged cohorts.

In addition to structural characterization of the bone material, nanoscale mechanical assessment of the femoral neck trabeculae between the young and elderly women provided direct evidence that the quality of bone material differs across age. The observed age-related alteration at the bone material level (less elastic behavior in the elderly) adds new experimental insight into the determinants of hip fractures in elderly women.

In contrast to trabecular bone, AFM analysis of the external cortical surface of the femoral neck revealed consistent qualitative and quantitative nanostructural features in young and elderly women. Our nanostructural findings of small mineral grains in both age groups and similar rate of mineral deposition along with unchanged Ca/P ratios suggest similar tissue age at the periosteal cortical surface both in young and elderly women. Beyond advanced morphological characterization of external cortical bone surface in young *versus* elderly women, our data may confirm that the femoral neck undergoes periosteal expansion with aging due to continuous periosteal new bone apposition.

The external cortical surface of the femoral neck in postmenopausal women with hip fracture displayed larger mineral crystals than in age-matched women without skeletal diseases. Based on observations that large-grained materials are accompanied by decreased mechanical properties in comparison with fine-grained fabrics, the

findings of larger crystals in the fracture group offer additional explanation for reduced toughness and decreased strength of the cortical bone observed in this study. In particular, considering that we analyzed the very surface where the fracture usually starts, these results contribute to the understanding of nanostructural basis of age-related bone fragility. Moreover, along with increased crystal size, a shift to a higher mineralization profile and a tendency to increased cortical porosity and reduced osteocyte lacunar network delineate that cortical bone of the superolateral femoral neck in the fracture group bears distinct signs of fragility at various levels of its structural organization. These results contribute to the understanding of osseous alterations involving several hierarchical levels in age-related bone fragility.

## 7. REFERENCES

- [1] Akkus O, Polyakova-Akkus A, Adar F, Schaffler MB. Aging of Microstructural Compartments in Human Compact Bone. *Journal of Bone and Mineral Research* 2003; 18: 1012-1019.
- [2] Allen MR, Burr DB. Human femoral neck has less cellular periosteum, and more mineralized periosteum, than femoral diaphyseal bone. *Bone* 2005; 36: 311-316.
- [3] An YH, Gruber HE. Introduction to Experimental Bone and Cartilage Histology. In: An YH, Martin KL, editors. *Handbook of Histology Methods for Bone and Cartilage*. Totowa - New Jersey: Humana Press; 2003, p. 3-31.
- [4] Anczykowski B, Gotsmann B, Fuchs H, Cleveland JP, Elings VB. How to measure energy dissipation in dynamic mode atomic force microscopy. *Applied Surface Science* 1999; 140: 376-382.
- [5] Bakker PMd, Manske SL, Ebacher V, Oxland TR, Cripton PA, Guy P. During sideways falls proximal femur fractures initiate in the superolateral cortex: Evidence from high-speed video of simulated fractures. *Journal of Biomechanics* 2009; 42: 1917-1925.
- [6] Banks E, Reeves GK, Beral V, Balkwill A, Liu B, Roddam A, for the Million Women Study C. Hip Fracture Incidence in Relation to Age, Menopausal Status, and Age at Menopause: Prospective Analysis. *PLoS Medicine* 2009; 6: e1000181.
- [7] Bar G, Delineau L, Brandsch R, Bruch M, Whangbo MH. Importance of the indentation depth in tapping-mode atomic force microscopy study of compliant materials. *Applied Physics Letters* 1999; 75: 4198-4200.
- [8] Barth HD, Launey ME, MacDowell AA, Ager JW, Ritchie RO. On the effect of X-ray irradiation on the deformation and fracture behavior of human cortical bone. *Bone* 2010; 46: 1475-1485.
- [9] Beck T. Extending DXA beyond bone mineral density: Understanding hip structure analysis. *Current Osteoporosis Reports* 2007; 5: 49-55.
- [10] Beck TJ, Looker AC, Mourtada F, Daphtary MM, Ruff CB. Age trends in femur stresses from a simulated fall on the hip among men and women: evidence of homeostatic adaptation underlying the decline in hip BMD. *Journal of Bone and Mineral Research* 2006; 21: 1425-32.

- [11] Beck TJ, Looker AC, Ruff CB, Sievanen H, Wahner HW. Structural trends in the aging femoral neck and proximal shaft: analysis of the Third National Health and Nutrition Examination Survey dual-energy X-ray absorptiometry data. *Journal of Bone and Mineral Research* 2000; 15: 2297-304.
- [12] Beck TJ, Ruff CB, Warden KE, Scott WW, Jr., Rao GU. Predicting femoral neck strength from bone mineral data. A structural approach. *Investigative Radiology* 1990; 25: 6-18.
- [13] Bell KL, Loveridge N, Jordan GR, Power J, Constant CR, Reeve J. A novel mechanism for induction of increased cortical porosity in cases of intracapsular hip fracture. *Bone* 2000; 27: 297-304.
- [14] Bell KL, Loveridge N, Power J, Garrahan N, Meggitt BF, Reeve J. Regional differences in cortical porosity in the fractured femoral neck. *Bone* 1999a; 24: 57-64.
- [15] Bell KL, Loveridge N, Power J, Garrahan N, Stanton M, Lunt M, Meggitt BF, Reeve J. Structure of the Femoral Neck in Hip Fracture: Cortical Bone Loss in the Inferoanterior to Superoposterior Axis. *Journal of Bone and Mineral Research* 1999b; 14: 111-119.
- [16] Bell KL, Loveridge N, Power J, Rushton N, Reeve J. Intracapsular Hip Fracture: Increased Cortical Remodeling in the Thinned and Porous Anterior Region of the Femoral Neck. *Osteoporosis International* 1999c; 10: 248-257.
- [17] Bell KL, Loveridge N, Reeve J, Thomas CDL, Feik SA, Clement JG. Superosteons (remodeling clusters) in the cortex of the femoral shaft: Influence of age and gender. *The Anatomical Record* 2001; 264: 378-386.
- [18] Bernhard A, Milovanovic P, Zimmermann EA, Hahn M, Djonic D, Krause M, Breer S, Püschel K, Djuric M, Amling M, Busse B. Micro-morphological properties of osteons reveal changes in cortical bone stability during aging, osteoporosis, and bisphosphonate treatment in women. *Osteoporosis International* 2013; 24: 2671-2680.
- [19] Binnig G, Quate CF, Gerber C. Atomic Force Microscope. *Physical Review Letters* 1986; 56: 930-933.
- [20] Bliziotis M, Sibonga JD, Turner RT, Orwoll E. Periosteal Remodeling at the Femoral Neck in Nonhuman Primates. *Journal of Bone and Mineral Research* 2006; 21: 1060-1067.

- [21] Bonnick S, Nichols D, Sanborn C, Payne S, Moen S, Heiss C. Right and left proximal femur analyses: Is there a need to do both? *Calcified Tissue International* 1996; 58: 307-310.
- [22] Bonucci E. Basic Composition and Structure of Bone. In: An YH, Draughn RA, editors. *Mechanical Testing of Bone and the Bone–Implant Interface*. Boca Raton: CRC Press; 2000, p. 3-22.
- [23] Bose S, Dasgupta S, Tarafder S, Bandyopadhyay A. Microwave-processed nanocrystalline hydroxyapatite: Simultaneous enhancement of mechanical and biological properties. *Acta Biomaterialia* 2010; 6: 3782-3790.
- [24] Boskey AL. Bone Mineralization. In: Cowin SC, editor. *Bone Mechanics Handbook*. Boca Raton: CRC Press; 2001, p. 5/1-5/33.
- [25] Boskey AL. Variations in bone mineral properties with age and disease. *Journal of Musculoskeletal Neuronal Interactions* 2002; 2: 532-4.
- [26] Boskey AL. Bone mineral crystal size. *Osteoporosis International* 2003; 14: 16-21.
- [27] Boskey AL. Mineralization of Bones and Teeth. *Elements* 2007; 3: 385-391.
- [28] Bousson V, Bergot C, Wu Y, Jolivet E, Zhou LQ, Laredo J-D. Greater tissue mineralization heterogeneity in femoral neck cortex from hip-fractured females than controls. A microradiographic study. *Bone* 2011; 48: 1252-1259.
- [29] Bozec L, De Groot J, Odlyha M, Nicholls B, Horton MA. Mineralised tissues as nanomaterials: Analysis by atomic force microscopy. *IEE Proceedings Nanobiotechnology* 2005; 152: 183-186.
- [30] Braithwaite RS, Col NF, Wong JB. Estimating Hip Fracture Morbidity, Mortality and Costs. *Journal of the American Geriatrics Society* 2003; 51: 364-370.
- [31] Brandi ML. Microarchitecture, the key to bone quality. *Rheumatology* 2009; 48: iv3-iv8.
- [32] Buchko CJ. Processing and characterization of protein polymer thin films for surface modification of neural prosthetic devices - PhD thesis. Michigan: University of Michigan; 1997.
- [33] Burr DB. Bone material properties and mineral matrix contributions to fracture risk or age in women and men. *Journal of Musculoskeletal Neuronal Interactions* 2002a; 2: 201-4.

- [34] Burr DB. Targeted and nontargeted remodeling. *Bone* 2002b; 30: 2-4.
- [35] Busse B, Djonic D, Milovanovic P, Hahn M, Püschel K, Ritchie RO, Djuric M, Amling M. Decrease in the osteocyte lacunar density accompanied by hypermineralized lacunar occlusion reveals failure and delay of remodeling in aged human bone. *Aging Cell* 2010a; 9: 1065-1075.
- [36] Busse B, Hahn M, Schinke T, Püschel K, Duda GN, Amling M. Reorganization of the femoral cortex due to age-, sex-, and endoprosthesis-related effects emphasized by osteonal dimensions and remodeling. *Journal of Biomedical Materials Research Part A* 2010b; 92A: 1440-1451.
- [37] Busse B, Hahn M, Soltau M, Zustin J, Püschel K, Duda GN, Amling M. Increased calcium content and inhomogeneity of mineralization render bone toughness in osteoporosis: Mineralization, morphology and biomechanics of human single trabeculae. *Bone* 2009; 45: 1034-1043.
- [38] Carter CB, Norton MG. *Ceramic materials*. Berlin: Springer Verlag; 2007.
- [39] Castro FA, Graeff CFO, Heier J, Hany R. Interface morphology snapshots of vertically segregated thin films of semiconducting polymer/polystyrene blends. *Polymer* 2007; 48: 2380-2386.
- [40] Chappard C, Bensalah S, Olivier C, Gouttenoire PJ, Marchadier A, Benhamou C, Peyrin F. 3D characterization of pores in the cortical bone of human femur in the elderly at different locations as determined by synchrotron micro-computed tomography images. *Osteoporosis International* 2013; 24: 1023-1033.
- [41] Chappard C, Marchadier A, Benhamou CL. Side-to-side and within-side variability of 3D bone microarchitecture by conventional micro-computed tomography of paired iliac crest biopsies. *Bone* 2008; 43: 203-208.
- [42] Chen H, Zhou X, Shoumura S, Emura S, Bunai Y. Age- and gender-dependent changes in three-dimensional microstructure of cortical and trabecular bone at the human femoral neck. *Osteoporosis International* 2010; 21: 627-636.
- [43] Chen P-Y, Toroian D, Price P, McKittrick J. Minerals Form a Continuum Phase in Mature Cancellous Bone. *Calcified Tissue International* 2011; 88: 351-361.
- [44] Ciarelli TE, Fyhrie DP, Schaffler MB, Goldstein SA. Variations in three-dimensional cancellous bone architecture of the proximal femur in female hip fractures and in controls. *Journal of Bone and Mineral Research* 2000; 15: 32-40.



- [45] Ciarelli TE, Tjhia C, Rao DS, Qiu S, Parfitt AM, Fyhrie DP. Trabecular packet-level lamellar density patterns differ by fracture status and bone formation rate in white females. *Bone* 2009; 45: 903-908.
- [46] Cole Z, Dennison E, Cooper C. Osteoporosis epidemiology update. *Current Rheumatology Reports* 2008; 10: 92-96.
- [47] Constantoudis V, Gogolides E. Fractal dimension of line width roughness and its effects on transistor performance. In: Allgair JA, Raymond CJ, editors. 1 ed. San Jose, CA, USA: SPIE; 2008. p. 692223-10.
- [48] Cooper C, Campion G, Melton LJ. Hip fractures in the elderly: A world-wide projection. *Osteoporosis International* 1992; 2: 285-289.
- [49] Cui WQ, Won YY, Baek MH, Lee DH, Chung YS, Hur JH, Ma YZ. Age-and region-dependent changes in three-dimensional microstructural properties of proximal femoral trabeculae. *Osteoporosis International* 2008; 19: 1579-1587.
- [50] Cui X, Hetke JF, Wiler JA, Anderson DJ, Martin DC. Electrochemical deposition and characterization of conducting polymer polypyrrole/PSS on multichannel neural probes. *Sensors and Actuators A: Physical* 2001; 93: 8-18.
- [51] Cullinane D, Einhorn T. Biomechanics of bone. In: Bilezikian J, Raisz L, Rodan G, editors. *Principles of Bone Biology*. San Diego: Academic Press; 2002, p. 17–32.
- [52] Cummings SR. Are patients with hip fractures more osteoporotic? Review of the evidence. *The American journal of medicine* 1985; 78: 487-494.
- [53] Currey J. Incompatible mechanical properties in compact bone. *Journal of Theoretical Biology* 2004; 231: 569-580.
- [54] Currey J. The structure and mechanics of bone. *Journal of Materials Science* 2012; 47: 41-54.
- [55] Currey JD. *Bones: structure and mechanics*. Princeton, N. J.: Princeton University Press; 2002.
- [56] Currey JD. The many adaptations of bone. *Journal of Biomechanics* 2003; 36: 1487-1495.
- [57] Dane S, Akar S, Hacibeyoglu I, Varoglu E. Differences Between Right-and Left-Femoral Bone Mineral Densities in Right-and Left-Handed Men and Women. *International Journal of Neuroscience* 2001; 111: 187-192.

- [58] De Laet CE, van Hout BA, Burger H, Hofman A, Pols HA. Bone density and risk of hip fracture in men and women: cross sectional analysis. *British Medical Journal* 1997; 315: 221-5.
- [59] Dempster DW, Compston JE, Drezner MK, Glorieux FH, Kanis JA, Malluche H, Meunier PJ, Ott SM, Recker RR, Parfitt AM. Standardized nomenclature, symbols, and units for bone histomorphometry: A 2012 update of the report of the ASBMR Histomorphometry Nomenclature Committee. *Journal of Bone and Mineral Research* 2013; 28: 2-17.
- [60] Diez-Perez A, Güerri R, Nogues X, Cáceres E, Peña MJ, Mellibovsky L, Randall C, Bridges D, Weaver JC, Proctor A, Brimer D, Koester KJ, Ritchie RO, Hansma PK. Microindentation for in vivo measurement of bone tissue mechanical properties in humans. *Journal of Bone and Mineral Research* 2010; 25: 1877-1885.
- [61] Dimri V. *Fractal behaviour of the earth system*. Heidelberg: Springer-Verlag; 2005.
- [62] Djonic D, Milovanovic P, Nikolic S, Ivovic M, Marinkovic J, Beck T, Djuric M. Inter-sex differences in structural properties of aging femora: implications on differential bone fragility: a cadaver study. *Journal of Bone and Mineral Metabolism* 2011; 29: 449-457.
- [63] Djuric M, Djonic D, Milovanovic P, Nikolic S, Marshall R, Marinkovic J, Hahn M. Region-Specific Sex-Dependent Pattern of Age-Related Changes of Proximal Femoral Cancellous Bone and Its Implications on Differential Bone Fragility. *Calcified Tissue International* 2010; 86: 192-201.
- [64] Djuric M, Milovanovic P, Djonic D, Hahn M, Marshall R, Amling M. Issues in interstudy comparisons of bone microarchitecture. *International Orthopaedics* 2013; 37: 2091-2092.
- [65] Dobrescu G, Crişan M, Zaharescu M, Ionescu NI. Fractal dimension determination of sol-gel powders using transmission electron microscopy images. *Materials Chemistry and Physics* 2004; 87: 184-189.
- [66] Donnelly E, Chen D, Boskey A, Baker S, van der Meulen M. Contribution of Mineral to Bone Structural Behavior and Tissue Mechanical Properties. *Calcified Tissue International* 2010; 87: 450-460.

- [67] Dougherty G, Henebry GM. Fractal signature and lacunarity in the measurement of the texture of trabecular bone in clinical CT images. *Medical Engineering and Physics* 2001; 23: 369-380.
- [68] Ebacher V, Guy P, Oxland TR, Wang R. Sub-lamellar microcracking and roles of canaliculi in human cortical bone. *Acta Biomaterialia* 2012; 8: 1093-1100.
- [69] Eppell SJ, Tong W, Lawrence Katz J, Kuhn L, Glimcher MJ. Shape and size of isolated bone mineralites measured using atomic force microscopy. *Journal of Orthopaedic Research* 2001; 19: 1027-1034.
- [70] Evans R, Ashwell JR, Dunstan CR. Lack of metabolic bone disease in patients with fracture of the femoral neck. *Australian and New Zealand Journal of Medicine* 1981; 11: 158-161.
- [71] Faccini JM, Exton-Smith AN, Boyde A. Disorders of bone and fracture of the femoral neck. *The Lancet* 1976; 307: 1089-1092.
- [72] Fan Z, Smith PA, Eckstein EC, Harris GF. Mechanical properties of OI type III bone tissue measured by nanoindentation. *Journal of Biomedical Materials Research Part A* 2006; 79A: 71-77.
- [73] Fan Z, Smith PA, Harris GF, Rauch F, Bajorunaite R. Comparison of Nanoindentation Measurements Between Osteogenesis Imperfecta Type III and Type IV and Between Different Anatomic Locations (Femur/Tibia versus Iliac Crest). *Connective Tissue Research* 2007; 48: 70-75.
- [74] Fang SJ, Haplepete S, Chen W, Helms CR, Edwards H. Analyzing atomic force microscopy images using spectral methods. *Journal of Applied Physics* 1997; 82: 5891-5898.
- [75] Fantner G, Hassenkam T, Kindt JH, Weaver JC, Birkedal H, Pechenik L, Cutroni JA, Cidade GAG, Stucky GD, Morse DE, Hansma PK. Sacrificial bonds and hidden length dissipate energy as mineralized fibrils separate during bone fracture. *Nature Materials* 2005; 4: 612.
- [76] Fantner GE, Birkedal H, Kindt JH, Hassenkam T, Weaver JC, Cutroni JA, Bosma BL, Bawazer L, Finch MM, Cidade GAG, Morse DE, Stucky GD, Hansma PK. Influence of the degradation of the organic matrix on the microscopic fracture behavior of trabecular bone. *Bone* 2004; 35: 1013-1022.

- [77] Fantner GE, Rabinovych O, Schitter G, Thurner P, Kindt JH, Finch MM, Weaver JC, Golde LS, Morse DE, Lipman EA, Rangelow IW, Hansma PK. Hierarchical interconnections in the nano-composite material bone: Fibrillar cross-links resist fracture on several length scales. *Composites Science and Technology* 2006; 66: 1202-1208.
- [78] Fratzl-Zelman N, Roschger P, Gourrier A, Weber M, Misof B, Loveridge N, Reeve J, Klaushofer K, Fratzl P. Combination of Nanoindentation and Quantitative Backscattered Electron Imaging Revealed Altered Bone Material Properties Associated with Femoral Neck Fragility. *Calcified Tissue International* 2009; 85: 335-343.
- [79] Fratzl-Zelman N, Roschger P, Misof B, Nawrot-Wawrzyniak K, Pötter-Lang S, Muschitz C, Resch H, Klaushofer K, Zwettler E. Fragility Fractures in Men with Idiopathic Osteoporosis Are Associated with Undermineralization of the Bone Matrix without Evidence of Increased Bone Turnover. *Calcified Tissue International* 2011: 1-10.
- [80] Fratzl P, Fratzl-Zelman N, Klaushofer K, Vogl G, Koller K. Nucleation and growth of mineral crystals in bone studied by small-angle X-ray scattering. *Calcified Tissue International* 1991; 48: 407-413.
- [81] Fratzl P, Gupta HS, Paschalis EP, Roschger P. Structure and mechanical quality of the collagen-mineral nano-composite in bone. *Journal of Materials Chemistry* 2004; 14: 2115-2123.
- [82] Gallant MA, Brown DM, Organ JM, Allen MR, Burr DB. Reference-point indentation correlates with bone toughness assessed using whole-bone traditional mechanical testing. *Bone* 2013; 53: 301-305.
- [83] Gan M, Samvedi V, Cerrone A, Dubey D, Tomar V. Effect of Compressive Straining on Nanoindentation Elastic Modulus of Trabecular Bone. *Experimental Mechanics* 2010; 50: 773-781.
- [84] García R, Magerle R, Perez R. Nanoscale compositional mapping with gentle forces. *Nature Materials* 2007; 6: 405-411.
- [85] Genant HK, Cooper C, Poor G, Reid I, Ehrlich G, Kanis J, Nordin BEC, Barrett-Connor E, Black D, Bonjour JP, Dawson-Hughes B, Delmas PD, Dequeker J, Eis SR, Gennari C, Johnell O, Johnston Jr CC, Lau EMC, Liberman UA, Lindsay R, Martin TJ, Masri B, Mautalen CA, Meunier PJ, Miller PD, Mithal A, Morii H, Papapoulos S,

Woolf A, Yu W, Khaltayev N. Interim Report and Recommendations of the World Health Organization Task-Force for Osteoporosis. *Osteoporosis International* 1999; 10: 259-264.

[86] Gourion-Arsiquaud S, Faibish D, Myers E, Spevak L, Compston J, Hodsman A, Shane E, Recker RR, Boskey ER, Boskey AL. Use of FTIR spectroscopic imaging to identify parameters associated with fragility fracture. *Journal of Bone and Mineral Research* 2009; 24: 1565-1571.

[87] Green M, Isaac DH, JenKins GM. Bone microstructure by collagenase etching. *Biomaterials* 1985; 6: 150-152.

[88] Grynblas M. Age and disease-related changes in the mineral of bone. *Calcified Tissue International* 1993; 53: S57-S64.

[89] Grynblas MD, Pilliar RM, Kandel RA, Renlund R, Filiaggi M, Dumitriu M. Porous calcium polyphosphate scaffolds for bone substitute applications in vivo studies. *Biomaterials* 2002; 23: 2063-2070.

[90] Güerri-Fernández RC, Nogués X, Quesada Gómez JM, Torres del Pliego E, Puig L, García-Giralt N, Yoskovitz G, Mellibovsky L, Hansma PK, Díez-Pérez A. Microindentation for in vivo measurement of bone tissue material properties in atypical femoral fracture patients and controls. *Journal of Bone and Mineral Research* 2013; 28: 162-168.

[91] Gupta HS, Wagermaier W, Zickler GA, Raz-Ben Aroush D, Funari SS, Roschger P, Wagner HD, Fratzl P. Nanoscale Deformation Mechanisms in Bone. *Nano Letters* 2005; 5: 2108-2111.

[92] Handschin RG, Stern WB. X-ray diffraction studies on the lattice perfection of human bone apatite (Crista Iliaca). *Bone* 1995; 16: S355-S363.

[93] Hansma P, Turner P, Drake B, Yurtsev E, Proctor A, Mathews P, Lulejian J, Randall C, Adams J, Jungmann R, Garza-de-Leon F, Fantner G, Mkrtchyan H, Pontin M, Weaver A, Brown MB, Sahar N, Rossello R, Kohn D. The bone diagnostic instrument II: Indentation distance increase. *Review of Scientific Instruments* 2008; 79: 064303-8.

[94] Hassenkam T, Fantner GE, Cutroni JA, Weaver JC, Morse DE, Hansma PK. High-resolution AFM imaging of intact and fractured trabecular bone. *Bone* 2004; 35: 4-10.

- [95] Hassenkam T, Jørgensen HL, Lauritzen JB. Mapping the imprint of bone remodeling by atomic force microscopy. *Anatomical Record - Part A Discoveries in Molecular, Cellular, and Evolutionary Biology* 2006; 288: 1087-1094.
- [96] Hassenkam T, Jørgensen HL, Pedersen MB, Kourakis AH, Simonsen L, Lauritzen JB. Atomic force microscopy on human trabecular bone from an old woman with osteoporotic fractures. *Micron* 2005; 36: 681-687.
- [97] Helvaci F, Cho J. A Nanoindentation Study of Thermally-Grown-Oxide Films on Silicon. *Materials Research Society Symposium Proceedings* 2005; 841: 1-6.
- [98] Hengsberger S, Kulik A, Zysset P. A combined atomic force microscopy and nanoindentation technique to investigate the elastic properties of bone structural units. *European Cells and Materials* 2001; 1: 12-7.
- [99] Hengsberger S, Kulik A, Zysset P. Nanoindentation discriminates the elastic properties of individual human bone lamellae under dry and physiological conditions. *Bone* 2002; 30: 178-184.
- [100] Hert J. A new attempt at the interpretation of the functional architecture of the cancellous bone. *Journal of Biomechanics* 1994; 27: 239-42.
- [101] Hildebrand T, Rüegsigger P. Quantification of Bone Microarchitecture with the Structure Model Index. *Computer Methods in Biomechanics and Biomedical Engineering* 1997; 1: 15-23.
- [102] Hoffler CE, Guo XE, Zysset PK, Goldstein SA. An application of nanoindentation technique to measure bone tissue Lamellae properties. *Journal of Biomechanical Engineering* 2005; 127: 1046-53.
- [103] Hoffler CE, Moore KE, Kozloff K, Zysset PK, Brown MB, Goldstein SA. Heterogeneity of bone lamellar-level elastic moduli. *Bone* 2000a; 26: 603-609.
- [104] Hoffler CE, Moore KE, Kozloff K, Zysset PK, Goldstein SA. Age, gender, and bone lamellae elastic moduli. *Journal of Orthopaedic Research* 2000b; 18: 432-437.
- [105] Homminga J, McCreadie BR, Ciarelli TE, Weinans H, Goldstein SA, Huiskes R. Cancellous bone mechanical properties from normals and patients with hip fractures differ on the structure level, not on the bone hard tissue level. *Bone* 2002; 30: 759-64.
- [106] Homminga J, Van-Rietbergen B, Lochmüller EM, Weinans H, Eckstein F, Huiskes R. The osteoporotic vertebral structure is well adapted to the loads of daily life, but not to infrequent "error" loads. *Bone* 2004; 34: 510-516.

- [107] Horcas I, Fernandez R, Gomez-Rodriguez JM, Colchero J, Gomez-Herrero J, Baro AM. WSXM: A software for scanning probe microscopy and a tool for nanotechnology. *Review of Scientific Instruments* 2007; 78: 013705-8.
- [108] Hordon LD, Peacock M. The architecture of cancellous and cortical bone in femoral neck fracture. *Bone and Mineral* 1990; 11: 335-345.
- [109] Hordon LD, Raisi M, Aaron JE, Paxton SK, Beneton M, Kanis JA. Trabecular architecture in women and men of similar bone mass with and without vertebral fracture: I. two-dimensional histology. *Bone* 2000; 27: 271-276.
- [110] Huja S, Beck F, Thurman D. Indentation Properties of Young and Old Osteons. *Calcified Tissue International* 2006; 78: 392-397.
- [111] Jandt KD. Atomic force microscopy of biomaterials surfaces and interfaces. *Surface Science* 2001; 491: 303-332.
- [112] Jee WSS. Integrated Bone Tissue Physiology: Anatomy and Physiology. In: Cowin SC, editor. *Bone mechanics handbook*. 2nd ed. Boca Raton: CRC Press; 2001, p. 1.1-1.68.
- [113] Jiang T, Hall N, Ho A, Morin S. Quantitative analysis of electrodeposited tin film morphologies by atomic force microscopy. *Thin Solid Films* 2005; 471: 76-85.
- [114] Jordan GR, Loveridge N, Bell KL, Power J, Rushton N, Reeve J. Spatial clustering of remodeling osteons in the femoral neck cortex: a cause of weakness in hip fracture? *Bone* 2000; 26: 305-313.
- [115] Kalmey JK, Lovejoy CO. Collagen fiber orientation in the femoral necks of apes and humans: do their histological structures reflect differences in locomotor loading? *Bone* 2002; 31: 327-332.
- [116] Kanis JA, Odén A, McCloskey EV, Johansson H, Wahl DA, Cooper C. A systematic review of hip fracture incidence and probability of fracture worldwide. *Osteoporosis International* 2012; 23: 2239-2256.
- [117] Kaptoge S, Dalzell N, Loveridge N, Beck TJ, Khaw K-T, Reeve J. Effects of gender, anthropometric variables, and aging on the evolution of hip strength in men and women aged over 65. *Bone* 2003; 32: 561-570.
- [118] Kindt JH, Fantner GE, Thurner PJ, Schitter G, Hansma PK. A new technique for imaging mineralized fibrils on bovine trabecular bone fracture surfaces by atomic force microscopy. *Materials Research Society Symposium Proceedings* 2005; 874: 59-65.

- [119] Kindt JH, Thurner PJ, Lauer ME, Bosma BL, Schitter G, Fantner GE, Izumi M, Weaver JC, Morse DE, Hansma PK. In situ observation of fluoride-ion-induced hydroxyapatite–collagen detachment on bone fracture surfaces by atomic force microscopy. *Nanotechnology* 2007; 18: 135102.
- [120] Kitching S, Williams PM, Roberts CJ, Davies MC, Tendler SJB. Quantifying surface topography and scanning probe image reconstruction. *Journal of Vacuum Science & Technology B* 1999; 17: 273-279.
- [121] Koehne T, Marshall RP, Jeschke A, Kahl-Nieke B, Schinke T, Amling M. Osteopetrosis, osteopetrorickets and hypophosphatemic rickets differentially affect dentin and enamel mineralization. *Bone* 2013; 53: 25-33.
- [122] Kuhn L, Grynopas M, Rey C, Wu Y, Ackerman J, Glimcher M. A Comparison of the Physical and Chemical Differences Between Cancellous and Cortical Bovine Bone Mineral at Two Ages. *Calcified Tissue International* 2008; 83: 146-154.
- [123] LaMothe JM, Zernicke RF. The relation between loading rate, strain gradients, and bone adaptation. *The Journal of Bone and Joint Surgery* 2008; 90-B: 78.
- [124] Landis WJ, Hodgens KJ, Song MJ, Arena J, Kiyonaga S, Marko M, Owen C, McEwen BF. Mineralization of Collagen May Occur on Fibril Surfaces: Evidence from Conventional and High-Voltage Electron Microscopy and Three-Dimensional Imaging. *Journal of Structural Biology* 1996; 117: 24-35.
- [125] Landis WJ, Song MJ, Leith A, McEwen L, McEwen BF. Mineral and Organic Matrix Interaction in Normally Calcifying Tendon Visualized in Three Dimensions by High-Voltage Electron Microscopic Tomography and Graphic Image Reconstruction. *Journal of Structural Biology* 1993; 110: 39-54.
- [126] Launey ME, Buehler MJ, Ritchie RO. On the Mechanistic Origins of Toughness in Bone. *Annual Review of Materials Research* 2010; 40: 25-53.
- [127] Lawrence TM, White CT, Wenn R, Moran CG. The current hospital costs of treating hip fractures. *Injury* 2005; 36: 88-91.
- [128] Legrand E, Chappard D, Pascaretti C, Duquenne M, Krebs S, Rohmer V, Basle MF, Audran M. Trabecular bone microarchitecture, bone mineral density, and vertebral fractures in male osteoporosis. *Journal of Bone and Mineral Research* 2000; 15: 13-9.
- [129] Legros R, Balmain N, Bonel G. Age-related changes in mineral of rat and bovine cortical bone. *Calcified Tissue International* 1987; 41: 137-144.



- [130] Lesić A, Bumbasirević M, Jarebinski M, Pekmezovic T. [Incidence of hip fractures in the population of Belgrade during the period 1990-2000. Projections for 2020]. *Acta Chirurgica Iugoslavica* 2005; 52: 95-99.
- [131] Lešić A, Jarebinski M, Pekmezović T, Bumbaširević M, Spasovski D, Atkinson H. Epidemiology of hip fractures in Belgrade, Serbia Montenegro, 1990–2000. *Archives of Orthopaedic and Trauma Surgery* 2007; 127: 179-183.
- [132] Lin Y, Xu S. AFM analysis of the lacunar-canalicular network in demineralized compact bone. *Journal of Microscopy* 2011; 241: 291-302.
- [133] Lips P, Netelenbos JC, Jongen MJM, van Ginkel FC, Althuis AL, van Schaik CL, van der Vijgh WJF, Vermeiden JPW, van der Meer C. Histomorphometric profile and vitamin d status in patients with femoral neck fracture. *Metabolic Bone Disease and Related Research* 1982; 4: 85-93.
- [134] Lita AE, Sanchez JE, Jr. Effects of grain growth on dynamic surface scaling during the deposition of Al polycrystalline thin films. *Physical Review B* 2000; 61: 7692-7699.
- [135] Lita AE, Sanchez JJE. Characterization of surface structure in sputtered Al films: Correlation to microstructure evolution. *Journal of Applied Physics* 1999; 85: 876-882.
- [136] Liu XS, Sajda P, Saha PK, Wehrli FW, Guo XE. Quantification of the roles of trabecular microarchitecture and trabecular type in determining the elastic modulus of human trabecular bone. *Journal of Bone and Mineral Research* 2006; 21: 1608-17.
- [137] Lochmuller EM, Matsuura M, Bauer J, Hitzl W, Link TM, Muller R, Eckstein F. Site-specific deterioration of trabecular bone architecture in men and women with advancing age. *Journal of Bone and Mineral Research* 2008; 23: 1964-73.
- [138] Lotz JC, Cheal EJ, Hayes WC. Stress distributions within the proximal femur during gait and falls: Implications for osteoporotic fracture. *Osteoporosis International* 1995; 5: 252-261.
- [139] Loveridge N, Power J, Reeve J, Boyde A. Bone mineralization density and femoral neck fragility. *Bone* 2004; 35: 929-941.
- [140] Lundeen GA, Vajda EG, Bloebaum RD. Age-related cancellous bone loss in the proximal femur of caucasian females. *Osteoporosis International* 2000; 11: 505-11.

- [141] Mackie I, Green M, Clarke H, Isaac D. Human bone microstructure studied by collagenase etching. *Journal of Bone and Joint Surgery, British Volume* 1989a; 71-B: 509-513.
- [142] Mackie IG, Green M, Clarke H, Isaac DH. Osteoporotic bone microstructure by collagenase etching. *Annals of the Rheumatic Diseases* 1989b; 48: 464-469.
- [143] Maravic M, Le Bihan C, Landais P, Fardellone P. Incidence and cost of osteoporotic fractures in France during 2001. A methodological approach by the national hospital database. *Osteoporosis International* 2005; 16: 1475-1480.
- [144] Marshall D, Johnell O, Wedel H. Meta-analysis of how well measures of bone mineral density predict occurrence of osteoporotic fractures. *British Medical Journal* 1996; 312: 1254-1259.
- [145] Martens M, Van Audekercke R, Delpont P, De Meester P, Mulier JC. The mechanical characteristics of cancellous bone at the upper femoral region. *Journal of Biomechanics* 1983; 16: 971-83.
- [146] Martin RB. Toward a unifying theory of bone remodeling. *Bone* 2000; 26: 1-6.
- [147] McCreadie BR, Morris MD, Chen T-c, Sudhaker Rao D, Finney WF, Widjaja E, Goldstein SA. Bone tissue compositional differences in women with and without osteoporotic fracture. *Bone* 2006; 39: 1190-1195.
- [148] McNally EA, Schwarcz HP, Botton GA, Arsenault AL. A Model for the Ultrastructure of Bone Based on Electron Microscopy of Ion-Milled Sections. *PLoS ONE* 2012; 7: e29258.
- [149] Melton LJ. Hip fractures: A worldwide problem today and tomorrow. *Bone* 1993; 14: 1-8.
- [150] Melton LJ, Atkinson EJ, O'Fallon WM, Wahner HW, Riggs BL. Long-term fracture prediction by bone mineral assessed at different skeletal sites. *Journal of Bone and Mineral Research* 1993; 8: 1227-1233.
- [151] Michelotti J, Clark J. Femoral Neck Length and Hip Fracture Risk. *Journal of Bone and Mineral Research* 1999; 14: 1714-1720.
- [152] Milovanovic P, Zimmermann EA, Hahn M, Djonic D, Püschel K, Djuric M, Amling M, Busse B. Osteocytic Canalicular Networks: Morphological Implications for Altered Mechanosensitivity. *ACS Nano* 2013; 7: 7542-7551.

- [153] Mishra P, Ghose D. The hardness study of oxygen implanted aluminum thin films. *Surface and Coatings Technology* 2006; 201: 965-970.
- [154] Mitchell MW, Bonnell DA. Quantitative topographic analysis of fractal surfaces by scanning tunneling microscopy. *Journal of Materials Research* 1990; 5: 2244-2254.
- [155] Mongiorgi R, Romagnoli R, Olmi R, Moroni A. Mineral alterations in senile osteoporosis. *Biomaterials* 1983; 4: 192-196.
- [156] Nakamura T, Turner CH, Yoshikawa T, Slemenda CW, Peacock M, Burr DB, Mizuno Y, Orimo H, Ouchi Y, Johnston CC. Do variations in hip geometry explain differences in hip fracture risk between Japanese and white Americans? *Journal of Bone and Mineral Research* 1994; 9: 1071-1076.
- [157] Nalla RK, Kruzic JJ, Kinney JH, Balooch M, Ager Iii JW, Ritchie RO. Role of microstructure in the aging-related deterioration of the toughness of human cortical bone. *Materials Science and Engineering: C* 2006; 26: 1251-1260.
- [158] Nenadović M, Potočnik J, Ristić M, Štrbac S, Rakočević Z. Surface modification of polyethylene by Ag<sup>+</sup> and Au<sup>+</sup> ion implantation observed by phase imaging atomic force microscopy. *Surface and Coatings Technology* 2012; 206: 4242–4248.
- [159] Nix WD, Gao H. Indentation size effects in crystalline materials: A law for strain gradient plasticity. *Journal of the Mechanics and Physics of Solids* 1998; 46: 411-425.
- [160] Njeh CF, Nicholson PH, Rho JY. Mechanical testing. In: Langton CM, Njeh CF, editors. *The Physical Measurement of Bone*. Bristol: Institute of Physics Publishing; 2004, p. 125-184.
- [161] Noble B. Bone microdamage and cell apoptosis. *European Cells and Materials* 2003; 6: 46-55.
- [162] Norman J, Shapter JG, Short K, Smith LJ, Fazzalari NL. Micromechanical properties of human trabecular bone: A hierarchical investigation using nanoindentation. *Journal of Biomedical Materials Research Part A* 2008a; 87A: 196-202.
- [163] Norman TL, Little TM, Yeni YN. Age-related changes in porosity and mineralization and in-service damage accumulation. *Journal of Biomechanics* 2008b; 41: 2868-2873.

- [164] Oliver WC, Pharr GM. An improved technique for determining hardness and elastic modulus using load and displacement sensing indentation experiments. *Journal of Materials Research* 1992; 7: 1564-1583.
- [165] Orwoll ES. Toward an Expanded Understanding of the Role of the Periosteum in Skeletal Health. *Journal of Bone and Mineral Research* 2003; 18: 949-954.
- [166] Ostertag A, Cohen-Solal M, Audran M, Legrand E, Marty C, Chappard D, de Vernejoul M-C. Vertebral fractures are associated with increased cortical porosity in iliac crest bone biopsy of men with idiopathic osteoporosis. *Bone* 2009; 44: 413-417.
- [167] Parfitt AM. Quantum concept of bone remodeling and turnover: implications for the pathogenesis of osteoporosis. *Calcified Tissue International* 1979; 28: 1-5.
- [168] Parfitt AM. Bone Remodeling and Bone Loss: Understanding The Pathophysiology of Osteoporosis. *Clinical Obstetrics and Gynecology* 1987; 30: 789-811.
- [169] Parfitt AM. Parathyroid Hormone and Periosteal Bone Expansion. *Journal of Bone and Mineral Research* 2002; 17: 1741-1743.
- [170] Parfitt AM. What is the normal rate of bone remodeling? *Bone* 2004; 35: 1-3.
- [171] Paschalis EP, Betts F, DiCarlo E, Mendelsohn R, Boskey AL. FTIR Microspectroscopic Analysis of Human Iliac Crest Biopsies from Untreated Osteoporotic Bone. *Calcified Tissue International* 1997a; 61: 487-492.
- [172] Paschalis EP, Betts F, DiCarlo E, Mendelsohn R, Boskey AL. FTIR Microspectroscopic Analysis of Normal Human Cortical and Trabecular Bone. *Calcified Tissue International* 1997b; 61: 480-486.
- [173] Passi N, Gefen A. Trabecular bone contributes to strength of the proximal femur under mediolateral impact in the avian. *Journal of Biomechanical Engineering* 2005; 127: 198-203.
- [174] Pfeifer P. Fractal dimension as working tool for surface-roughness problems. *Applications of Surface Science* 1984; 18: 146-164.
- [175] Pidaparti RMV, Chandran A, Takano Y, Turner CH. Bone mineral lies mainly outside collagen fibrils: Predictions of a composite model for osteonal bone. *Journal of Biomechanics* 1996; 29: 909-916.
- [176] Pierre MA, Zurakowski D, Nazarian A, Hauser-Kara DA, Snyder BD. Assessment of the bilateral asymmetry of human femurs based on physical,

densitometric, and structural rigidity characteristics. *Journal of Biomechanics* 2010; 43: 2228-2236.

[177] Power J, Loveridge N, Lyon A, Rushton N, Parker M, Reeve J. Osteoclastic cortical erosion as a determinant of subperiosteal osteoblastic bone formation in the femoral neck's response to BMU imbalance. Effects of stance-related loading and hip fracture. *Osteoporosis International* 2005; 16: 1049-1056.

[178] Power J, Loveridge N, Rushton N, Parker M, Reeve J. Evidence for bone formation on the external "periosteal" surface of the femoral neck: a comparison of intracapsular hip fracture cases and controls. *Osteoporosis International* 2003; 14: 141-145.

[179] Qiu S, Sudhaker Rao D, Fyhrie DP, Palnitkar S, Parfitt AM. The morphological association between microcracks and osteocyte lacunae in human cortical bone. *Bone* 2005; 37: 10-15.

[180] Rao AD, Reddy S, Rao DS. Is There a Difference Between Right and Left Femoral Bone Density? *Journal of Clinical Densitometry* 2000; 3: 57-61.

[181] Rauch F. Bone Accrual in Children: Adding Substance to Surfaces. *Pediatrics* 2007; 119: S137-S140.

[182] Regelsberger J, Milovanovic P, Schmidt T, Hahn M, Zimmermann E, Tsokos M, Zustin J, Ritchie R, Amling M, Busse B. Changes to the cell, tissue and architecture levels in cranial suture synostosis reveal a problem of timing in bone development. *European Cells and Materials* 2012; 24: 441-458.

[183] Reich T, Gefen A. Effect of trabecular bone loss on cortical strain rate during impact in an in vitro model of avian femur. *BioMedical Engineering OnLine* 2006; 5: 45.

[184] Reilly GC, Knapp HF, Stemmer A, Niederer P, Knothe Tate ML. Investigation of the Morphology of the Lacunocanalicular System of Cortical Bone Using Atomic Force Microscopy. *Annals of Biomedical Engineering* 2001; 29: 1074-1081.

[185] Rey C, Combes C, Drouet C, Glimcher M. Bone mineral: update on chemical composition and structure. *Osteoporosis International* 2009; 20: 1013-1021.

[186] Rezwan K, Chen QZ, Blaker JJ, Boccaccini AR. Biodegradable and bioactive porous polymer/inorganic composite scaffolds for bone tissue engineering. *Biomaterials* 2006; 27: 3413-3431.

- [187] Rho JY, Pharr GM. Effects of drying on the mechanical properties of bovine femur measured by nanoindentation. *Journal of Materials Science: Materials in Medicine* 1999a; 10: 485-488.
- [188] Rho JY, Pharr GM. Nanoindentation Testing of Bone. In: An YH, Draughn RA, editors. *Mechanical Testing of Bone and the Bone–Implant Interface*. Boca Raton: CRC Press; 1999b, p. 257-269.
- [189] Rho JY, Roy ME, Tsui TY, Pharr GM. Elastic properties of microstructural components of human bone tissue as measured by nanoindentation. *Journal of Biomedical Materials Research* 1999a; 45: 48-54.
- [190] Rho JY, Tsui TY, Pharr GM. Elastic properties of human cortical and trabecular lamellar bone measured by nanoindentation. *Biomaterials* 1997; 18: 1325-30.
- [191] Rho JY, Zioupos P, Currey JD, Pharr GM. Variations in the individual thick lamellar properties within osteons by nanoindentation. *Bone* 1999b; 25: 295-300.
- [192] Rho JY, Zioupos P, Currey JD, Pharr GM. Microstructural elasticity and regional heterogeneity in human femoral bone of various ages examined by nano-indentation. *Journal of Biomechanics* 2002; 35: 189-198.
- [193] Ritchie RO. The conflicts between strength and toughness. *Nature Materials* 2011; 10: 817-22.
- [194] Rizzoli R. Microarchitecture in focus. *Osteoporosis International* 2010; 21: 403-406.
- [195] Roberts SE, Goldacre MJ. Time trends and demography of mortality after fractured neck of femur in an English population, 1968–98: database study. *British Medical Journal* 2003; 327: 771-775.
- [196] Roschger P, Fratzl P, Eschberger J, Klaushofer K. Validation of quantitative backscattered electron imaging for the measurement of mineral density distribution in human bone biopsies. *Bone* 1998; 23: 319-26.
- [197] Roschger P, Paschalis EP, Fratzl P, Klaushofer K. Bone mineralization density distribution in health and disease. *Bone* 2008; 42: 456-466.
- [198] Rudman K, Aspden R, Meakin J. Compression or tension? The stress distribution in the proximal femur. *BioMedical Engineering OnLine* 2006; 5: 12.

- [199] Sahoo NK, Thakur S, Tokas RB. Fractals and superstructures in gadolinia thin film morphology: Influence of process variables on their characteristic parameters. *Thin Solid Films* 2006; 503: 85-95.
- [200] Saito M, Marumo K. Collagen cross-links as a determinant of bone quality: a possible explanation for bone fragility in aging, osteoporosis, and diabetes mellitus. *Osteoporosis International* 2010; 21: 195-214.
- [201] Sasaki N, Tagami A, Goto T, Taniguchi M, Nakata M, Hikichi K. Atomic force microscopic studies on the structure of bovine femoral cortical bone at the collagen fibril-mineral level. *Journal of Materials Science: Materials in Medicine* 2002; 13: 333-337.
- [202] Schaffler MB, Choi K, Milgrom C. Aging and matrix microdamage accumulation in human compact bone. *Bone* 1995; 17: 521-525.
- [203] Schuit SC, van der Klift M, Weel AE, de Laet CE, Burger H, Seeman E, Hofman A, Uitterlinden AG, van Leeuwen JP, Pols HA. Fracture incidence and association with bone mineral density in elderly men and women: the Rotterdam Study. *Bone* 2004; 34: 195-202.
- [204] Seeman E. Periosteal Bone Formation — A Neglected Determinant of Bone Strength. *New England Journal of Medicine* 2003; 349: 320-323.
- [205] Seeman E. The periosteum—a surface for all seasons. *Osteoporosis International* 2007; 18: 123-128.
- [206] Seeman E. Bone quality: the material and structural basis of bone strength. *Journal of Bone and Mineral Metabolism* 2008; 26: 1-8.
- [207] Senohradski K, Markovic-Denic L, Lesic A, Bumbasirevic V, Bumbasirevic M. Trends in the incidence of hip fractures. *Osteoporosis International* 2013; 24: 1759-1763.
- [208] Shuman D. Atomic Force Microscope Indentation Measurement Software. In: Wilkening G, Koenders L, editors. *Nanoscale Calibration Standards and Methods*: Wiley-VCH Verlag GmbH & Co. KGaA; 2006, p. 463-480.
- [209] Shuman DJ, Costa ALM, Andrade MS. Calculating the elastic modulus from nanoindentation and microindentation reload curves. *Materials Characterization* 2007; 58: 380-389.

- [210] Silk T, Hong Q, Tamm J, Compton RG. AFM studies of polypyrrole film surface morphology II. Roughness characterization by the fractal dimension analysis. *Synthetic Metals* 1998; 93: 65-71.
- [211] Simmons ED, Pritzker KPH, Grynblas MD. Age-related changes in the human femoral cortex. *Journal of Orthopaedic Research* 1991; 9: 155-167.
- [212] Skedros JG, Bloebaum RD, Bachus KN, Boyce TM, Constantz B. Influence of mineral content and composition on graylevels in backscattered electron images of bone. *Journal of Biomedical Materials Research* 1993; 27: 57-64.
- [213] Skedros JG, Knight AN, Farnsworth RW, Bloebaum RD. Do regional modifications in tissue mineral content and microscopic mineralization heterogeneity adapt trabecular bone tracts for habitual bending? Analysis in the context of trabecular architecture of deer calcanei. *Journal of Anatomy* 2012; 220: 242-255.
- [214] Smith LJ, Schirer JP, Fazzalari NL. The role of mineral content in determining the micromechanical properties of discrete trabecular bone remodeling packets. *Journal of Biomechanics* 2010; 43: 3144-3149.
- [215] Stone KL, Seeley DG, Lui LY, Cauley JA, Ensrud K, Browner WS, Nevitt MC, Cummings SR. BMD at Multiple Sites and Risk of Fracture of Multiple Types: Long-Term Results From the Study of Osteoporotic Fractures. *Journal of Bone and Mineral Research* 2003; 18: 1947-1954.
- [216] Strbac S, Nenadovic M, Rajakovic L, Rakocevic Z. Chemical surface composition of the polyethylene implanted by Ag<sup>+</sup> ions studied by phase imaging atomic force microscopy. *Applied Surface Science* 2010; 256: 3895-3899.
- [217] Su X, Sun K, Cui FZ, Landis WJ. Organization of apatite crystals in human woven bone. *Bone* 2003; 32: 150-162.
- [218] Szulc P, Seeman E, Duboeuf F, Sornay-Rendu E, Delmas PD. Bone Fragility: Failure of Periosteal Apposition to Compensate for Increased Endocortical Resorption in Postmenopausal Women. *Journal of Bone and Mineral Research* 2006; 21: 1856-1863.
- [219] Tai K, Dao M, Suresh S, Palazoglu A, Ortiz C. Nanoscale heterogeneity promotes energy dissipation in bone. *Nature Materials* 2007; 6: 454-62.
- [220] Tai K, Ulm F-J, Ortiz C. Nanogranular Origins of the Strength of Bone. *Nano Letters* 2006; 6: 2520-2525.



- [221] Tanck E, Hannink G, Ruimerman R, Buma P, Burger EH, Huiskes R. Cortical bone development under the growth plate is regulated by mechanical load transfer. *Journal of Anatomy* 2006; 208: 73-79.
- [222] Thompson D, Posner A, Laughlin W, Blumenthal N. Comparison of bone apatite in osteoporotic and normal Eskimos. *Calcified Tissue International* 1983; 35: 392-393.
- [223] Thurner PJ. Atomic force microscopy and indentation force measurement of bone. *Wiley Interdisciplinary Reviews: Nanomedicine and Nanobiotechnology* 2009; 1: 624-649.
- [224] Thurner PJ, Müller R, Kindt JH, Schitter G, Fantner GE, Wyss P, Sennhauser U, Hansma PK. Novel techniques for high-resolution functional imaging of trabecular bone. In: *Proceedings of the SPIE*; 2005. p. 515-526.
- [225] Thurner PJ, Oroudjev E, Jungmann R, Kreuz C, Kindt JH, Schitter G, Okouneva TO, Lauer ME, Fantner GE, Hansma HG, Hansma PK. Imaging of Bone Ultrastructure using Atomic Force Microscopy. In: Méndez-Vilas A, Díaz J, editors. *Modern Research and Educational Topics in Microscopy*. 3rd ed. Badajoz: Formatex; 2007, p. 37-48.
- [226] Tong W, Glimcher MJ, Katz JL, Kuhn L, Eppell SJ. Size and Shape of Mineralites in Young Bovine Bone Measured by Atomic Force Microscopy. *Calcified Tissue International* 2003; 72: 592-598.
- [227] Tosteson ANA, Gottlieb DJ, Radley DC, Fisher ES, Melton LJ, III. Excess mortality following hip fracture: the role of underlying health status. *Osteoporosis International* 2007; 18: 1463-1472.
- [228] Tsangari H, Findlay DM, Fazzalari NL. Structural and remodeling indices in the cancellous bone of the proximal femur across adulthood. *Bone* 2007; 40: 211-7.
- [229] Uitewaal P, Lips P, Netelenbos J. An analysis of bone structure in patients with hip fracture. *Bone and Mineral* 1987; 3: 63-73.
- [230] Ulmeanu M, Serghei A, Mihailescu IN, Budau P, Enachescu M. C–Ni amorphous multilayers studied by atomic force microscopy. *Applied Surface Science* 2000; 165: 109-115.
- [231] Uusi-Rasi K, Sievänen H, Heinonen A, Beck TJ, Vuori I. Determinants of changes in bone mass and femoral neck structure, and physical performance after

menopause: a 9-year follow-up of initially peri-menopausal women. *Osteoporosis International* 2005; 16: 616-622.

[232] van der Meulen MCH, Ashford MW, Kiratli BJ, Bachrach LK, Carter DR. Determinants of femoral geometry and structure during adolescent growth. *Journal of Orthopaedic Research* 1996; 14: 22-29.

[233] Veenland JF, Link TM, Konermann W, Meier N, Grashuis JL, Gelsema ES. Unraveling the Role of Structure and Density in Determining Vertebral Bone Strength. *Calcified Tissue International* 1997; 61: 474-479.

[234] Verhulp E, van Rietbergen B, Huiskes R. Load distribution in the healthy and osteoporotic human proximal femur during a fall to the side. *Bone* 2008; 42: 30-5.

[235] Viguet-Carrin S, Garnero P, Delmas P. The role of collagen in bone strength. *Osteoporosis International* 2006; 17: 319-336.

[236] Wagoner Johnson AJ, Herschler BA. A review of the mechanical behavior of CaP and CaP/polymer composites for applications in bone replacement and repair. *Acta Biomaterialia* 2011; 7: 16-30.

[237] Wallace JM. Applications of atomic force microscopy for the assessment of nanoscale morphological and mechanical properties of bone. *Bone* 2012; 50: 420-427.

[238] Wallace JM, Erickson B, Les CM, Orr BG, Banaszak Holl MM. Distribution of type I collagen morphologies in bone: Relation to estrogen depletion. *Bone* 2010; 46: 1349-1354.

[239] Wang J, Shaw LL. Nanocrystalline hydroxyapatite with simultaneous enhancements in hardness and toughness. *Biomaterials* 2009; 30: 6565-6572.

[240] Weiner S, Wagner HD. The Material Bone: Structure-Mechanical Function Relations. *Annual Review of Materials Science* 1998; 28: 271-298.

[241] Wiktorowicz ME, Goeree R, Papaioannou A, Adachi JD, Papadimitropoulos E. Economic Implications of Hip Fracture: Health Service Use, Institutional Care and Cost in Canada. *Osteoporosis International* 2001; 12: 271-278.

[242] Wu Y, Bergot C, Jolivet E, Zhou LQ, Laredo J-D, Bousson V. Cortical bone mineralization differences between hip-fractured females and controls. A microradiographic study. *Bone* 2009; 45: 207-212.

[243] Xin R, Leng Y, Wang N. HRTEM Study of the Mineral Phases in Human Cortical Bone. *Advanced Engineering Materials* 2010; 12: B552–B557.

- [244] Yates LB, Karasik D, Beck TJ, Cupples LA, Kiel DP. Hip structural geometry in old and old-old age: similarities and differences between men and women. *Bone* 2007; 41: 722-32.
- [245] Yerramshetty JS, Akkus O. The associations between mineral crystallinity and the mechanical properties of human cortical bone. *Bone* 2008; 42: 476-482.
- [246] Yerramshetty JS, Lind C, Akkus O. The compositional and physicochemical homogeneity of male femoral cortex increases after the sixth decade. *Bone* 2006; 39: 1236-1243.
- [247] Zawada DG, Brock JC. A Multiscale Analysis of Coral Reef Topographic Complexity Using Lidar-Derived Bathymetry. *Journal of Coastal Research* 2009: 6-15.
- [248] Zinke-Allmang M, Feldman LC, Grabow MH. Clustering on surfaces. *Surface Science Reports* 1992; 16: 377-463.
- [249] Zysset PK, Edward Guo X, Edward Hoffler C, Moore KE, Goldstein SA. Elastic modulus and hardness of cortical and trabecular bone lamellae measured by nanoindentation in the human femur. *Journal of Biomechanics* 1999; 32: 1005-1012.

## **Curriculum Vitae**

Dr. Petar Milovanović was born on March 9th 1984 in Zemun. He finished elementary school "Sutjeska" in 1999, and Gymnasium in Zemun in 2003 as the best pupil in the generation. He was enrolled in University of Belgrade - School of Medicine in 2003, graduated in 2009 with GPA 10/10 and was awarded as the best graduate student. Subsequently, he was enrolled in Doctoral Studies (course: Skeletal biology) at University of Belgrade - School of Medicine in 2009/2010. Since 2005, he has been participating in research projects within the Laboratory for Anthropology, Institute of Anatomy, University of Belgrade - School of Medicine, under guidance of Prof. Dr. Marija Djurić. For his achievements during studies and scientific work, he won numerous national and international awards. In 2012, he was awarded with DAAD research grant for scientific work at the Institute of Osteology and Biomechanics in Hamburg, Germany. He was appointed to the position of a teaching assistant at Institute of Anatomy, University of Belgrade - School of Medicine in December 2010, and to the position of assistant professor in November 2012. Since 2011, he has been working as a research fellow on the project III45005 funded by Ministry of Education and Science of the Republic of Serbia. He is an author or co-author of 23 papers published in peer-reviewed international journals indexed in Journal Citation Report list.

## **Биографија кандидата**

Др Петар Миловановић је рођен 9. марта 1984. године у Земуну. Завршио је основну школу „Сутјеска“ 1999. године, а 2003. године и Земунску гимназију као Бак генерације. На Медицински факултет у Београду уписан је 2003. године, а дипломирао је 2009. године са просечном оценом 10 и награђен као Најбољи дипломирани студент. Докторске студије - смер Биологија скелета (на енглеском језику) уписао је 2009. године на Медицинском факултету у Београду. Од 2005. године активно учествује у научним пројектима Лабораторије за антропологију Института за анатомију Медицинског факултета у Београду којом руководи проф. др Марија Ђурић. Добитник је бројних домаћих и међународних признања за стручни и научни рад. Добитник је DAAD стипендије за истраживачки рад 2012. године, на основу које је боравио на научном усавршавању на Институту за остеологију и биомеханику у Хамбургу, Немачка. У звање сарадника у настави на катедри за анатомију Медицинског факултета у Београду изабран је децембра 2010. године, а новембра 2012. године изабран је у звање асистента. Од 2011. године ради на пројекту III45005 који финансира Министарство просвете и науке Републике Србије. Аутор је или коаутор у 23 рада штампана у целини у часописима индексираним у JCR листи.

Прилог 1.

## Изјава о ауторству

Потписани: Петар Д. Миловановић

### Изјављујем

да је докторска дисертација под насловом

„Наноструктурне и микроархитектонске карактеристике врата бутне кости: утицај на повећану коштану фрагилност са старењем код жена“

- резултат сопственог истраживачког рада,
- да предложена дисертација у целини ни у деловима није била предложена за добијање било које дипломе према студијским програмима других високошколских установа,
- да су резултати коректно наведени и
- да нисам кршио ауторска права и користио интелектуалну својину других лица.

Потпис докторанда

У Београду, 02.11.2013.



Прилог 2.

## Изјава о истоветности штампане и електронске верзије докторског рада

Име и презиме аутора: Петар Д. Миловановић

Студијски програм: биологија скелета

Наслов рада: Наноструктурне и микроархитектонске карактеристике врата бутне кости: утицај на повећану коштану фрагилност са старењем код жена

Ментор: проф. др Марија Ђурић

Изјављујем да је штампана верзија мог докторског рада истоветна електронској верзији коју сам предао/ла за објављивање на порталу **Дигиталног репозиторијума Универзитета у Београду**.

Дозвољавам да се објаве моји лични подаци везани за добијање академског звања доктора наука, као што су име и презиме, година и место рођења и датум одбране рада.

Ови лични подаци могу се објавити на мрежним страницама дигиталне библиотеке, у електронском каталогу и у публикацијама Универзитета у Београду.

Потпис докторанда

У Београду, 02.11.2013.

  
др Петар Д. Миловановић

Прилог 3.

## Изјава о коришћењу

Овлашћујем Универзитетску библиотеку „Светозар Марковић“ да у Дигитални репозиторијум Универзитета у Београду унесе моју докторску дисертацију под насловом:

„Наноструктурне и микроархитектонске карактеристике врата бутне кости: утицај на повећану коштану фрагилност са старењем код жена“

која је моје ауторско дело.

Дисертацију са свим прилозима предао сам у електронском формату погодном за трајно архивирање.

Моју докторску дисертацију похрањену у Дигитални репозиторијум Универзитета у Београду могу да користе сви који поштују одредбе садржане у одабраном типу лиценце Креативне заједнице (Creative Commons) за коју сам се одлучио.

1. Ауторство
2. Ауторство - некомерцијално
3. Ауторство – некомерцијално – без прераде
4. Ауторство – некомерцијално – делити под истим условима
5. Ауторство – без прераде
6. Ауторство – делити под истим условима

(Молимо да заокружите само једну од шест понуђених лиценци, кратак опис лиценци дат је на полеђини листа).

Потпис докторанда

У Београду, 02.11.2013.

